The Dissertation Committee for William Reynolds Murray Certifies that this is the approved version of the following dissertation:

Modification and Control of the Interface of High Temperature Cuprate Superconductors Using Self-Assembled Monolayers

Committee:

John T. McDevitt, Supervisor

Alan Cowley

Alan Campion

John Markert

Keith Stevenson

Modification and Control of the Interface of High Temperature Cuprate Superconductors Using Self-Assembled Monolayers

by

William Reynolds Murray, B.S.

Dissertation

Presented to the Faculty of the Graduate School of

The University of Texas at Austin

in Partial Fulfillment

of the Requirements

for the Degree of

Doctor of Philosophy

The University of Texas at Austin

August 2003

Dedication

This dissertation is dedicated to my parents, Richard and Rachel, and my brother Jim, for all their support and encouragement throughout the years.

I also dedicate this work to all the teachers and professors who have encouraged and believed in me; especially Dr. Erich Uffelman for making chemistry fun again, and Dr. Lad Sessions for bringing me back to school after my hiatus in the real world. I still remain an “academic tourist”

Acknowledgements

I would like to thank Dr. McDevitt for his patience, assistance, and allowing me to pursue the chemistry and PLD system where it needed to go.

I would also like to thank Dr. Keith Stevenson for his availability to answer my electrochemistry questions.

I would like to thank my co-workers throughout my time here for all of their insight into my research and the entertainment they provided when things got stressful. Thanks to Dr. Steve Savoy for the ready jokes and chemical pop-quizzes. Thanks to Dr. Jason Ritchie for the instruction in the RAIRS measurements and your endless, humorous torment of a certain co-worker. Thanks to Dr. Cyndi Wells for the long conversations about chemistry and making the problems in my life look small. Thanks to Dr. Andrea Wells for the friendship and understanding when things got rough. Thanks to Dr. Sara Eames for putting up with our good-natured ribbing and for all the assistance in characterization of the films when there were too many to handle by myself. I have to include this in type for posterity, Sara, "Wot?" Thanks to Chris E. Jones for the computer "assistance." Thanks to Katherine Kershan for her grunt work

acquiring the atomic adsorption data. Thanks to Dr. Steen Schougaard for playing the devil's advocate about research and pushing me on when I needed it. Thanks to Sung-Wook Kim for taking over the pulse laser deposition system so that I could get on with my research, and also for acquiring SEM's when I really needed them. Your help has been invaluable towards the end of this long process during the last minute sprint to the PhD finish line. Thanks to Jorge Wong and Alex Pavel for the entertainment in lab and staying out of my way.

Considering all the time spent in the machine shops during my tenure, I would be remiss if I didn't thank the chemistry machine shop for ideas and assistance solving some particularly thorny issues with the design of the PLD system. Research would not happen without Grady, Lee, Terry, Charles and Kenneth. Thanks to Jack Chalmers in the physics machine shop for teaching me how to machine my own parts.

I would especially like to thank Jamie Jones for her support and encouragement during this phase of the journey. Hopefully, I'll be able to provide the same for you when it is your turn.

Modification and Control of the Interface of High Temperature Cuprate Superconductors Using Self-Assembled Monolayers

Publication No._____

William Reynolds Murray, Ph.D.

The University of Texas at Austin, 2003

Supervisor: John T. McDevitt

High temperature superconductors are plagued by numerous material problems that have hampered the commercial development of these complex copper oxides. One of the most problematic material characteristics is the propensity of the cuprates to undergo reduction in the presence of water, acids, CO and CO_2. One of the solutions to prevent corrosion developed in the McDevitt lab entails protecting the material with a monolayer coating of alkyl-amine reagents. While previous work has shown that these monolayers hinder the corrosion of cuprate superconductors, the mechanism and energetics of the formation process is poorly understood. The goal of this dissertation is to examine the mechanism and kinetics of formation of self-assembled amine monolayers atop cuprate superconductors.

This dissertation is organized as follows: In Chapter 1, the theory of the materials and thin film deposition processes used in this dissertation are described. The specifics of the methods and materials employed are described Chapter 2. In order to examine these phenomena, a new pulsed laser deposition system capable of generating larger quantities of corrosion free thin film superconductors has been built and optimized as described in Chapter 3. In Chapter 4, experimental evidence for the removal of previously exposed corroded material by the alkyl-amine monolayer reagent has been provided using x-ray photoelectron spectroscopy, atomic absorption spectroscopy, and scanning electron micrography. Evidence of the alkyl-amines role in planarizing the superconductors is also provided. Finally, in Chapter 5, the kinetics of adsorption have been examined using a redox active monolayer reagent, providing the first documentation of adsorption isotherms atop cuprate thin films.

Table of Contents

List of Tables

List of Figures

1 Introduction and Theory

1.1 Overview

Since the early 1980's there has been resurgence in the study of thin films of organic molecules, and their effects on the interface of numerous materials.[1] These thin films, often only the thickness of a single molecule, serve as ideal systems for modeling numerous interfacial effects, and provide the impetus for the development of new analytical techniques and electronic devices. One of the goals of research in the McDevitt group has been to bridge the gap between the interfacial chemistry of high-temperature superconductors (HTSC) and the material stability issues inherent in the copper oxide based superconductors. By overcoming these stability issues, novel devices and improved functionality of high-T_c materials is expected. Since nearly all solid-state chemical transformations happen at interfaces, in the case that of the superconductor and the atmosphere or chemical solution, it has been necessary and useful to develop a set of tools to determine how these interfaces behave from a microscopic level. To provide this control of the interface, self-assembly of amine monolayers atop these superconductors has been developed.[2-8] Previous work has show the enhanced stability of the cuprate materials with monolayer protection, but little is understood about the dynamics of the process and rate of formation of these protective adsorbate layers.

The work contained in this dissertation covers the mechanism and kinetics of monolayer formation of amine reagents atop the common cuprate superconductors for the express purpose of assisting and modifying the interfacial

properties of these superconductors. In this first Chapter, theoretical and relevant background information about the materials and processes involved this research will be described. At the conclusion of this Chapter, a brief outline of the remaining experimental studies, which constitute the backbone of the dissertation, will be described.

1.2 SELF-ASSEMBLY

1.2.1 Introduction

In 1920, Irving Langmuir introduced us to a world different than our own. In his world there were only two dimensions. As he would later write,

> "We live in a world of three dimensions. We measure objects by their length, breadth, and thickness. The position of a point can be described by three coordinates, x, y, and z…Today…I propose to tell you of a real two-dimensional world in which phenomena occur that are analogous to those described in *Flatland*. I plan to tell you about the behavior of molecules and atoms that are held at the surface and solids and liquids."[9]

Langmuir's definition of this two dimensional world, with the assistance of Katherine Blodgett, occurred at the air liquid interface of a trough now referred to as a Langmuir-Blodgett (LB) trough, although originally developed by Agnes Pockels. Langmuir and Blodgett began the first systematic study of amphiphilic monolayers using this tool. It was their work and this device that provided the first reproducible ordered monolayers for study.[1]

The LB trough controls the formation of well-ordered molecular assemblies at the interface of a liquid and a gas. This ordering occurs as a moveable barrier controls the surface area of the film, and thus how tightly molecules that bridge the interface must be to one another. With Modern

adaptation of this instrumentation, this packing is measured with sensitive automated scales that determine the surface pressure and control the precise area of the surface through an automated system.

The close packed assemblies of amphiphiles were then transferred to substrates for study of thickness and other properties of interest. These LB films are still extensively studied today, and LB troughs remain a common method for depositing monolayer films.

More recently, organized monolayer films have been created with the use of certain adsorbate molecules and the appropriate choice of flat substrate materials. The new technique, self-assembly, owes much of its theoretical background to the LB films, but differs in one crucial way. Instead of requiring a complex instrument to create a well-ordered monolayer, the assemblies are created spontaneously through the interactions of the monolayer with the chosen substrate.

The development of self-assembled monolayers (SAMs) has been extensively investigated recently with the gold-thiol system becoming the model structure for investigation.[1] Although other assemblies have been described, including carboxylic acids on aluminum and silver, alcohols and amines atop platinum, and silicon containing reagents on hydroxylated surfaces, the bulk of the studies seem to have been for the adsorption of sulfur reagents on gold surfaces.[1] This prevalence of research atop gold is a result of its noble character, no stable surface oxide in known to exist,[10] so the films can be handled without the need for expensive or difficult inert atmosphere techniques.

Due to the predominance of gold thiol assemblies further discussion in this section will be described in terms of those monolayers.

1.2.2 Theory of Self-Assembly

As mentioned above, self-assembled monolayers can be formed without the need for expensive equipment; the process happens spontaneously due to the favorable energetics of the reaction of the reagent with the surface. For a monolayer to form, three conditions must be satisfied. First, the surfactant must possess an active head group that is capable of chemisorbing to the substrate, Figure 1.1. This chemisorption provides the majority of the exothermic energy minimization, with the formation of polar covalent bonds for thiols atop gold. The energies of this interaction are reported to be >10 kcal/mol.[11-13] The head group is assumed to pin on the surface due to molecule substrate interactions at a specific site although mobility of the molecule across the surface still occurs. This exothermic chemisorption serves to lower the total energy of the system by packing all available sites which leads to the second condition for good monolayer formation, tail group packing.

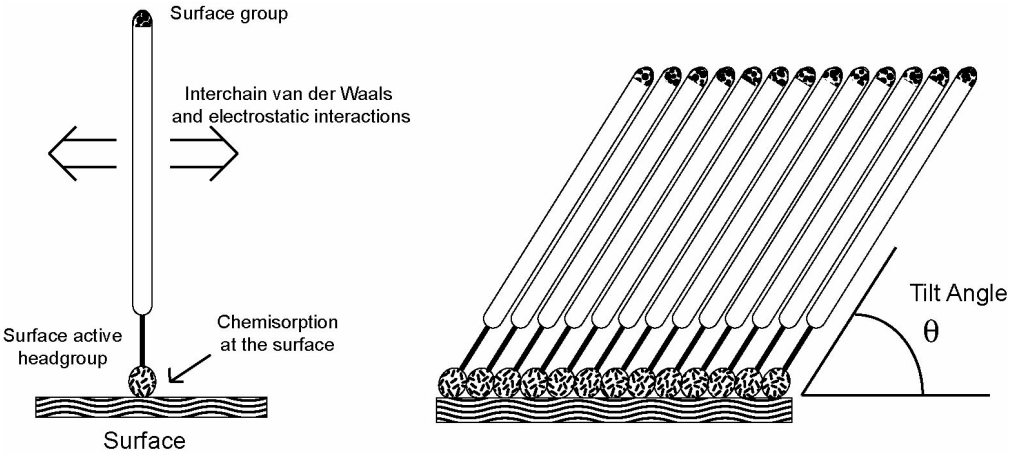

Figure 1.1 A schematic view of the forces and packing of a self-assembled monolayer.

Likewise, the largest degree of ordering becomes possible when the tail groups are able to interact on a short distance. The van der Waals interactions and occasional electrostatic interactions help to hold the monolayer together. For this reason, bulky tail groups sterically hinder the formation of high quality monolayers by restricting the availability of active sites on the substrate and by poorly holding the tail groups together. These tail group interactions (<10 kcal/mol)[1] influence the overall ordering of the SAM. These tail group interactions lead to the tilting of monolayers as seen in Figure 1.1, since by tilting the alkyl chains are closer together minimizing the interatomic energy. Reflection adsorption FTIR measurements of the carbon-hydrogen and carbon-carbon stretching of adsorbed monolayers have shown that a well ordered film shows packing approaching those of the pure crystalline reagent[14,15].

Thirdly, the terminal group of the monolayer plays a role in the order of the monolayer. These end groups are useful for imparting desirable qualities to

the monolayer for purposes of interfacial control, but play a small role energetically. The last few methylene units tend to be disordered with each gauche bond having a value of ~0.7 kcal/mol. These gauche conformations are endothermic in nature, detracting from the overall energy minimization of the monolayer formation.[1]

The above three conditions can be summarized with a few simple rules; Regardless of the head group interactions with the surface, straight chain hydrocarbon tail groups will lead to better packing atop the substrate because of lower steric hindrance. The longer the chain of alkyl groups, the more crystalline the monolayer due to increased tail interaction, with the transition from liquid like to crystalline monolayers occurring with chains of at least 9 carbon units.[16]

1.2.3 Uses of Self-Assembled Monolayers

Self-assembled monolayers provide ideal model surfaces for the study of interfacial phenomena. The ability to create atomically smooth surfaces with films of organic reagents atop them provides the models for the study of wetting, tribology, adhesion and related interfacial effects. By tethering electroactive groups to the exterior or interior of the monolayer, basic chemical and electrochemical theories can be tested.[17]

In the commercial arena, attempts are underway to develop molecular electronics based on monolayer assemblies[18,19]. The inclusion of groups capable of acting as switches opens the possibility of ultra small interactive electronics. Single layers of alkane thiols atop gold have also been used as resists for lithographic patterning of gold substrates leading to the development of “soft”

lithographic processes that do not require expensive lithographic machinery.[20-22] Numerous research groups are developing sensors based on molecular recognition atop monolayer structures.[23-31]

The use of self-assembled monolayers atop high temperature superconductors will be discussed in detail in Chapters 4 and 5 where the mechanism and kinetics of alkylamine adsorption atop cuprate superconductors will be described.

1.3 SUPERCONDUCTIVITY

1.3.1 History and Introduction

At the beginning of the twentieth century, H. K.–Onnes was competing with Dewar to liquefy all the known gases. Helium was the last to be liquefied on July 10, 1908 with the production of 60 ml. The impetus for the liquification of the gases arose from the desire to study the temperature resistance characteristics of common metals, a topic that was debated strongly at the time by the physics community. Since it was known from experimental studies that the purity of the metals affects the overall resistivity of the metals, mercury was selected as an ideal metal to study since it could easily be purified by distillation. In the process of studying the temperature dependence of the resistivity of purified mercury samples, Onnes and co-workers were surprised to find that mercury abruptly looses its electrical resistance at a temperature close to 4.2K. In investigations of the resistivities of the metal, a sleeping research assistant failed to note an anomalous disappearance of resistance upon cooling. Upon heating, the transition from the zero resistance superconducting state to the normal resistivity was

recorded. This discovery of the unexpected superconductivity lead to Onnes being awarded the Nobel Prize in physics in 1913, for "his investigations on the properties of matter at low temperatures which led *inter alia* to the production of liquid helium."[32]

Once superconductivity was discovered, other elements were examined and found to superconduct as well. Eventually, niobium was found to have the highest elemental superconductivity at 9.25K. Research into other compounds and alloys raised the transition temperature (T_c) where the material becomes superconducting by about 3K every decade. The important "normal" superconductors are shown in Figure 1.2.

Research into superconductivity branched out from the metals to alloys in the 1920s and 1930s. Empirical evidence suggested that the materials with an average of 5 to 7 valence electrons were the best superconductors. This empirical basis was established by Matthias and coworkers in the 1950s, and led to the development of many new superconductors. Work in the 1960s using "Matthias's rules" centered around the niobium in a β-Tungsten structure commonly called "A15" with a formula of A_3B. This binary structure and other ternary structures derived from it approached 20 K, but could not break the liquid hydrogen barrier. In 1971, Webb at RCA broke this barrier with a metastable Nb_3Ge compound that retained the record T_c of 23.2 K until 1986. Many researchers in the filed speculated that that the superconductivity transition temperature would be limited to below 30 K.[33]

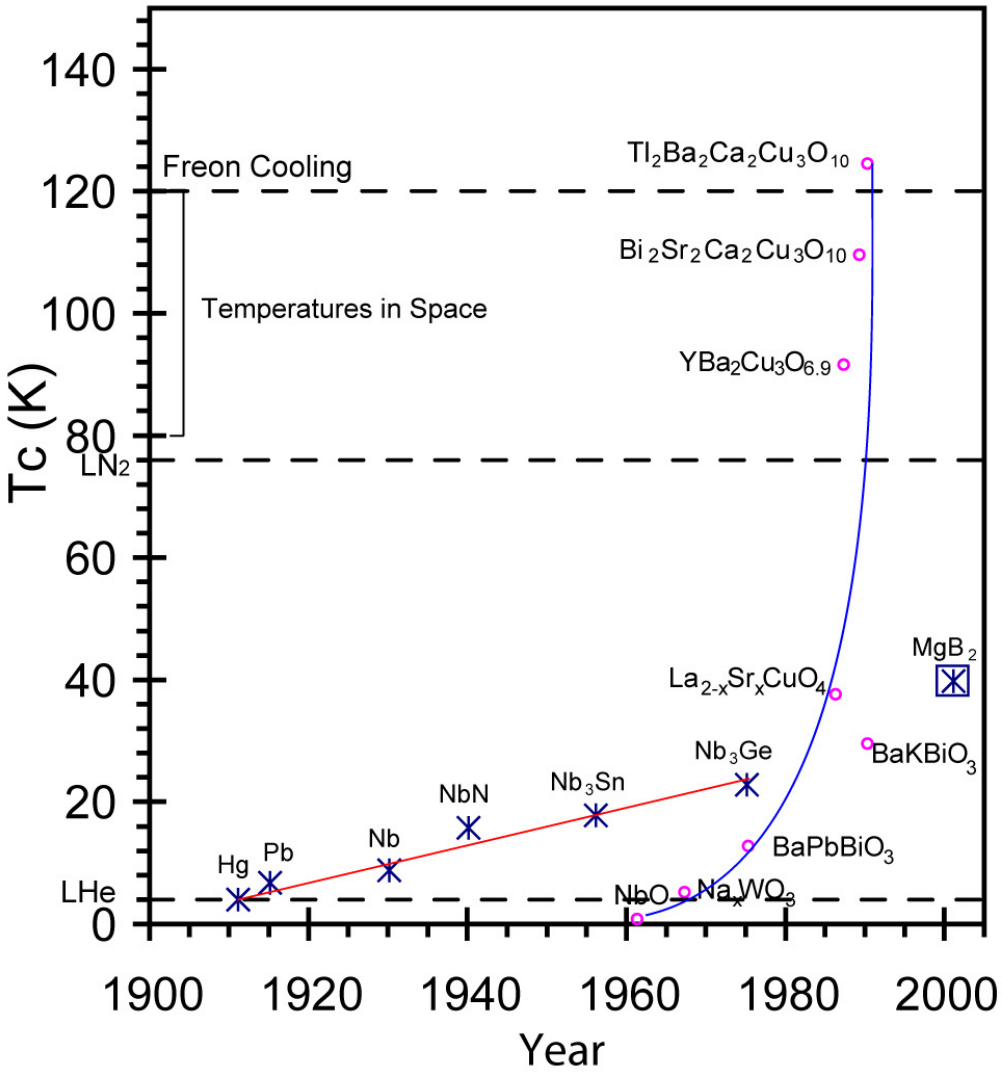

Figure 1.2 Evolution of the transition temperatures of both normal and high temperature superconductors. The so-called normal superconductors are shown on the straight line beginning with Hg in 1911. The high-temperature superconductors are shown on the curved line. The new addition to the superconductor family is MgB_2, discovered in 2001.

Bednorz an Muller shattered expectations and changed the field of superconductivity dramatically with the discovery of $La_{1.83}Ba_{0.15}CuO_4$ in 1986.[34] With this material, a new world record was set with a T_c of 35K. This work followed up on previous work Michel and Raveau who had described the normally insulating metal oxides to have unusual metal-like properties.[35] Bednorz and Müller's discovery caused a massive research effort in complex copper oxides for more materials with higher transition temperatures. The research in these "high-temperature" superconductors rapidly raised the temperature at which superconductivity could exist, with the important 77K mark being passed by M.K. Wu and C.W. Chu with their collaborative development of $YBa_2Cu_3O_{7-\delta}$.[36,37] This material with a transition temperature of 92K was the first to exhibit superconductor properties above the boiling point of liquid nitrogen (77K). Robert Hazen best describes the importance of the liquid nitrogen boiling pointing the following way:

> Seventy-seven Kelvin is like the sound barrier of the four minute mile. It is *the* technological and psychological barrier against which all things cold are gauged. Below 77 K any phenomena, no matter how remarkable, is an esoteric curiosity with few practical uses. But anyone can buy liquid nitrogen. Above 77K there is almost no limitation to the material's applications, because almost anything can be refrigerated easily to that temperature. Paul Chu's team had discovered a material that…could transform superconductivity from an oddity to a day-to-day reality.[38]

In the frenzy of research following the discovery of $YBa_2Cu_3O_{7-\delta}$, numerous other cuprate superconductors were discovered that quickly pushed the record transition temperature above 120K. Maeda and co-workers reported a T_c of 105K in 1988 in the material $BiSrCaCu_2O_{10}$.[39] Shortly after the discovery of

the bismuth superconductors, Sheng and Hermann reported the synthesis of a TlBaCuO system with a transition of ~90K.[40] Within weeks, the same group reported that doping calcium into the superconductor lead to an increased T_c of ~120K. This new system was later found to be two distinct phases, $Tl_2Ba_2CaCu_2O_4$ (2212) and $Tl_2Ba_2Ca_2Cu_2O_{10}$ (2222), both of which become superconducting above 120K.[41] The record of the TlBaCaCuO systems held until the discovery of $HgBa_2Ca_2Cu_2O_{10}$ by Schilling *et. al.* several years later with a 130K T_c which was increased to 150K by the application of pressure by Paul Chu's group.[42,43] This remains the current record for the transition temperature of the copper oxide superconductors, but a new class of superconducting materials based on MgB_2 was discovered in 2001 and is now the focus of intense study.[44,45]

1.3.2 Theory and Properties of Superconductivity

Once superconductivity was verified from an experimental vantage point in 1911, others began to try to develop a model to explain the effect. Prior to an explanation of the lack of resistance, Meissner and Ochsenfeld discovered a new property of superconductors in 1933. They found that once cooled below the critical temperature, superconductors respond to modest external magnetic fields so as to expel them from their interior regions thereby displaying prefect diamagnetism. This expulsion is the true test of all superconductors and has been named the Meissner effect. This effect is the basis for popular demonstration of superconductivity, floating magnets above cooled samples. Following discovery of the Meissner effect, the first phenomenological attempt to explain superconductivity was presented by F. London and H. London. The Londons

postulated a two-fluid model that accurately predicted the Meissner effect and depth of penetration of a magnetic field into a superconductor, the penetration depth, λ. In 1950, Ginzburg and Landau, who would later win a Nobel Prize for his investigations into liquid hydrogen, developed an intuitive macroscopic theory that explained most of the characteristic properties of superconductors. The development of the Ginzburg-Landau theory was followed in 1957 by Abrikosov's discovery that the magnetic field is expelled from the superconductor in two different ways. In the Type I superconductors, the field is expelled completely from the interior of the superconductor, while Type II superconductors expel the field totally at low intensities, and only partially at higher intensities. These Type II, mixed state, materials remain superconductive in higher fields (<10 Tesla) and are of interest for many commercial applications (*vide infra*). While all of these theoretical ideas are important, the most useful explanation for both the diamagnetism and supercurrent were yet to come.

To explain conventional superconductivity from a microscopic perspective, John Bardeen, Leon Cooper, and Robert Schrieffer developed a theory in 1957. Called BCS theory, it derives from quantum mechanics, the pairing of electrons via phonon interactions with the lattice of the material to form Cooper pairs.[46] For their work, they were awarded the Nobel Prize in Physics in 1972.

Cooper pairs are the heart of conventional superconductivity. Following the ideas of Cooper, electrons in a superconductor are weakly attracted to one another. Once this interaction occurs, the electrons will be scattered from one

momentum state to another. Since all the momentum states below the Fermi level, are full the system, the electrons must go to energy level higher than the Fermi level. The Fermi level is the level of maximum occupation in a system. This would lead to an increase in kinetic energy since unfilled orbitals of higher energy are being filled, an inherently unstable system. Cooper then realized that the overall potential energy of the system would decrease by allowing states above the Fermi level to be filled. Beginning with the many electron Schrödinger equation, he reformulated the potential energy, V, for electrons if pairing is allowed to occur. In this formulation, V accounts for the interaction of the electrons through the phonons of the sea of electrons. This potential energy term is assumed to work only in the narrow energy region between 0 and $\hbar\omega_D$, the energy of a phonon in the lattice. Continuing to derive the total energy, he arrived at the following relation:

$$E \approx -2\hbar\omega_D \exp\left(-\frac{2}{V_O D(E_F)}\right) \qquad \text{Eq} \quad 1.1$$

In creating this equation, where V_O is the ground state potential for interaction between electrons and $D(E_F)$ is the density of states at the Fermi levels, Cooper shows that the energy of the pair will always have a lower energy than the ground state. Given the equation above, electrons attracted to one another will always bind without the imposition of a large potential. So in a sea of electrons, pairing of electrons can lead to lower energies when the energy is lower than $\hbar\omega_D$. This can be viewed in a simplistic manner as an electron preparing the lattice by polarizing it, which attracts another electron. The formation of the

Cooper pairs and the contrast to normal electron conduction can be seen in Figure 1.3.

While Cooper's theory works for a two-electron system, Bardeen and Schrieffer helped extend the formalism to a many electron system. In their theory, Bardeen, Cooper and Schrieffer created a set of highly correlated electrons that move in a single coherent motion, similar to a Bose-Einstein (BE) condensate trapped in a lattice. Like a BE condensate, the Cooper pairs drop down in energy into a quantum state where they all have the same properties, thus creating a gap in the density of states of the material, Figure 1.4. While this description is overly simplistic, it does provide a useful basis for understanding the motivation for the formation of Cooper pairs. Further, the diamagnetism of superconductors is explained as the magnetic field inducing a current of Cooper pairs that creates a field equal to the inducing current, but have opposite direction. This cancels out the inducing field, expelling it from the superconductor (Type I) or pinning it in magnetic vortices localized within the material (Type II).

The equations that arose from BCS theory allow a few predictions to be made about superconductors. One essential property is the critical temperature (T_c) of the sample that is related to the energy gap (E_g) that forms as the electrons coalesce into Cooper pairs.

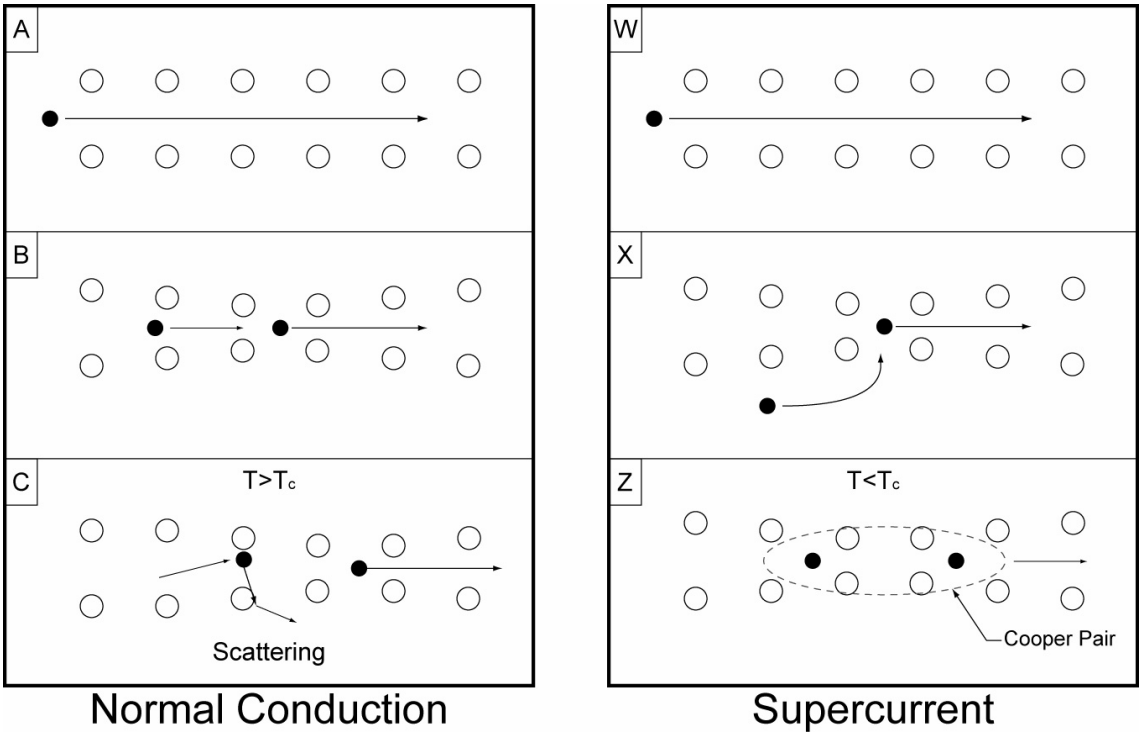

Figure 1.3 Schematic of normal electron conduction and supercurrent. In normal electron conduction, an electron moves as a result of a potential (A) and attracts the lattice towards it (B). Other electrons moving through the lattice would be attracted to this area of higher than normal electric charge, but are scattered as a result of the lattice vibrations (C) that do not allow the attractive forces between the electrons to develop. In a superconductor below T_c the electron moving through the lattice (W) creates the same lattice distortion (X) that attracts another electron. Because of the low temperature and reduced lattice vibrations, the two electrons interact with one another through the lattice vibrations forming a stable Cooper pair (Z) that is resistant to scattering.

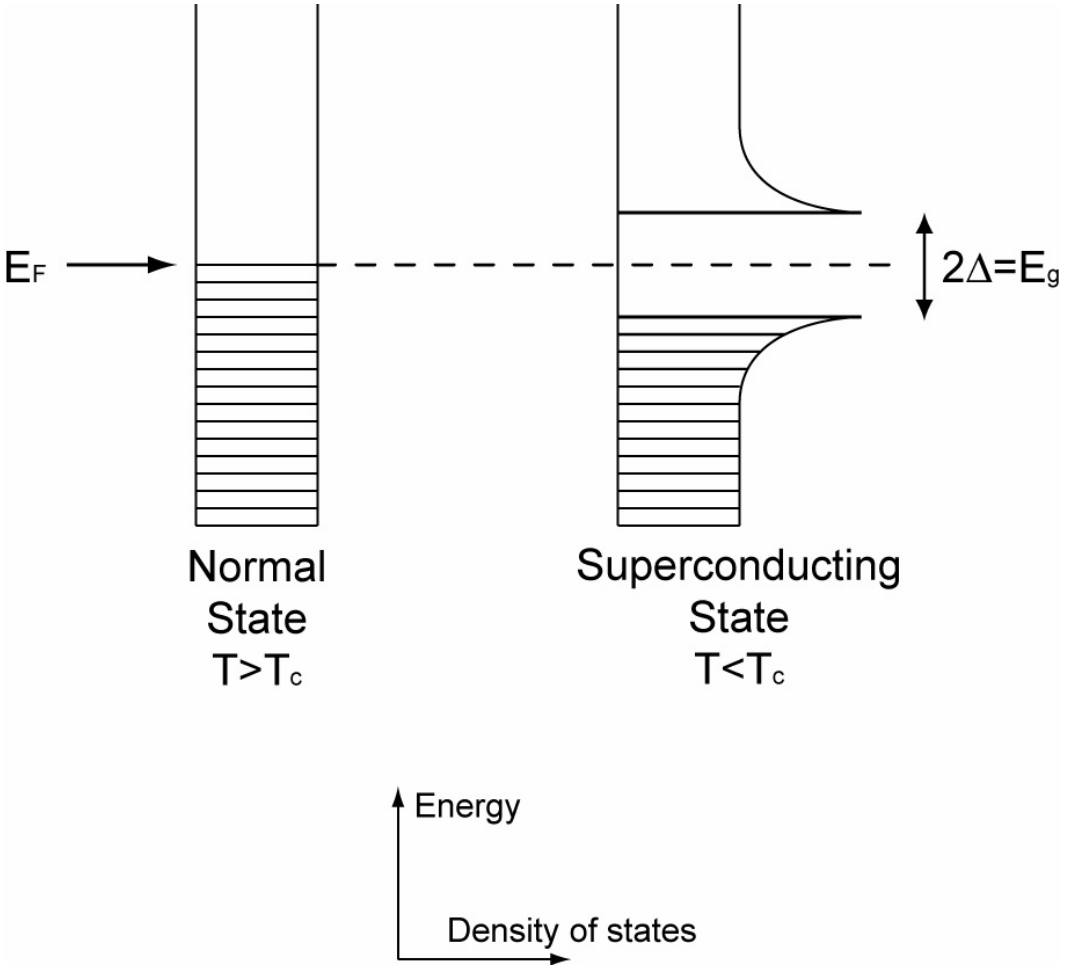

Figure 1.4 Density of state diagrams for a superconductor above and below the transition temperature. When the superconductor is above the transition temperature (A) the material behaves as a normal metal with conduction occurring by electrons thermally activated above the Fermi level (E_F). As the superconductor is cooled below T_c (B), a gap forms at the Fermi level as the electrons form into Cooper pairs, lowering their overall energy.

$$E_g = 3.5 k_B T_c \qquad \text{Eq 1.2}$$

Given the energy of the gap, the transition can be predicted or vise versa. Based on the energetics of the Cooper pairs, the distance over which the electrons can interact and couple, the coherence length of the pair ξ, is determined given $E_g=2\Delta$ and ν_F, the Fermi velocity.

$$\xi = \frac{\hbar \nu_F}{\pi \Delta} \qquad \text{Eq 1.3}$$

The coherence length will be important in discussion of the material properties of the superconductor in the following section.

Another useful predictive device is the relationship between the transition temperature and the Debye temperature of the material. The Debye temperature (Θ_D) is a temperature characteristic of a crystal lattice and can be calculated. Given Θ_D and the electron phonon coupling constant (λ), the transition temperature is given by the following equation.

$$T_c = 1.134 \Theta_D e^{-1/\lambda} \qquad \text{Eq 1.4}$$

This equation has proven useful for predicting the transition temperatures of many of the "normal" superconductors. Without modification, the equation also predicted a maximum T_c of ~30K as mentioned previously.

Because of this limitation, the work of Bednorz and Muller was very exciting to the physics community. The Swiss group had shattered the theoretical limit to transition temperatures and were awarded the Nobel Prize for their work in 1987. While not explaining completely all the subtleties of the superconductivity of the copper oxides, the BCS theory does serve as a basis for the on going search for a better explanation.

Brian Josephson postulated a novel use for superconductors in 1962. He theorized that unusual quantum tunneling effects should happen when a Cooper pair tunnels through an extremely thin layer of an insulator or normal metal. Because the tunneling length decays across the gap created by the insulating material, slight changes in either magnetic fields or temperature at the gap would be disruptive to the supercurrent in the system. For his development of this theory, Josephson was awarded the Nobel Prize in 1973.

1.3.3 High Temperature Superconductors

The development of superconductor theory, and the creation of devices based on Josephson's theory, stimulated research in the field of superconductivity. The high temperature superconductors developed in the 1980's are a direct result of the success of the BCS theory in formalizing the relationship between lattice vibrations and the formation of Cooper pairs. After the discovery of Bednorz and Muller, C.W. Chu was successful in his research, because he recognized that the creation of a rigid lattice would lead to better formation of Cooper pairs.

Considering the class of copper oxide superconducting materials, they have a few qualities in common. First, most are anisotropic layered structures. They consist of alternating layers of copper oxide with other metal layers in between. For example, in $YBa_2Cu_3O_{7-\delta}$, the CuO_2 sheets are separated by the yttrium ion and sandwiched by the BaO sheets, Figure 1.5. Second, these metallic oxides are conductive. Most metal oxides are insulators, but these materials

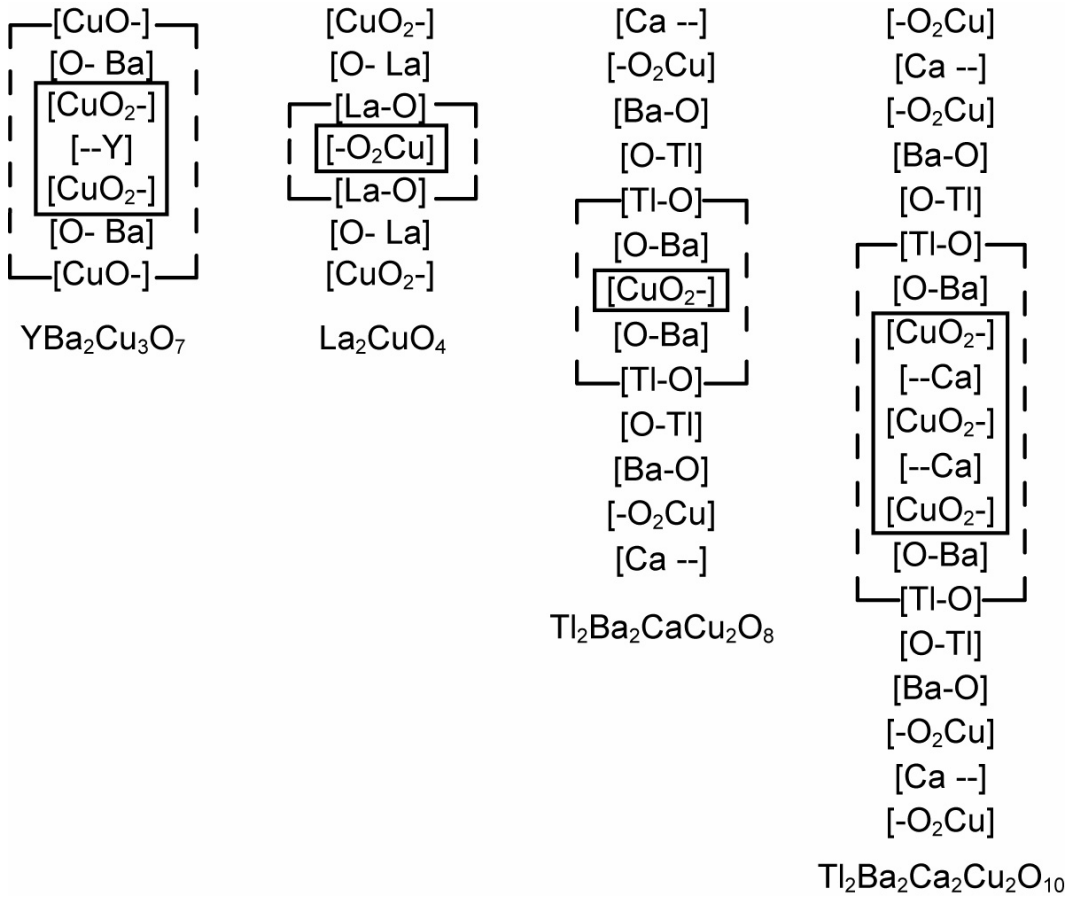

Figure 1.5 Layer structure of a few common copper oxide based superconductors. The dashed lines indicate the unit cell of the material and the box encloses the copper oxide sheets.

transport electrical current primarily along the copper oxide sheets. Conduction still occurs across the sheets, but to a lesser extent. Third, these materials are ceramics, consisting of small grains of material. As a ceramic, they contain numerous voids, imperfections and grain boundaries. Some of these imperfections and grain boundaries will be shown in the later Chapters dealing with the preparation and characterization of thin film and monolayer structures.

Considering the structure of $YBa_2Cu_3O_{7-\delta}$ in finer detail, it is a triple perovskite structure. As shown in Figure 1.6 this structure consists two distinct copper polyhedra. Looking at the structure along the a-axis (100), the four coordinate CuO chains are visible at the top and bottom as are the five coordinate CuO sheets on either side of the yttrium ion. In the copper oxides, the amount of oxygen in the lattice plays a central role in the transport properties and the superconducting transition temperature. Diffraction studies have shown that most oxygen lost form the lattice is removed from the CuO chains. The "doping" of the oxygen affects the superconductivity of the material by changing the oxidation state of the copper in the lattice. More typically, copper ions within solid-state components exist with formal valence values of +1 and +2. In $YBa_2Cu_3O_{7-\delta}$, Cu exhibits an oxidation state of +2.3. This can be thought of as a mix of Cu^{2+} and Cu^{3+} in the lattice. This mixed valent state is key to the conductivity of the material. The differing ionizations allow for mobility of the electrons (or holes) that would not occur for a fully oxygenated sample.[47] Careful control of the oxygen content is critical to the superconductivity of the system and will be addressed in Chapter 3.

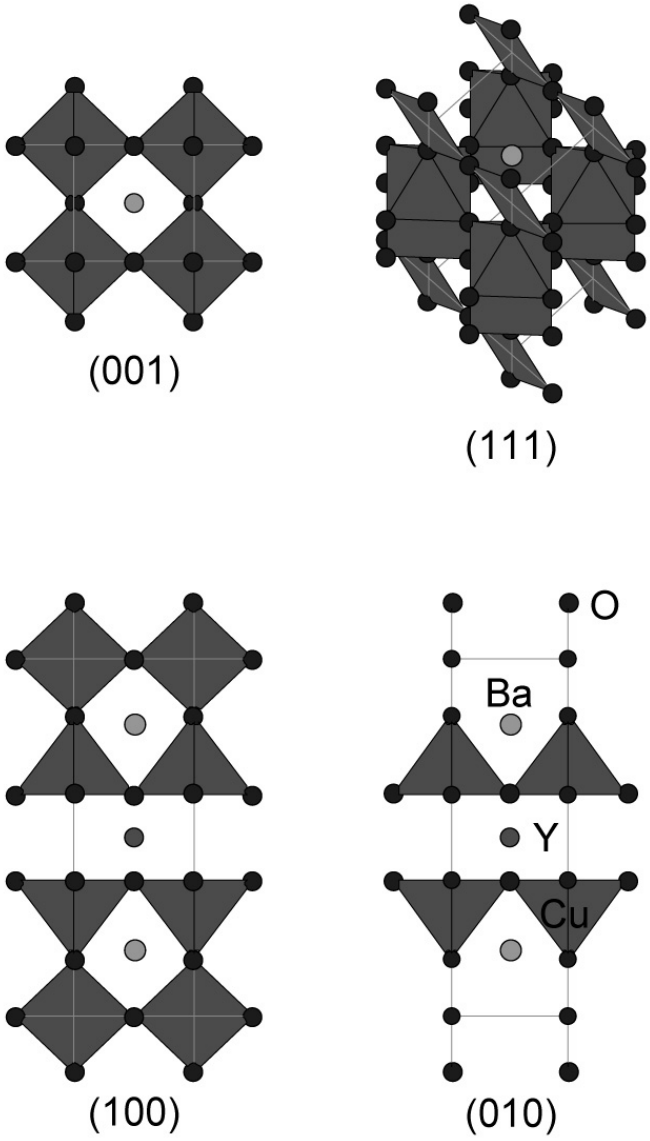

Figure 1.6 Crystalline projections of the $YBa_2Cu_3O_{7-\delta}$ lattice along various crystallographic planes. In these representations, the Cu ions are shown as polyhedra surrounded by oxygen. The square polyhedra visible in the (100) projection are the CuO sheets verifiable by their appearance in the (010) projection. The triangular polyhedra are the CuO sheets where conductivity occurs.

The presence of the Cu^{3+} in $YBa_2Cu_3O_{7-\delta}$ materials affects the stability of the material, and thus limits applications where superconducting materials may be used. The Cu^{3+} is an unusually high oxidation state for copper that normally prefers a +1 or +2 state. This Cu^{3+} has been shown to oxidize gold in order to be reduced to the more common Cu^{2+}. This reduction is a driving force in the corrosion of the complex copper oxide materials (along with lattice strain)[48,49].

The corrosion of superconducting materials is known to occur through the following reaction scheme:[48]

$$2YBa_2Cu_3O_7 + 3H_2O \rightarrow Y_2BaCuO_5 + 5CuO + 3Ba(OH)_2 + \tfrac{1}{2}O_2$$
$$Ba(OH)_2 + CO_2 \rightarrow BaCO_3 + H_2O \qquad \text{Eq 1.5}$$

As a result of these reactions, the $YBa_2Cu_3O_{7-\delta}$ material is converted into insulating phases, which cover the surface of the materials. This corrosion is a serious hindrance to the utilization of high temperature superconductors and will be addressed in the Chapters 4 and 5 where the process of self-assembly atop thin films of superconductors will be described.

One of the methods developed to prevent corrosion does not rely on a organic overlayer. In work performed in the McDevitt lab, new superconductors were engineered to limit the ability of water to penetrate the lattice and relieve lattice strain, thus preventing the corrosion.[49-57] The most promising of these materials was $YBa_2Cu_3O_{7-\delta}$ doped with Ca and La. The formula with $Y_{0.6}La_{0.4}Ba_{1.6}Ca_{0.4}Cu_3O_{7-\delta}$ (TX-YBCO) was found to be 100 times more resistant to corrosion than the $YBa_2Cu_3O_{7-\delta}$. Importantly, the T_c of $Y_{0.6}La_{0.4}Ba_{1.6}Ca_{0.4}Cu_3O_{7-\delta}$ is 80K, three degrees above the boiling point of nitrogen. This material will be

described later in this dissertation along with the regular $YBa_2Cu_3O_{7-\delta}$ in the studies of SAM adsorption because its inherent corrosion resistance protects the surface.

The understanding of the corrosion and surface chemistry of the superconductors is useless if the knowledge is not utilized. The application of cuprate superconductors will be examined briefly in the next section.

1.3.4 Applications

The most common uses of superconductors are for high magnetic field generation and superconducting electronics. Large scale high current applications will be considered first, followed by and examination of useful electronic devices.

Superconductors are already being employed on a large scale in numerous research institutions around the world, or in any other industry where large magnetic fields are required. One of the most common uses is in nuclear magnetic resonance spectroscopy and magnetic resonance imaging. Other uses of high field devices are for motors and generators. The U.S Navy is currently testing superconductive motors for ship and submarine propulsion due to the smaller size requirements of superconducting motors with horsepower comparable to normal electrical motors. Installation of high-T_c copper oxide wire into power grids is being tested as of this writing. Numerous other uses, where power backup and conditioning are important are being developed.[58]

The fields where protection of superconductors against corrosion will have the biggest impact will be in the area of electronic thin film applications. The work of Brian Josephson (*vide supra*) has led to the development of a Josephson junction. This device based on the tunneling of supercurrent through thin layers of

an insulator of normal metal are used as switches and components of Superconducting QUantum Interference Detectors (SQUIDs). As of 1991, single junctions made of Nb had switching times of less than 1 ps.[59] These SQUIDs are pairs of junctions that in the proper configuration are exquisitely sensitive to small changes in magnetic fields. Due to their sensitivity, SQUIDs are being used in ultra-sensitive magnetometers.

Other thin film devices are based on the low impedance of superconducting thin films. Due to their low impedance, thin films of superconductors are being used as passive microwave frequency filters and antenna. They are also used as bolometers to convert visible radiation into voltage signals. Superconductor filter are superior to conventional semiconductor technology in the far infrared and usable across the entire electromagnetic spectrum. The inclusion of high-T_c copper oxide components into other electronic devices is an ongoing research interest as well.

As mentioned previously, all of these thin films suffer from the danger of environmental degradation. The research in this work is focused on understanding the chemistry of self-assembled amines as protective layers for $YBa_2Cu_3O_{7-\delta}$ and related compounds. Once fully developed, the work may aid the implementation of thin films into useful devices.

1.4 ELECTROCHEMICAL INVESTIGATION OF SURFACES

1.4.1 Introduction

The primary focus of this dissertation is placed on the development of an understanding of the interfacial chemistry of adsorbates atop $YBa_2Cu_3O_{7-\delta}$

and related compounds. In addition to high vacuum surface science techniques (*vide infra*), electrochemistry is one of the most sensitive, yet simple, means of probing the surfaces of conductors. The presence of thin corrosion layers atop films prevents the use of the popular atomic resolution technique, scanning tunneling microscopy, but electrochemistry allows the indirect analysis of the surface. The electrochemistry of the high temperature superconductors has been examined previously in the McDevitt lab, and the effects of corrosion on the electrochemical signature of the material are well documented.[60-64] Chapter 5 of this dissertation will focus on using electrochemical methods to determine the ability of amines to clean and protect thin films through measurement of the rates of adsorption.

Before delving into the experimental aspects of the electrochemical investigations, some background discussion is deemed to be appropriate.

1.4.2 Theory

The vast majority of all electrochemical processes happen at interfaces, whether that interface is two solids, a solid and a liquid or even a liquid-liquid layer. Regardless of the system, a few basic ideas apply to process that can occur at the interface. The main processes in interfacial chemistry are shown in Figure 1.7.

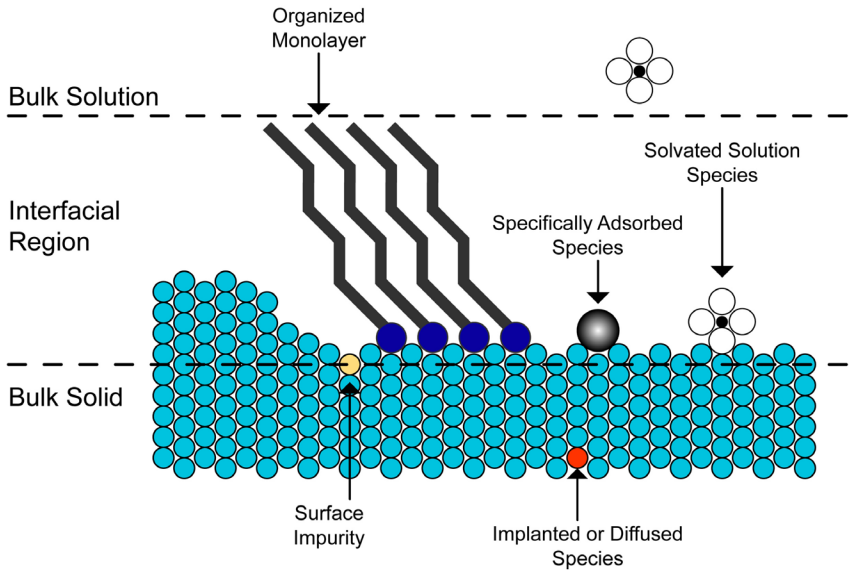

Figure 1.7 Processes that can occur at the liquid solid interface.

For this research we will be interested in the organized monolayers and impurities of the surface. A general discussion of the electrode interface follows.

The interface can be thought of as an intermediate layer between the bulk of the film and the solution. Organization of dissolved species occurs in this layer as defined by Helmholtz.[65] For this model, the solvated solution species (supporting electrolyte) and solvent molecules specifically adsorb to the electrode in what is called the inner Helmholtz plane (IHP) with charge balancing counter ions organizing into a second plane right behind the inner plane. This second plane is known as the outer Helmholtz plane (OHP) and these ions are assumed to be too distant to interact with the electrode. They are non-specifically adsorbed and diffuse into solution as a result of thermal motion. Any excess charge in the electrode is thought to reside in this region between the OHP and the surface.

While this layer interacts as a capacitor would, further independent development of theory by Gouy and Chapman fit experimental results better.

Gouy and Chapman derived a potential dependant, statistical distribution of ions in solution from statistical mechanics. They assume that the distribution follows Boltzman statistics and that ions are point charges. Unfortunately, their models failed in concentrated solutions. Stern developed a model in 1924 that is a mix of the Helmholtz model and the Gouy-Chapman diffusion model. In this model the portion of the charge on the electrode is restricted to the IHP or compact layer, and the remainder is distributed according to Gouy-Chapman in the diffuse double layer. By treating the two charges as capacitances, the sum of the two accounts for either high concentration, modeled well by Helmholtz or low concentration modeled by Gouy-Chapman. Unfortunately, both Stern and Gouy-Chapman characterize the potential distribution of ions based on the valence of the ions. This was found to be experimentally incorrect. Grahame proposed a solution to this where hydrated ions in solution can shed their water shell at the surface of the electrode and approach closer than previously predicted. The differing abilities of ions to de-solvate, accounted for the observed experimental errors. His theory also creates yet another layer, this one the inner plane of closest approach, which is actually identical to the IHP. The OHP becomes the plane of closest approach for solvated ions, and the rest of solution the diffuse layer.[65]

Having described the distribution of ions in solution, the response to electrochemical processes is now defined. Often the expected potential of a reaction as derived from thermodynamics is not measured experimentally. The

reason for this overpotential (excess potential required to drive the reaction) is the nature of the process that occurs at the electrode. Some of the processes that can cause overpotentials are shown in Figure 1.8

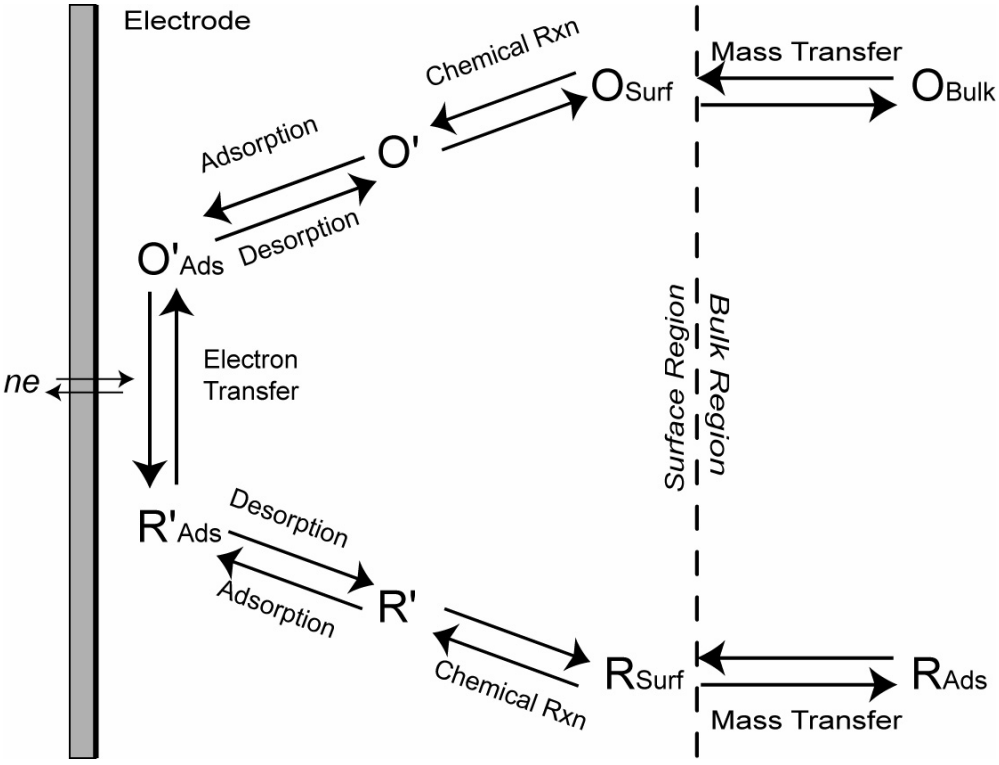

Figure 1.8 Processes at the electrode surface. (Adapted from [65]).

Summarizing the possible routes of a reaction at the electrode, the rate of electron transfer is governed by the rates of four processes:[65]

1) Mass transfer of the species to the surface region.
2) Electron transfer at the surface of the electrode.
3) Chemical reactions prior to or after the electron transfer.
4) Adsorption, desorption or crystallization.

As expected, the rate constants for some of these processes are potential dependant.

Bearing in mind the above processes and structure of the electrochemical interface, the characteristics of the current response to applied potential will be described. The main electrochemical technique used in this dissertation work is cyclic voltammetry. In a standard three-electrode cell, a potential is varied linearly with time between two desired potentials. Upon reaching either end potential, the direction of the potential sweep is reversed. The current is measured between the working electrode, where the desired measurement is taking place, and a large area counter (auxiliary) electrode. While this current flow is established, a reference electrode is positioned in between the working and counter electrode to measure the potential resulting from the electrode processes at the working electrode.

Examination of the magnitude of the current traces and areas of the peaks that arise as species are oxidized or reduced reveals both qualitative and quantitative information about the electroactive species. The peak current can be related to the concentration of dissolved or adsorbed species and are system dependant. The actual quantitative equations used for the examination of the

adsorbed monolayer species atop cuprate superconductors will be developed in Chapter 5.

1.5 ADSORPTION ISOTHERMS

The energetics and kinetics of the monolayer formation studied in this dissertation were derived from adsorption isotherms, and thus require an introduction to the theory of the basic adsorption isotherms used here.

The adsorption of various reagents atop surfaces has been a subject of great interest since before the turn of the 20th century. The first systematic experiments to determine the conditions of this interfacial chemistry were performed by Irving Langmuir. He developed one of the first successful models to approximate the interactions occurring upon surfaces. With theses words, "The plane faces of a crystal must consist of atoms forming a regular plane lattice structure … When molecules of gas are adsorbed by such a surface these molecules take up definite positions with respect to the surface lattice and thus tend to form a new lattice above the old[66]" Irving Langmuir began an exposition of his theory of adsorption of gases to flat surfaces. This adsorption isotherm applies also to liquid interfaces and will be derived briefly[66]. When the gas is in equilibrium with the surface the rate of condensation ($\alpha\theta\mu$) is equal to the rate of evaporation ($\nu_1\theta_1$), where α is the rate of adsorption, θ is the fractional surface coverage, μ is the number of moles arriving at the surface every second, and ν_1 is the rate of desorption. Thus given:

$$\alpha\theta\mu = \upsilon_1\theta_1 \qquad \text{Eq 1.6}$$

and assuming only a monolayer forms, number of sites covered and the number of sites of evaporation equal the total number of normalized sites,

$$\theta + \theta_1 = 1 \qquad \text{Eq 1.7}$$

Substitution and rearrangement gives,

$$\theta_1 = \frac{\alpha\mu}{\nu_1 + \alpha\mu} \qquad \text{Eq 1.8}$$

Substituting $\sigma_1=\alpha/\nu_1$, where $\sigma_1$is the "relative life" of an adsorbed atom or the observed rate, the final form becomes:

$$\theta_1 = \frac{\sigma_1\mu}{1 + \sigma_1\mu} \qquad \text{Eq 1.9}$$

If η is the gram density of molecules adsorbed per unit area, and N_0 is the number of active sites for adsorption, the following relationship can be derived.

$$\frac{N_a}{N_0}\eta = \theta_1 = \frac{\sigma_1\mu}{1 + \sigma_1\mu} \qquad \text{Eq 1.10}$$

Langmuir proceeds to derive the "average life" of the atom on the surface, τ,

$$\tau = \frac{N_0\alpha}{N_a\nu_1} = \frac{N_0\sigma_1}{N_a} \qquad \text{Eq 1.11}$$

by saying that the average life of the atoms condensed on the surface is equal to the first term, while the average of all the atoms is equal to the last term. Substituting τ into $\theta_1 = \frac{\sigma_1\mu}{1 + \sigma_1\mu}$ Eq 1.9, the following is derived,

$$\eta = \frac{\tau\mu}{1 + \sigma_1\mu} \qquad \text{Eq 1.12}$$

.

At low pressures (concentration), the relative lifetime of atoms on the surface approaches zero and $\eta = \tau\mu$. At higher pressure, the relative lifetime becomes large and a saturation value η_∞ can be determined.

$$\eta_\infty = \frac{\tau}{\sigma_1} = \frac{N_0}{N_a} \qquad \text{Eq 1.13}$$

While the amount of coverage is important, the kinetics of the adsorption is also important. Langmuir used an analogous derivation to show that the rate of adsorption is given by the following:

$$\frac{N_0}{N_a}\frac{d\theta'}{dt} = \alpha\mu - (\nu_1 + \alpha\mu)\theta' \qquad \text{Eq 1.14}$$

where θ′ is the instantaneous coverage. Integrating for time gives,

$$t = \frac{N_0}{N_a \nu_1 (1 + \sigma_1 \mu)} \ln \frac{\theta'}{\theta_1 - \theta'} \qquad \text{Eq 1.15}$$

Converting to the more commonly used notation in use today gives the following equation:

$$\theta(t) = \frac{C}{C + (k_d / k_a)} \left[1 - e^{-(k_a C + k_d)t}\right] \qquad \text{Eq 1.16}$$

more commonly shown below after substituting $k_{obs} = k_a C + k_d$ and $K' = C/(C + (k_d/k_a))$:

$$\theta(t) = K'\left[1 - e^{-k_{obs} t}\right] \qquad \text{Eq 1.17}$$

where C is concentration, k_{obs} is the observed rate, and k_a and k_d refer to the rates of adsorption and desorption, respectively.[67] See Figure 1.9 for example isotherms of a 1 M solution at different k_{obs}.

$$R(NH_2) + M \underset{k_d}{\overset{k_a}{\leftrightarrow}} R(H_2N)M$$

This equation can then be fit to empirically measured data, as Blanchard has done with his QCM experiments, to determine the k_{obs} of the system. Knowing the

Figure 1.9 Theoretical Langmuir adsorption isotherms. The effect of various adsorption rates can be seen for a 1M solution.

concentration. By changing concentrations of the adsorbant, and plotting k_{obs} vs. C for a system, the linear plot gives a slope of k_a and an intercept of k_d.

There are a few caveats to using the Langmuir isotherms however. Single monolayer coverage is assumed[68]. Only one type of adsorption site exists and the adsorption to a site is independent of the coverage of nearby sites. While the prior experiments in the McDevitt lab using the same deposition methods have determined single monolayer coverage, the possibility of only one type of adsorption site is difficult given the roughness of the films. The independence of adsorption to a site remains to be determined.

1.6 METHODS OF SUPERCONDUCTOR THIN FILM DEPOSITION

The majority of this dissertation work is performed on thin films of superconductors. In order to better understand the deposition chamber developed and optimized in chapter 3, the methods growth of high temperature superconductors with be discussed below.

1.6.1 Introduction

Devices manufactured from thin film superconductors play an important role in today's technological advancement. The thin films are used in superconducting quantum interference detectors (SQUIDs), microwave frequency filters, bolometers, and high-speed communication circuits. While these devices make inroads into everyday use, many research problems still exist. The stability and sample to sample variability of the high temperature superconductors are

problematic at best. Efforts are under way to both modify the structure of the superconductors and develop protective coatings for these materials. The rapidly formed passivation layer of corrosion products inhibits any research involving the interface of these thin films.

Since the majority of the work in this dissertation occurred on thin films of superconductors, the methods of deposition, and the intricacies of the chosen method will be explored next. The information will be useful for understanding the processes that occur and affect the quality of the thin films used in Chapters 4 and 5 as related to the adsorption of monolayers atop cuprate superconductors. The processes of developing a specialized deposition chamber are also intricately tied to an understanding of the deposition parameters and will be described in Chapter 3.

1.6.2 Overview of Techniques for Thin Film Superconductor Deposition

Many techniques have been developed for the creation of thin film superconductors. Methods of deposition currently used include molecular beam epitaxy (MBE), sputtering, chemical vapor deposition, and pulsed laser deposition (PLD). The first three methods will be described briefly, with a more detailed description of PLD as used for this work following.

1.6.2.1 Molecular beam epitaxy of superconductors

The evaporation of materials at high temperature and reduced pressure is one of the simplest methods for the formation of thin films of metals, dielectrics, and other non-refractory materials when compared to other methods of

deposition. A single pellet may be used as a source, but due to a lack of control of the deposition rate atomic deficiencies result. Use of multiple single element sources and precise control of the deposition of each species allows better control. Deposition rate are anywhere between 0.1 and 1 nm/s. Another layer of sophistication can be added however to achieve atomic layer control of the deposition.

The precision control is achieved using molecular beam epitaxy. In this method each atomic layer is deposited shuttered single source crucibles. A flux gauge stationed behind the substrate measures the rate of deposition and can be used to control the shutters. The heated substrate is usually mounted so it can be rotated towards each crucible in turn to achieve the complex multilayered structures. For the high temperature superconductors that require lattice oxygen, oxygen plasma is created from the bleed valve and high temperature of the evaporated materials. This oxygenation allows *in situ* growth without any need for post deposition processing. Reflection high-energy electron diffraction (RHEED) concurrently monitors the atomic structure of the deposition. The high level of control inherent in this method has allowed the creation of very strained, pure, or unusual structures that can be manufactured only using MBE. This precision control comes at a cost, however, the deposition rates can be very slow and ultra high vacuum is required. These two conditions lead to a slow throughput and expensive equipment costs.

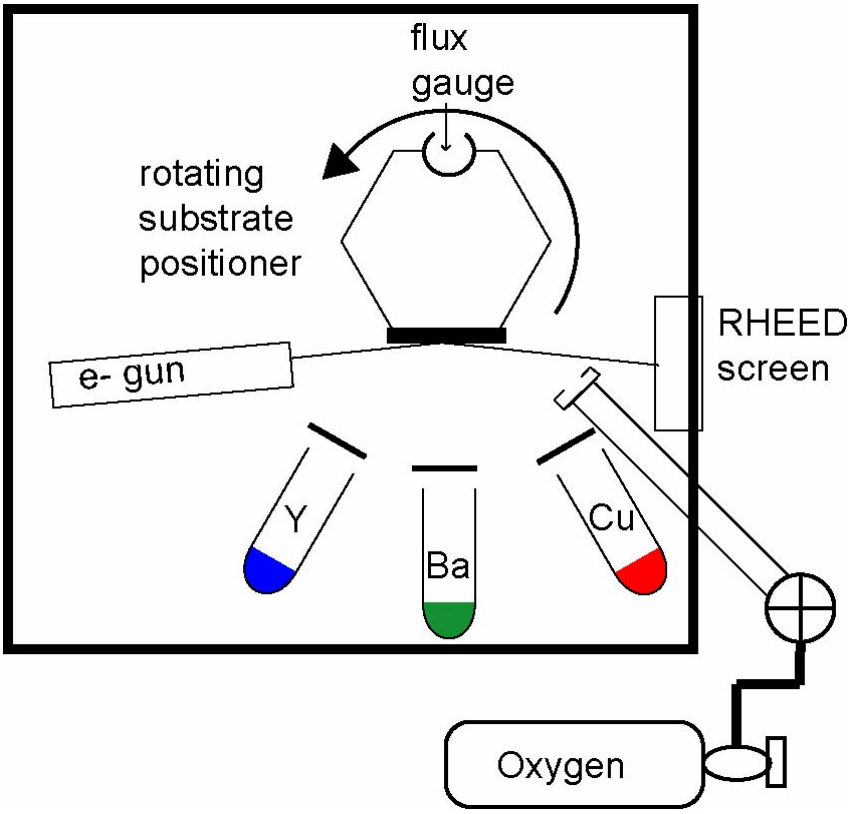

Figure 1.10 Schematic of an MBE system for $YBa_2Cu_3O_{7-\delta}$

In addition to thermal evaporation, electron beams commonly are used to evaporate the target materials. The ultra high vacuum requirements (~10^{-7} torr) of e-beam evaporation preclude the use of an oxygen bleed, preventing the *in situ* processing of materials.[69,70]

Sputtering

In sputtering depositions, higher pressures are used than in e-beam or thermal evaporation, usually with a partial pressure of argon between 1mtorr and a few hundred torr. This argon gas is excited by a radio frequency excitation or a

direct current discharge with a resulting energy of 5 kV. This excitation forms an argon plasma that are accelerated towards the target material, blasting the components from the surface to be collected on the substrate (Figure 1.11). Both single and multiple targets may be used. On axis sputtering, where the target and substrate are perpendicular to one another, leads to deposition rates near 0.1 nm/s. Unfortunately, the deposited film is subject to bombardment by the plasma resulting in removal of oxygen and redeposition of the heavier species. This changes the films composition and is a serious limitation of sputtering complex copper oxide superconductors.

To prevent damage to the deposited films, off axis techniques are used. In this set-up, the substrates are 90° to the plasma and outside of the area of the plasma. This geometry leads to a slower deposition rate, typically 0.3 nm/s, but avoids the resputtering effects.

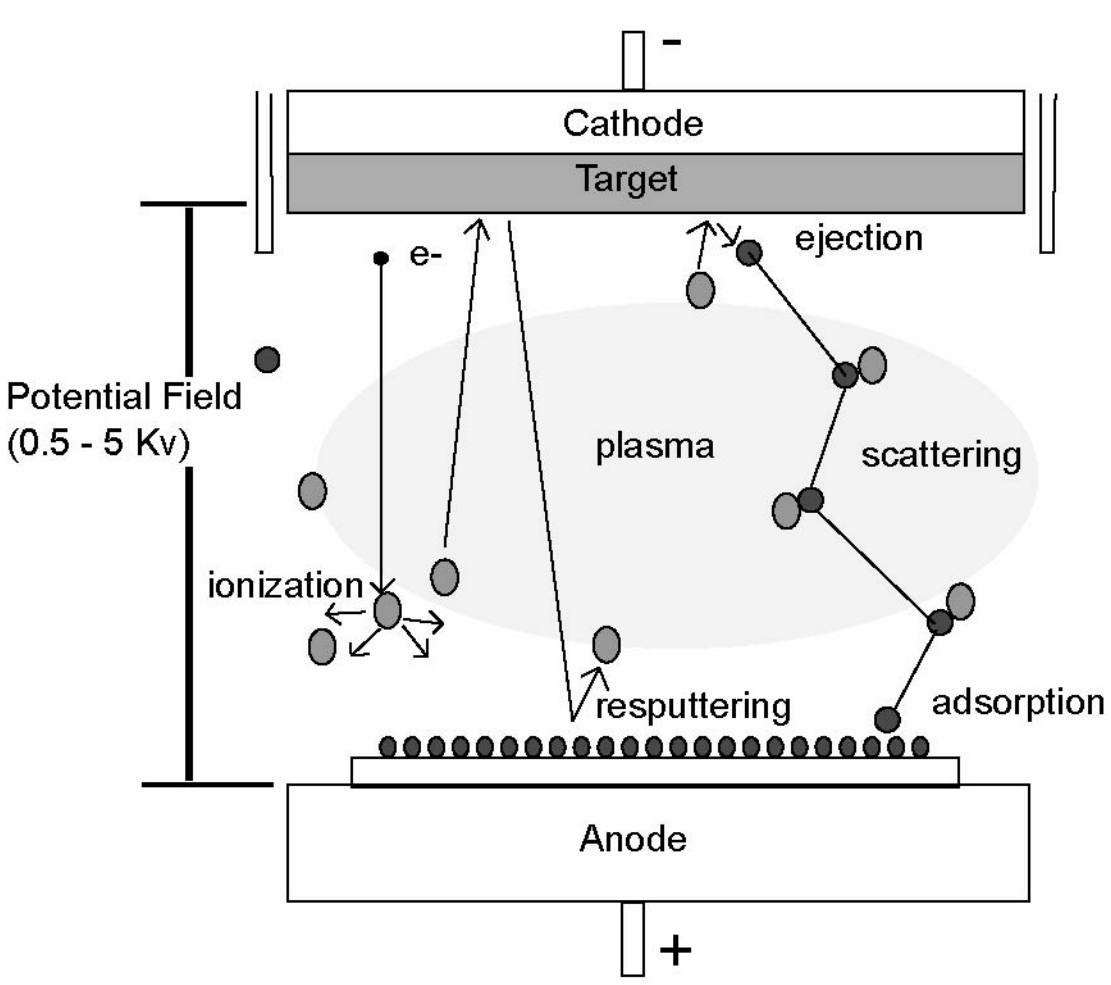

Figure 1.11 Illustration of sputtering mechanism and related processes

Magnetron sputtering can also be used to minimize resputtering effect. Here a strong magnet is used to confine or deflect the plasma. A balanced magnetron uses a permanent magnet surrounding the target to attract the plasma back towards the target, allowing only weak plasma to interact with the film. An unbalanced magnetron uses only a small magnet centered behind the target to prevent the plasma from impacting the target.[69,70]

1.6.2.2 Chemical vapor deposition

While the other cuprate film preparation techniques described are limited by high vacuum requirements, small deposition areas, and slow deposition rates, chemical vapor deposition (CVD) and metal organic chemical vapor deposition (MOCVD) avoid all these limitations. With these techniques, a volatile source of the desired metal precursors passes into a reaction chamber under an oxygen/inert gas flow. Once in the chamber, the species either deposit or thermally decompose on the heated substrate to produce epitaxial films. For successful depositions the precursor must have a) a suitably high vapor pressure for transport, b) chemical and volatile stability at the operating temperatures, and c) stability for long-term storage. These requirements can be viewed as the main limitations of CVD and MOCVD. Suitable precursors are few and far between. Many of the metals are deposited using 2,2,6,6-tetra-methyl-3,5-heptandionates (thd). Barium deposition still remains a problem due to the lack of suitable precursors. Residual carbon contamination is another inevitable serious limitation, leading to defects and film degradation.[69,70]

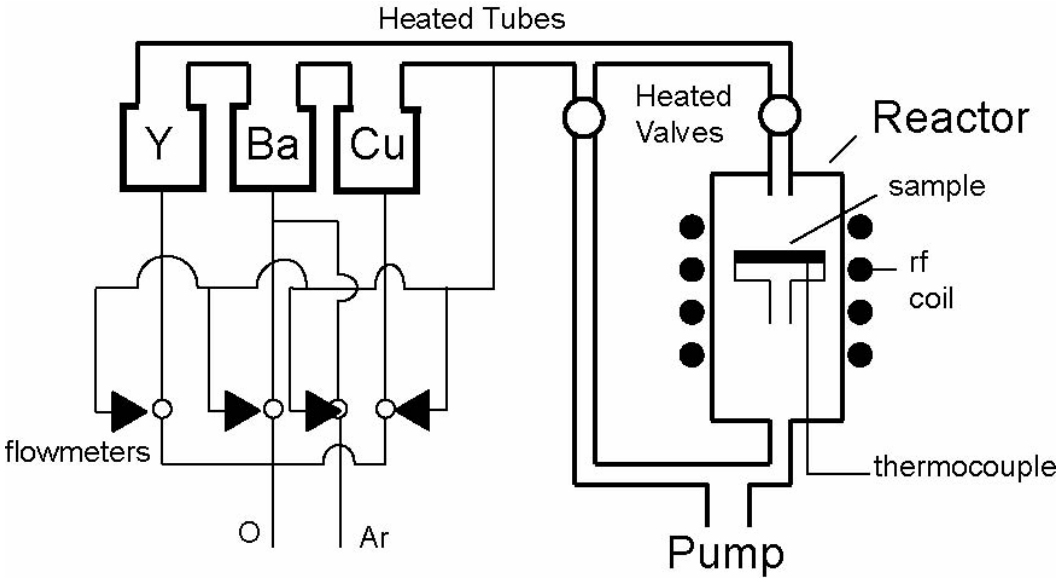

Figure 1.12 MOCVD apparatus

1.6.2.3 Pulsed laser deposition

While MBE and sputtering are well established in the semiconductor production industry, PLD is arguably one of the best methods for deposition of high quality thin films of high temperature superconductors. The method of PLD lacks the developmental time and focus that have been applied to other deposition methods, and has only been emphasized since the successful growth of high temperature superconducting films in 1987. "The pioneering work led by Venkatesan (then located at) Bellcore convinced those people who were previously skeptical about this technique and opened the flood gate that led to numerous studies".[71,72] Since the high temperature superconductor work, PLD research has been expanded to include semiconductors and other technologically relevant multilayer devices. To date, wide band gap semiconductors, optically clear conductors, plastics, bioceramics, tribological coatings, and optical modulating materials have been successfully deposited using PLD.

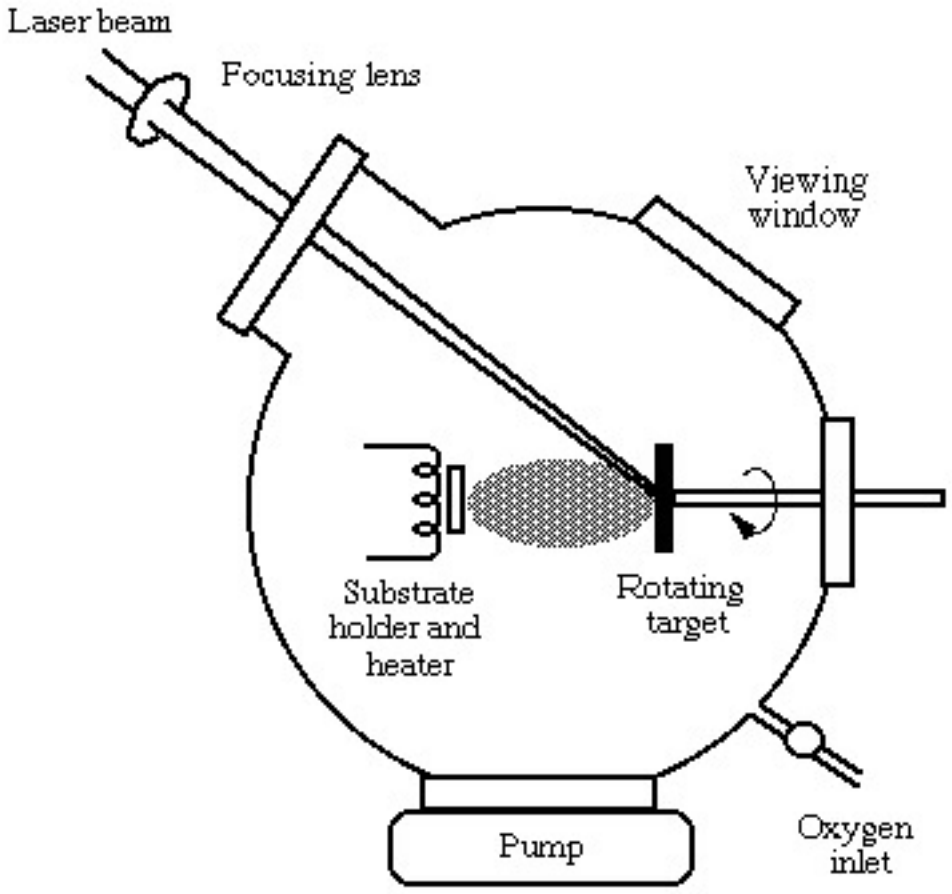

Figure 1.13 Schematic of a pulsed laser deposition chamber

The PLD method is unique because of a number of intrinsic advantages over conventional deposition processes. Primarily, the main benefits of PLD stem from the source of energy used to dislodge the atoms from the target surface. In other techniques, ions and electrons must be controlled and manipulated to achieve the desired morphology and composition of films. In PLD, the primary control is the ultraviolet (UV) laser pulse that deposits the energy for evaporation

into the target. This laser beam is frequently easier to manipulate, and given the correct wavelength, interactions with the gas-phase species are negligible. The dynamic range of the deposition process is also quite varied. The ubiquitous coupling of the laser pulse to most materials below the 250 nm wavelength allows almost any material to be ablated. The decoupling of the laser target interaction from other deposition conditions also increases the versatility. The most important advantage is the ability of PLD to deposit materials with very complex stoichiometries from a single target. As Venkatesan states, "The process is so different in many ways from conventional deposition processes that is will be many years before all the unique features of PLD are fully realized and utilized[73]."

Although PLD is a very versatile technique, there are still issues to be addressed using this technique. One issue is cost of the system. The lasers used previously were very expensive to purchase and maintain, but the prices are coming down for the hardware as durability is improving. The laser may also be spread over multiple deposition systems, in effect lowering the cost of the system. The McDevitt laboratory currently has two deposition chambers that use a single KrF (λ=248 nm) excimer laser. Experimental studies using these facilities will be described further in chapter 3.

One of the major limitations of PLD is the small deposition area, limited by the size of the plume of evaporated material. For large surface area films or wires, the target and/or beam are rastered to provide better coverage over large areas. Diameters of over 3 inches are now common as are tapes limited in length

only by the size of the spools. There are numerous ways to circumvent this limited area problem and our solution will be discussed in a coming section.

The other major limitation inherent in PLD is the creation of particulates that may be incorporated into the film. Since PLD is a forward directed process similar to a spray application of a coating, any material evaporated or ejected from the target has a probability of landing on the substrate. Droplets are frequently encountered as a result of the laser melting the target. The collision of evaporated species with the background gas can also lead to formation of particulates in the gas phase. Most notably for high temperature superconductors, the oxides of the main components have all been detected as crystallites on the surface of films using electron micrographs. Various methods of mechanically preventing the deposition of particles have been explored, but perhaps the easiest method of controlling particulate formation is careful regulation of the laser target interaction. Likewise, a more detailed discussion of the control of laser target interactions will follow.

Another limitation of the PLD process is also the deposition rate. While deposition rates of nanometers per second rates are possible, the best lattices are formed at lower deposition rates equivalent to 1Å/s. The creation of highly oriented cuprate films with good film morphological characteristics is an important goal of this dissertation. Consequently, the details of the rate control will be discussed in detail later.

1.6.3 Theory of the PLD Deposition of High Temperature Superconductors

Deposition of thin films has been compared to people entering a theater. In CVD, the people enter through a door and find their seats a few at a time. However, in an analogous sense with PLD, everyone is dropped from the ceiling all at once.[74] In order for everyone to be able to find a seat (next to their friends in the case of complex copper oxide superconductors) requires very precise control of the condition of the deposition. For this control to be achieved, the factors that affect the growth during pulsed laser deposition must be understood. The interaction of lasers with materials, the chemical processes occurring in the plume of ejected material, and the growth mechanisms of thin films will be described briefly.

1.6.3.1 Interaction of Lasers with the Target Surface [75]

The primary benefit of pulse laser deposition is the ability of lasers to interact with almost all materials. As stated earlier, lasers of the appropriate wavelength will interact with almost all materials if the wavelength is sufficiently short. This interaction is a result of the electrons absorbing the energy of the incident photon resulting in either ejection from the atom or heating. The four primary mechanisms of interaction and ablation of the target materials will be investigated.

Research in mechanisms of material from a target, or sputtering, has mainly been conducted using electrons and ions, but the results are shown to correlate with those of laser-solid interactions. In this sense, the ablation process

is analogous to sputtering and will be referred to as such in the discussions on mechanim of material ablation The primary ablation mechanisms are electronic, collisional, thermal, exfoliational, and hydrodynamic.

Electronic ablation, commonly described a group of related processes involving excitation or ionization, is one of the main methods of forming the ejected plume of target material. At high laser pulse energies, a rapid energy deposition model has been proposed. The pulse leads to dense electron excitation, with number densities exceeding 10^{22} cm^{-3}. These excited electrons increase the energy of each atom as given with the following expression:

$$E_{increase} = \frac{n_e \times E_{gap}}{n_c} \qquad \text{Eq} \quad 1.18$$

where n_e and n_c are the number densities of electrons, excited and condensed respectively. E_{gap} is the band gap of the material. This increase in total energy of the atoms increases the vapor pressure of the material by orders of magnitude. The increased vapor pressure, the primary reason for ablation, is responsible for the explosive propulsion of the ejecta to temperatures in excess of 10,000 K. A low energy mechanism alternatively proposes the creation of trapped excitons and decay products that may occur near the surface. These defects lead to the energetic ejection of individual atoms. Regardless of the mechanism, Kelly [75]has proposed five key features of electronic sputtering: (1) existence of an energy density threshold for particle emission; (2) kinetic energies of order of a few eV; (3) low internal energy due to the inability to establish an equilibrium during the short laser pulse; (4) a high degree of directionality resulting from the close

packing of the starting material; (5) a non thermodynamic yield of molecules and ions.

In PLD, the laser pulse is not directly involved in collisional sputtering, the momentum impact between solids, due to the comparatively low momentum of a photon The resulting plasma from the other processes does create conditions where indirect collisions with the surface can occur. "It has been shown that if a plasma forms for any reason during laser–surface interactions in vacuum or air, then an explicit laser plasma interaction begins[75]." Ions created in the plasma are accelerated by the electric field of the photons to as much as 100 eV resulting in bombardment of surfaces nearby.

Thermal sputtering, the vaporization of material due to increased temperature, occurs due to localized heating of the material, but its quantification is difficult. The thermal sputtering requires heating of the target above its critical temperature, which has not been conclusively observed. The best evidence is the presence of a frozen wavelike surface structure often missing in electron micrographs of target materials. Isolated surface temperature measurements of irradiation show insufficient heating to boil the material from the surface, in this case Al_2O_3.[76,77] Alternative methods of thermal effects have been developed and will be explained shortly.

While electronic sputtering is desirable and collisional and thermal sputtering are beneficial, both exfoliational and hydrodynamic sputtering may hinder quality film formation. Exfoliational sputtering is when the target material flakes off as a result of thermal shocks. Exfoliation occurs most frequently in

materials, such as $YBa_2Cu_3O_{7-\delta}$, with high melting temperatures that resist deformation due to stress and strain. Flaking is postulated to occur as a result of the high thermal expansion of the material without subsequent melting. This repeated cycling finally leads to localized failure of the target. Hydrodynamic sputtering is the formation of melted droplets formed and emitted from the surface as a result of transient melting. If the material has a relatively low melting point, each pulse can form a melt layer that accelerates the away from the target due to the turbulence created by the volume change upon melting and expansion of the liquid. Both exfoliation and droplet formation result in inconsistencies in the target that may be imaged using electron micrographs. These droplets and flakes also interact in the plume with other ejected material to form droplets on the surface of the deposited film.

These laser-target interactions hint at the necessary optimization of the laser fluence to minimize droplet formation and yet still achieve optimum stoichiometries of the films. Thusly, the control of laser energy, the spot size and resulting energy density are of vast importance in depositing good quality films.

1.6.3.2 Laser Induced Target Modification

The pre–treatment of target materials is important to the production of quality thin films. After the initial pulse and emission of material, the target is still undergoing changes that over time will affect the composition of multicomponent film. The electronic excitation that leads to sputtering also leads to a localized heating of the material. This heating forms a melt front that propagates into the target inducing changes in the material. This melt front leads

to the aforementioned exfoliation and hydrodynamic sputtering. At low photon fluence levels, those that occur at the edges of the laser spot, cones of material form that often differ in composition from the bulk material. The incongruity of these cones is a result of the differential sputtering and hydrodynamic effects, resulting in the formation of a vaporization resistant layer shell. The differential sputtering is a result of the repeated short thermal cycles. After each melt formation, the higher melting point components will freeze first driving still molten materials towards the surface. In the case of $YBa_2Cu_3O_{7-\delta}$, Yttria (Y_2O_3) and Y_2BaCuO_5 solidify first driving the copper and barium towards the surface. These Cu and Ba compounds evaporate more quickly, leaving behind a Y_20_3 shell. This shell is more transparent to the UV laser pulse, leading to an increased interaction depth.[78]

These surface modifications require a pretreatment step in any deposition. A steady state develops after repeated pulses since the Cu material must diffuse through the overarching yttria. This diffusion leads to a self-limiting of the surface enrichment. The recommended solution to the surface composition changes is to simply ablate the target for a few minutes prior to the deposition. The pre-ablation conditions the target to ensure that a uniform composition is vaporizing once the steady state has been reached. Surprisingly, little change in the stoichiometry is noted in the deposited product, most likely as a result of the preconditioning.

1.6.3.3 The Ablation Plume

The reactions of the ejected material before deposition influence the final quality of the thin film. When material is emitted from the surface after a pulse of only a few nanoseconds, a high pressure 10-500 atm bubble of hot plasma forms. This bubble expands supersonically, creating a beam of species with varying angular distributions, which can affect the final stoichiometry of the film. Interactions with a background gas may also occur to change the composition of materials in flight. For these reasons, understanding the processes that occur mid-flight is important for successful production of pristine films.

The actual composition of the plasma affects the final structure of the films, although methods of monitoring the plasma are few. "For example, some of the most sensitive diagnostics are overwhelmed by the robust environment of dense laser plasmas, while rugged diagnostics are insensitive to low-density plumes[79]". Regardless of the method of investigation used, the resulting information is useful in depositions especially when a background gas is present or when reduction of particulates is important.

When a background gas is present, the plume is scattered, shortened and thermalized. These effects modify the deposition rate, the spatial distribution, and the kinetic energy of the species. All these factors will have an important effect on the final film quality. In $YBa_2Cu_3O_{7-\delta}$, a partial pressure of oxygen is necessary to incorporate oxygen into the final deposited film. This occurs through a reaction of yttrium with the background gas to form YO^+ species that are subsequently deposited. Geohegan has summarized the effect of a

background gas on the plume as follows: "(1) an increase in the fluorescence from all species due to collisions on the expansion front and subsequent interplume collisions; (2) a sharpening of the plume boundary, indicative of a shock front,; (3) a slowing of the plume relative to the propagation in vacuum, resulting in (4) spatial confinement of the plume."[79] In effect, the more gas present the shorter and narrower the plume becomes. Since scattering is also dependant upon the mass of the species involved, angular distributions of the ejected material also vary more greatly, based on the amount of gas present. In $YBa_2Cu_3O_{7-\delta}$, the heavier barium species do not scatter as much as the lighter yttrium and copper species leading to an enrichment of barium in the films if conditions are not adjusted to limit this effect.

In addition to controlling the scattering of the species in plume, background gas also leads to the growth of particulates. Interplume collisions can cause the growth of non-stoichiometric particles in the films[72]. Improved film quality, as determined by improved superconductor characteristics, has been noted when a second laser is used to irradiate the plume and photodissociate the condensing species in the plume.[80,81] Since gas phase interactions are necessary to import oxygen into the films but because they can lead to impurities in the film, the pressure of oxygen present must be carefully controlled. As a result, oxygen pressure in one of the most important variables in high-T_c cuprate thin film deposition.

1.6.3.4 Mechanisms of Film Growth[74]

High quality thin film growth requires more than just the correct conditions at the target and in the plume. In order to achieve smooth continuous films, both the rate of incoming species and temperature of the surface must be controlled. Importantly, both factors affect the orientation, continuity, and film morphology by determining the method(s) of growth.

The deposition of a film requires that a supersaturation of materials exist to form nucleation sites atop the substrate. The importance of supersaturation and its effect on growth is best understood by considering the growth of crystals as developed in the La Mer model, Figure 1.10. According to this model when a solution (in this case the area of film substrate interactions) becomes oversaturated, nucleation occurs.[74] The resulting nucleation lowers the concentration below the critical nucleation density and leads to the further growth of clusters from the original nuclei.[47] Each nucleation growth event can be expected to occur for each pulse of the laser.

The overall growth of the film from a string of successive pulses depends on both the thermodynamics relating to the surface energies, and the film substrate surface energy. Thermodynamically, for a film to growth, the overall Gibbs free energy for the cluster of atoms on the surface must decrease. This energy is summarized in the equation,

$$\Delta G = a_1 r^2 \Gamma_{C-V} + a_2 r^2 \Gamma_{S-C} + a_2 r^2 \Gamma_{S-V} + a_3 r^3 \Delta G_V \qquad \text{Eq} \quad 1.19$$

where r is cluster radius, the Γ's are the interface energies, ΔG_V is the change in volume free energy on condensation, and a's are shape dependant constants. Here C, S and V refer to the cluster, the substrate, and the vapor.[74]

The volume free energy, ΔG_V, is the easiest of the factors to control in a deposition since it is dependant upon the supersaturation of the plume.

$$\Delta G_v = -\frac{kT}{\Omega} \ln\left(\frac{P}{P_e}\right) = -\frac{kT}{\Omega} \ln(\zeta) \qquad \text{Eq} \quad 1.20$$

where k is Boltzmann's constant, T is the absolute temperature (Kelvin), P is the arriving atom pressure, P_e is the film atom pressure, Ω is the atomic volume, and ς is the supersaturation. According to this equation, as developed by Greene, any excess of atoms arriving with a pressure greater than the pressure of the atoms in the film will result in a negative volume free energy. This pressure is controlled by the amount and velocity of atoms leaving the target that successfully traverse the plume. So by controlling the laser energy, to provide a sufficient number of energetic atoms, the supersaturation of the film can be adjusted. The distance of the substrates from the targets also becomes critical since the atoms slow from their initial supersonic speeds in the presence of a background gas. If the target is too far away, the atoms will not have enough velocity to provide and over pressure and the deposition will be negatively affected.

The temperature of the substrate also affects the supersaturation of the area near the substrate since it controls the vapor pressure of the atoms. If the temperature is too high, the P_e term will be come large limiting the ability of

nucleation and film formation. In effect the atoms of the film are boiling off of the surface.

The surface free energy terms are also important for film formation and morphology. Given the inequality,

$$\Gamma_{C-V} + \Gamma_{S-C} > \Gamma_{S-V} \qquad \text{Eq} \quad 1.21$$

the surface free energy terms will be positive. In this form the inequality dictates that energetics favor incoming atoms will bead up and nucleate/grow atop one another. If the reverse were true, the atoms would rather form a continuous film atop the substrate. This inequality is the basis for two of the three formalizations of film growth, Figure 1.15. The first formalization, Volmer-Weber nucleation, occurs when the surface energetics favor beading. The second, Frank-van der Merwe growth, occurs when the continuous films form. A third form, Stranski-Krastinov growth, is intermediate between the others. In this situation, a few complete monolayers form prior to nucleation and growth of clusters atop the monolayers. Unrelieved stress arising from lattice mismatch with substrate causes this unusual mechanism.

Judicious choice of the substrates and their temperature control the surface energetics. Smooth films favor substrates with surface energies close to those of the target material and similar lattice spacings. These similar spacings prevent later stress and orient the deposition of the films. Going back to the theater analogy, the substrate serves as the seats, in the form of low energy sites, which if precisely spaced, allow all of the patrons to find seats close to their friends. The better the lattice match, the lower the surface–cluster interfacial energy and the

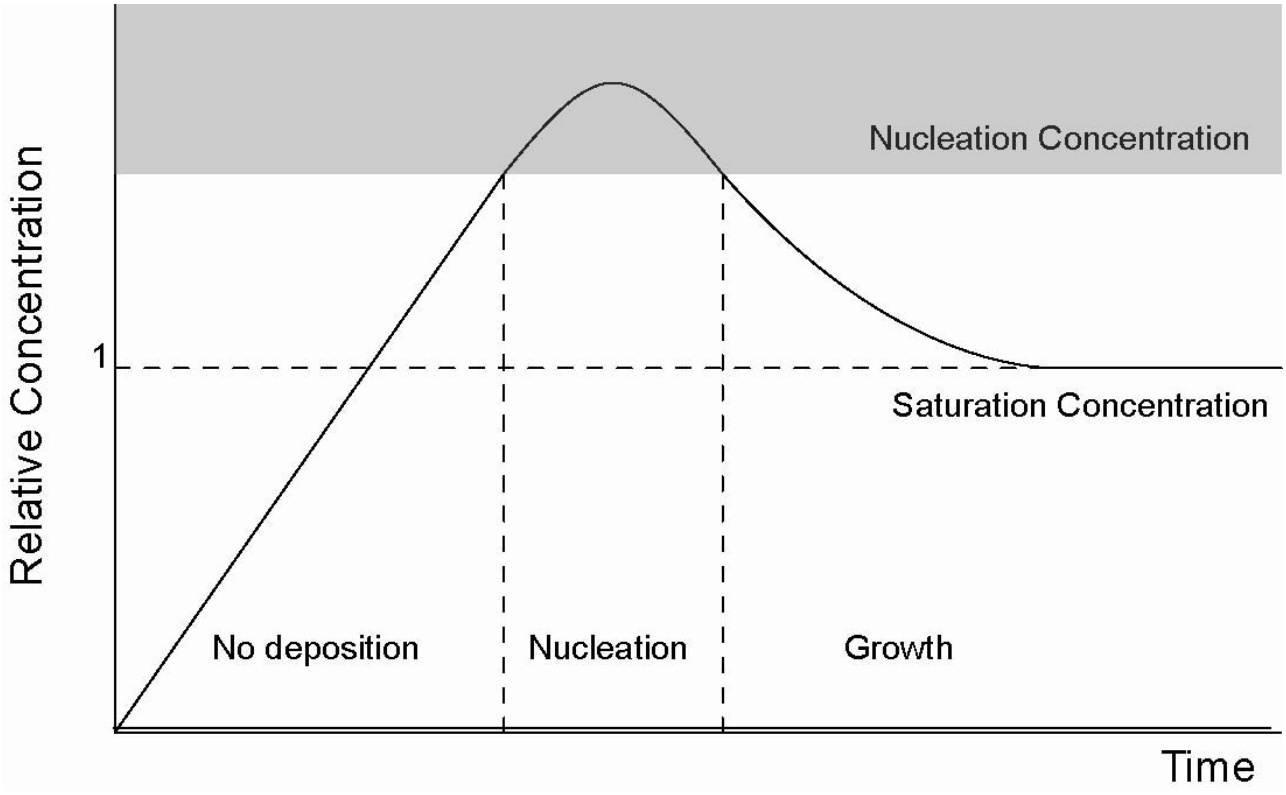

Figure 1.14 La Mer nucleation and growth as a function of time and concentration

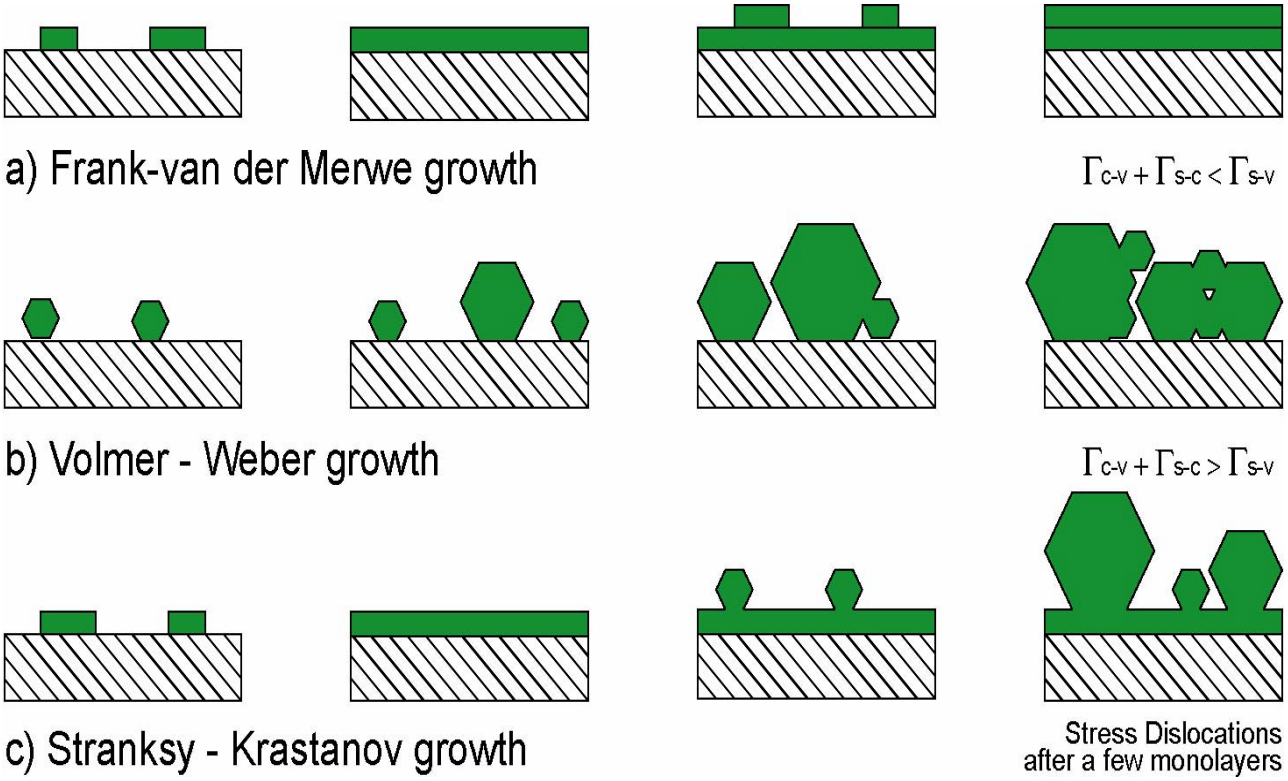

Figure 1.15 Three mechanisms of thin film growth

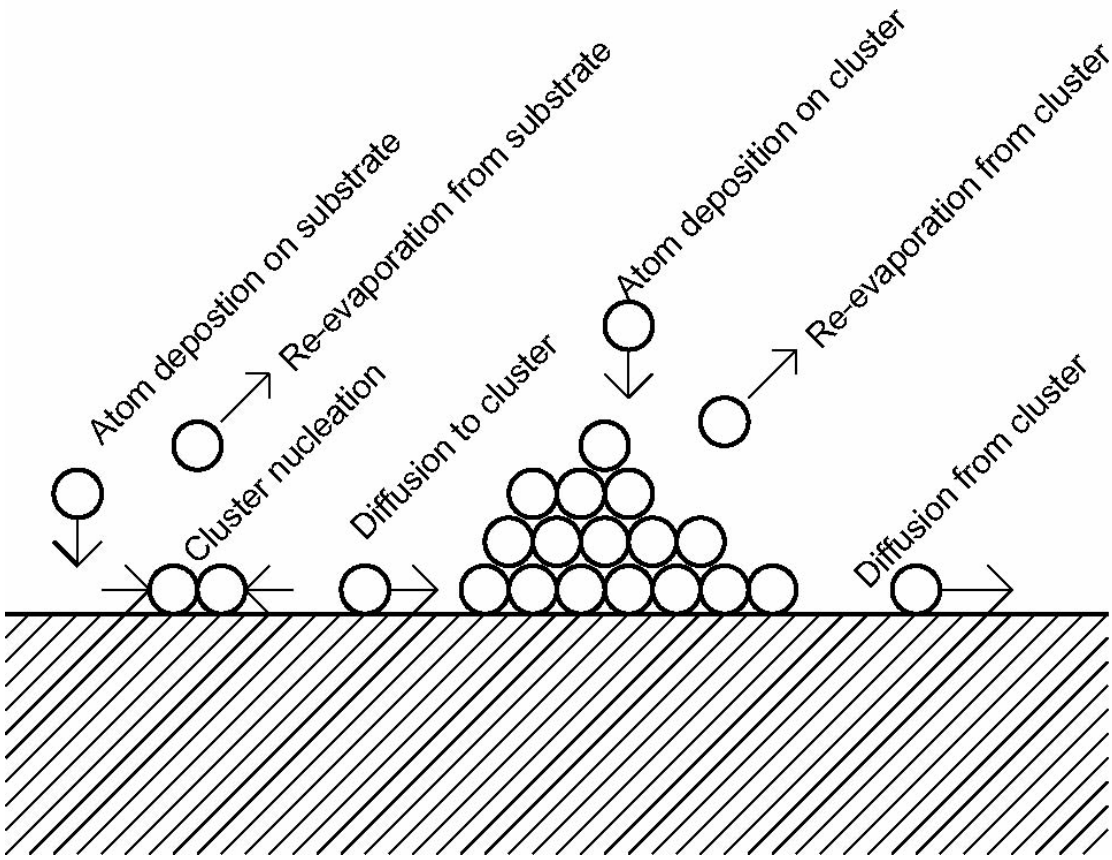

Figure 1.16 Processes occurring during deposition

film will adhere to the surface better. The choice of substrate also affects the final crystalline orientation of the films due to the lattice spacing.

The temperature of the substrate also controls the interfacial energetics in a fine balancing act. For ideal film growth, the atoms need sufficient energy upon arriving at the surface to find a suitable spot in the lattice. Heating the substrate provides energy to allow those atoms that have decelerated and cooled allowing them to diffuse across the surface. Ideally, only enough energy is supplied so that the atoms move across the substrate but do not re-evaporate into the chamber, lowering the volume free energy and nucleation as well, Figure 1.17.

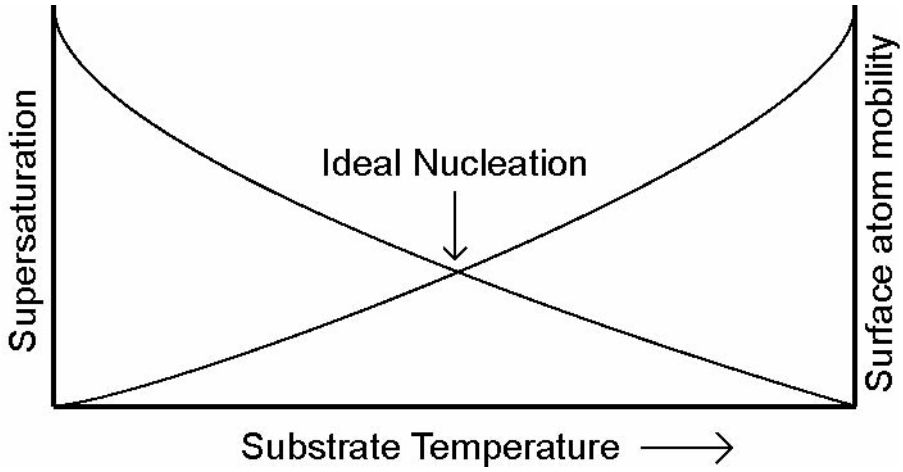

Figure 1.17 Control of nucleation and morphology with substrate temperature

Balancing the deposition rate and the substrate temperature are critical for the production of high quality cuprate films. As the substrate temperature increases, re-evaporation increases and nucleation becomes more difficult. Accordingly, as the deposition rate increases, nucleation increases and clusters grow faster. The ideal conditions would occur with low substrate temperature at

very high rates. Unfortunately, the requirement for sufficient atom mobility requires a certain substrate temperature.

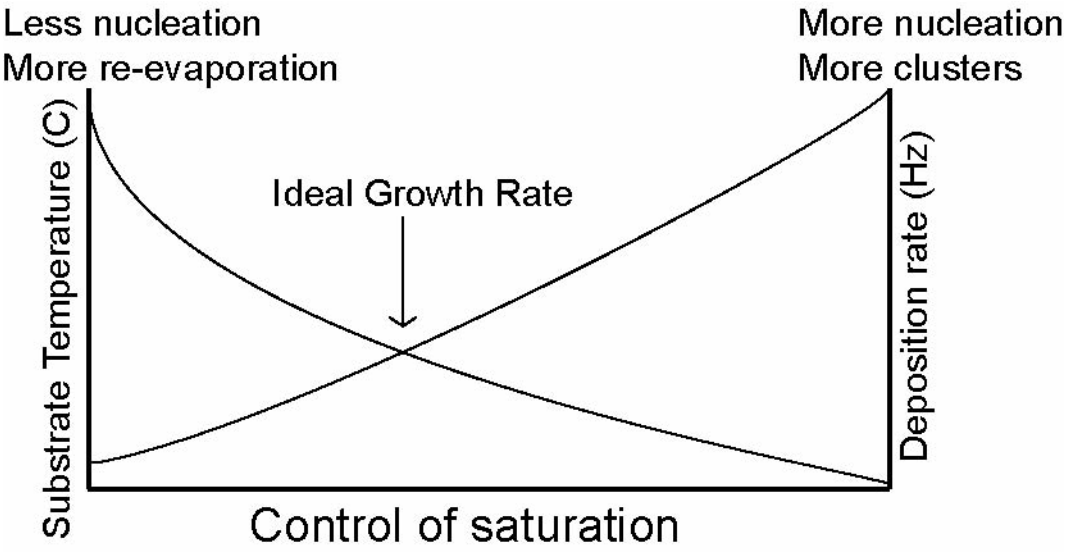

Figure 1.18 The ideal growth rate is a combination of ideal deposition rate and substrate temperature

So two different conditions, nucleation and crystalline structure, are controlled by the substrate temperature. Both must be balanced against the deposition rates and the required surface saturation of the vapor phase atoms. Luckily, any problems associated with the deposition rates are alleviated if the pulse rate of the laser is different than the time scale of any surface reaction. Interference with the surface reactions are only expected to occur in the frequency of the laser near the time scale of the surface diffusion, agglomeration, and dissociation. This is not a problem for most PLD since the laser frequencies are usually close to 10 Hz.

1.6.4 PLD Essentials

Understanding the effects of laser energy density, background gas, substrate selection, and substrate temperature can control the formation qualities of films. By judicious choice of these parameters, high quality films can be deposited as will be described in Chapter 3.

1.7 X-RAY PHOTOELECTRON SPECTROSCOPY

In order to study the chemical environment of the HTSC thin films, a sensitive analytic method is needed. Due to the intrinsic reactivity of the cuprate superconductors to ambient conditions, a method of determining the cleanliness and quality of the surface of high-T_c cuprate samples is needed. In this dissertation, X-ray photoelectron spectroscopy is used to qualitatively measure the cleanliness and the effects self-assembly on the surface of the thin films of superconductors.

X-ray photoelectron spectroscopy (XPS) is a sensitive surface characterization method. The method of XPS characterizes the first few nanometers of the surface by examining the kinetic energy, E_{kin}, of a photoelectron ejected from an atom due to irradiation from an X-ray photon. The unique binding energy of electrons to atoms allows examinations of the fundamental structure of atoms and determination of the chemical environment of atoms of interest.

Knowing the energy of the x-ray ($h\nu$) and the work function of the analyzer (Φ), the binding energy is determined from the relationship, $E_B = h\nu - E_{Kin} - \Phi$, as shown in Figure 1.19. The work function in the above

equation should be that of the surface, but in reality is that of the surface and the analyzer since the photoelectron must pass through a field created by the difference between the two. Photoelectrons having binding energies below ~1500 eV can be studied. This limitation results from the inherent energy limitation of the illuminating x-ray, usually an Al K_α, the energy of which is 1486.6 eV. Another popular source is the Mg K_α line with a photon energy of 1253.6 eV.

Once known, the binding energy is compared to tabulated values or reference compounds to determine the emitting atom. This allows simple determination of the elemental composition, but more information may be gained from a scan of the region of interest.

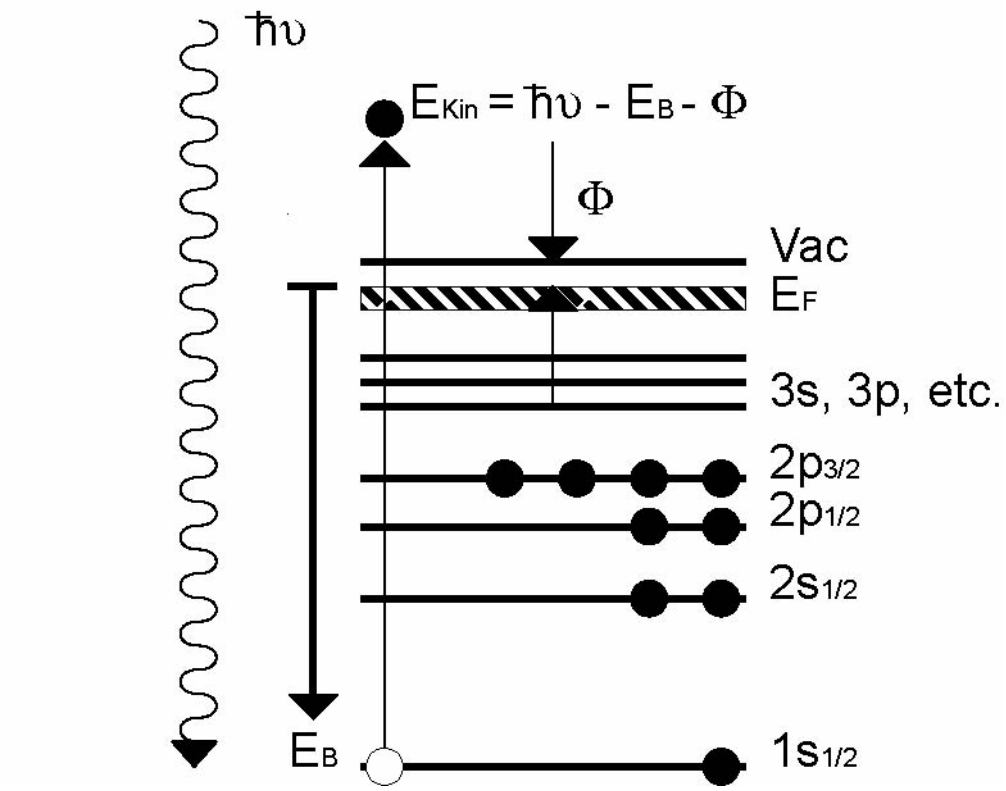

Figure 1.19 Schematic illustration of photoelectron emission.

The above equation explains the ideal one photoelectron situation, but actual measured energies represent the effect of other electrons on the photoelectron. This allows the determination of the chemical environment in addition to mere elemental composition. The chemical shift of the peak arises as a result of these electron interactions. The effect of the environment on the binding energy is best explained if the measured binding energy is described as a sum of the resulting ion and a potential arising from its environment. This summation is described by the equation:

$$E_B(k) = E_B(k,q_A) = V \qquad \text{Eq 1.22}$$

where $E_B(k, q_a)$ is the free ion binding energy of the free ion A, q_A is the net charge, and V is the potential at the position of A as a result of all nearby atoms.

It is the potential V that allows the determination of the chemical environment. As a general rule, creation of a positive ion by removing the valence electrons increases the binding energy of the remaining electrons while negative ionization reduces the binding energy. Comparison of the binding energies to reference compounds allows determination of the chemical state.

In addition to chemical identity, the position in relation to the surface can be determined by modifying the geometry of the analysis. As shown in Figure 1.20, the angle of the detector, Θ, can be varied with respect to the plane of the surface of interest. At high angles a greater proportion of the electrons ejected from the deeper atoms are observed, compared to the surface. At low angles, only the surface region is observed due to the limited mean free path length of ejected

photoelectrons. The rest of the atoms on and near the surface serve to shield the deeper atoms from the detector.

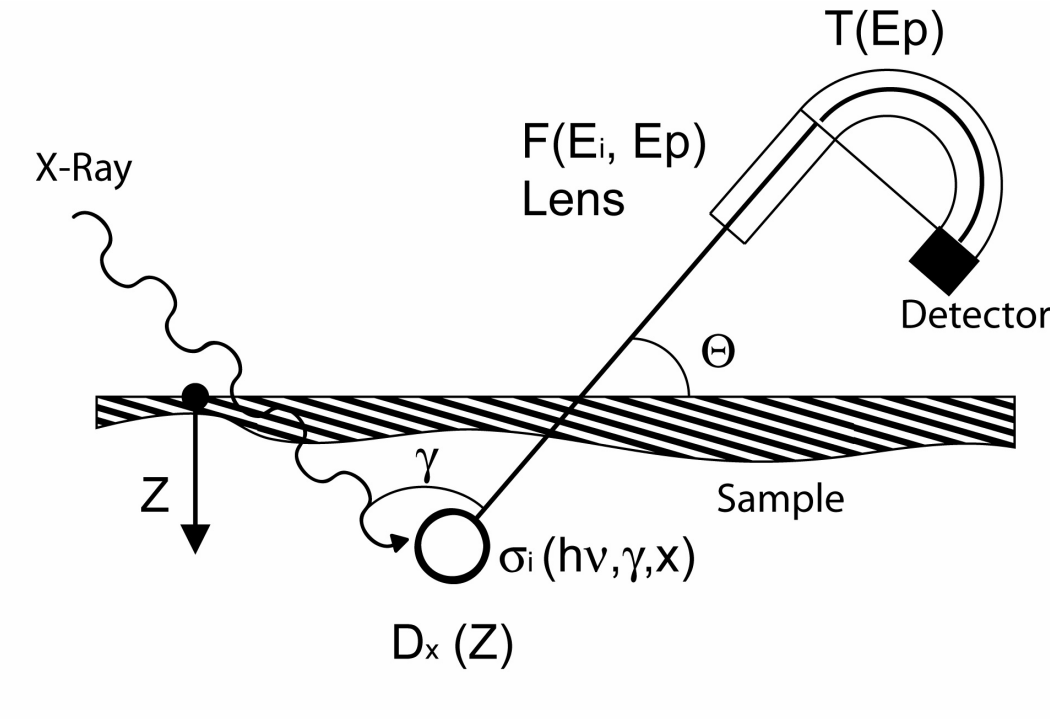

Figure 1.20 XPS analysis geometry. The total intensity of the signal is a function of the angle of emission θ, the angle dependent cross section of the atom of interest σ_I, and the analyzer functions F and T.

1.8 X-RAY DIFFRACTION MEASUREMENTS

Due to the anisotropic nature of cuprate superconductors, the crystalline orientation of films determines the behavior of the material. Films with the c-axis oriented normal to the substrate will have better conduction across the film due to the contiguous alignment of the CuO planes. The ability of water and other corrosion products to move into the lattice is determined by the orientation of the lattice as well. Likewise the phase purity and stoichiometry of the materials is

important for proper superconductive behavior. Both of these qualities are experimentally measured using x-ray diffraction.

In order to understand the chemistry of the films produced for study, the orientation and degree of crystallinity must be understood. For the optimization of the deposition conditions in Chapter 3, X-ray diffraction provided the means of measuring the orientation order.

X-ray diffraction is useful for determination of the periodic arrangement of atoms in a structure. The ability to detect the atomic positions is based on the diffraction of photons by regularly repeating atoms. In an x-ray experiment, the incident beam of photons impinges on the sample and the intensity of reflections are quantified based on the 2Θ angle of the diffractometer[82]. The series of peaks detected can only occur when the 2Θ angle is such that reflections from planes of atoms constructively interfere. Such constructive interference can only occur from planes where the difference in path length is an integral number of wavelengths. This requirement is shown geometrically in Figure 1.21.

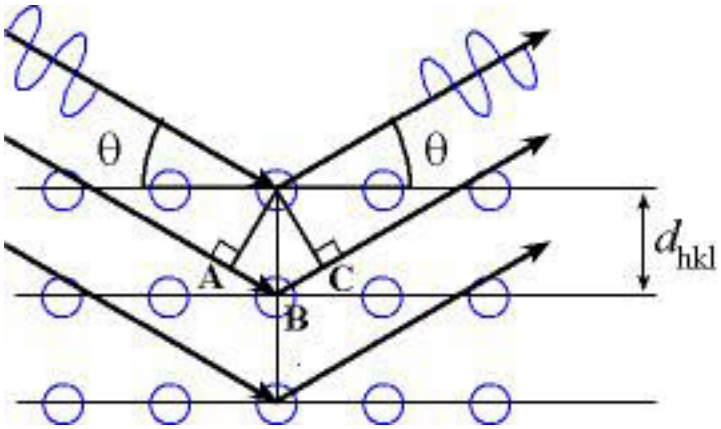

Figure 1.21 Illustration of diffraction geometry in x-ray analysis

In the experiment, photons incident at the angle Θ penetrate the surface and are scattered by the cloud of electrons surrounding the atoms at the angle Θ. The photons striking the second plane travels a distance AB + BC further than the ray of photons impinging the plane above it. These rays can only be in constructively interfere if they are in phase, meaning that AB + BC = nλ must be true. The relationship AB = BC = d sin Θ can be determined geometrically leading to the equation:

$$2d\sin\theta = n\lambda \qquad \text{Eq} \quad 1.23$$

This relation has been formalized as Bragg's law and is indispensable for the calculation of atomic positions. [83]

Given that reflections only occur from planes of periodically spaced atoms, a system has been developed to quickly identify the plane of discussion. These Miller indices, given as (abc), correspond to the number of unit cells the plane is removed from a chosen origin in reciprocal lattice space. For example, in our figure below, with the x-y (a-b) direction perpendicular to the plane on the page and the z-y (b-c) direction in the plane of the page, a miller index of (00h) would be given for the various planes of atoms shown. In modified triple perovskite structures of $YBa_2Cu_3O_{7-\delta}$, the BaO planes and CuO sheets correspond to the different (001), (002), (00n) . . . peaks detected in powder diffraction (Figure 1.22).

For this dissertation, most attention has been placed on determination of the predominant orientation of thin film crystalline unit cells in reference to the underlying substrate. A typical experiment to determine whether a thin film was

predominantly a-axis oriented, with the a-axis perpendicular to the face of the substrate, or c-axis oriented would consist of the film being aligned in the path of the x-ray and collecting a 2-theta scan from 10° to 60° theta. The resulting peaks are compared to the literature positions for peaks of known crystallographic planes. In this way, determination of the predominant orientation of the thin film is easily accomplished. While comparing the known peaks for the film or pellet of interest, anomalous peaks are sometimes detected. By comparing those peaks to the know diffraction patterns of starting materials and other undesirable phases of superconductors, we can determine the uniformity and purity of the samples. A sample X-ray diffraction with the inset resistance versus temperature graph is provided in Figure 1.23. Representative X-ray diffractions will be provided in Chapter 3 to elucidate the quality and orientation of the deposited films.

1.9 CONCLUSION

In summary, the first chapter has laid a foundation and provided background for a description of a dissertation program that centers on the definition of adsorbate chemistry atop common cuprate superconductor samples. The remaining chapters are organized in the following way: Chapter 2 describes the materials and methods used in this dissertation. Chapter 3 relates the creation of a novel pulsed laser deposition system and the optimization entailed in creation of high quality thin films. Chapter 4 explores the mechanism of amine adsorption atop superconductors. Chapter 5 reports on initial studies of the kinetics of monolayer formation on superconductors. Overall, the dissertation program has targeted the development of a more complete understanding of amine adsorbate

chemistry atop cuprate superconductors using oriented samples and a variety of adsorbate molecules.

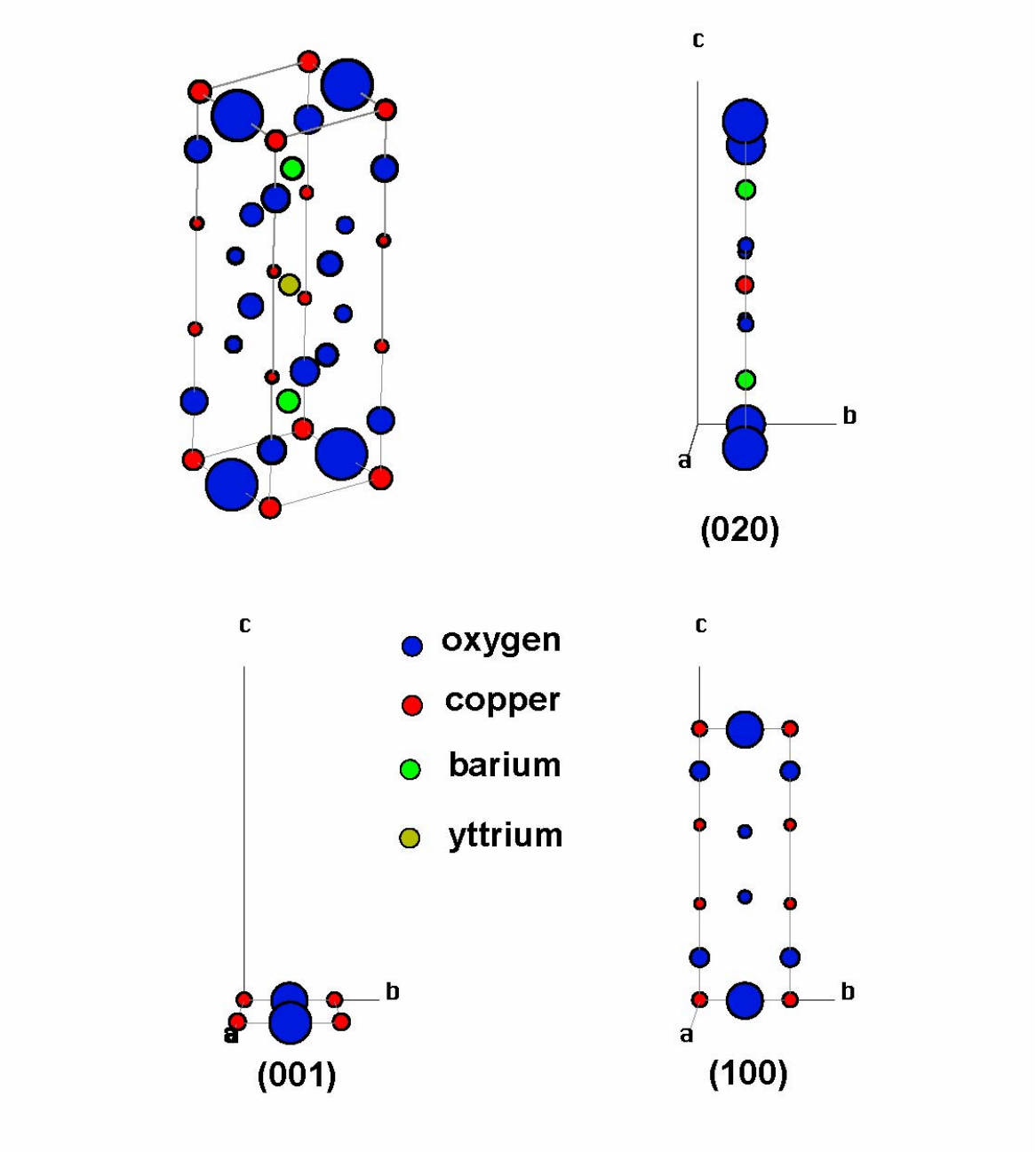

Figure 1.22 $YBa_2Cu_3O_{7-\delta}$ lattice and example Miller indices

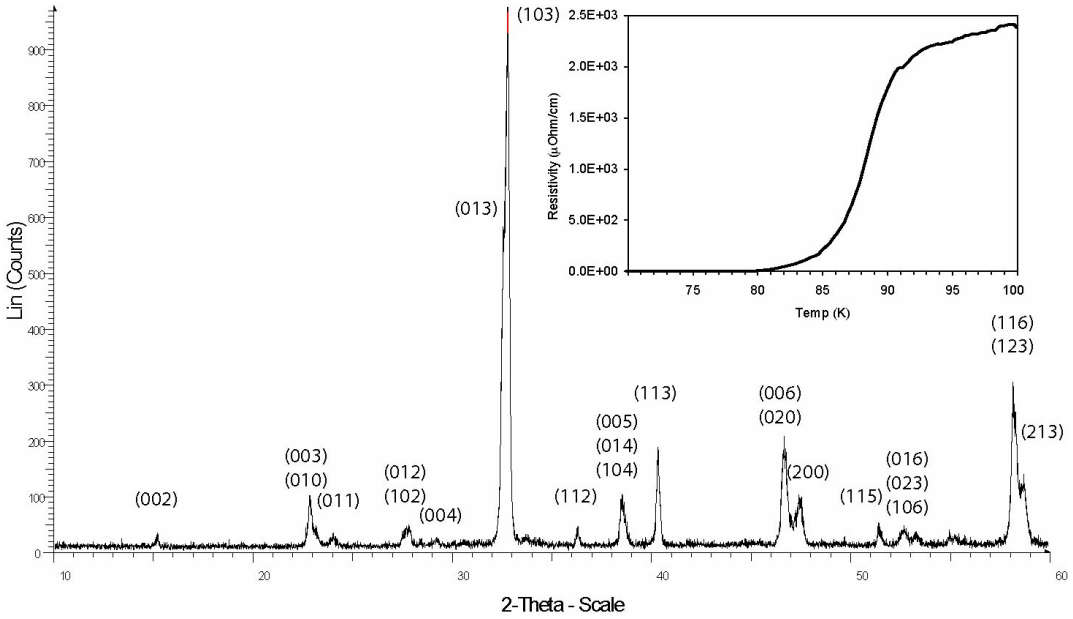

Figure 1.23 Sample XRD of a Y1 pellet manufactured as a target. The inset is the resistance versus temperature plot for the sample.

1.10 REFERENCES

(1) Ulman, A. *An introduction to ultrathin organic films: from Langmuir-Blodgett to self-assembly*; Academic Press: San Diego, CA, 1991.

(2) Wells, C. A. In *Department of Chemistry and Biochemistry*; University of Texas at Austin: Austin Texas, 1999, p 176.

(3) Ritchie, J. E.; Wells, C. A.; Zhou, J.-P.; Zhao, J.; McDevitt, J. T.; Ankrum, C. R.; Jean, L.; Kanis, D. R. *J. Am. Chem. Soc.* **1998**, *120*, 2733-2745.

(4) Ritchie, J. E. In *Department of Chemistry and Biochemistry*; University of Texas at Austin: Austin, Texas, 1998, p 166.

(5) McDevitt, J. T.; Mirkin, C. A.; Lo, R.-K.; Chen, K.; Zhou, J.-P.; Xu, F.; Haupt, S. G.; Zhao, J.; Jurbergs, D. *Chem. Mat.* **1996**, *8*, 811-813.

(6) Mirkin, C. A.; Xu, F.; Zhu, J. *Adv. Mat.* **1997**, *9*, 167-172.

(7) Chen, K.; Mirkin, C. A.; Lo, R.-K.; Zhao, J.; McDevitt, J. T. *J. Am. Chem. Soc.* **1995**, *117*, 6374-6375.

(8) Chen, K.; Xu, F.; Mirkin, C. A.; Lo, R.-K.; Nanjundaswamy, K. S.; Zhou, J.-P.; McDevitt, J. T. *Langmuir* **1996**, *12*, 2622-2624.

(9) Langmuir, I. **1936**, *Science*, 379-383.

(10) Sugi, M.; Nembach, K.; Mobius, D. *Thin Solid Films* **1974**, *27*, 205.

(11) Dubois, L. H.; Zegarski, B. R.; Nuzzo, R. G. *J. Am. Chem. Soc.* **1990**, *112*, 570-579.

(12) Schessler, H. M.; Karpovich, D. S.; Blanchard, G. J. *J. Am. Chem. Soc.* **1996**, *118*, 9645-9651.

(13) Hackett, D. W.; Uibel, R. H.; Stevenson, K. J.; Harris, J. M.; White, H. S. *Journal of the American Chemical Society* **1998**, *120*, 1062-1069.

(14) Nuzzo, R. G.; Fusco, F. A.; Allara, D. L. *J. Am. Chem. Soc.* **1987**, *109*, 2358-2368.

(15) Chidsey, C. E. D.; Loiacono, D. N. *Langmuir* **1990**, *6*, 682-691.

(16) Porter, M. D.; Bright, T. B.; Allara, D. L.; Chidsey, C. E. D. *J. Am. Chem. Soc.* **1987**, *109*, 3559.

(17) Finklea, H. O. In *Electroanalytical Chemistry*; Bard, A. J., Rubinstein, I., Eds.; Marcel Dekker, Inc.: New York, 1996; Vol. 19, pp 110-337.

(18) Mirkin, C. A.; Ratner, M. A. *Annu. Rev. Phys. Chem.* **1992**, *43*, 719-754.

(19) Gorman, C. B.; Biebuyck, H. A.; Whitesides, G. M. *Chem. Mat.* **1995**, *7*, 526-529.

(20) Kumar, A.; Abbott, N. L.; Kim, E.; Biebuyck, H. A.; Whitesides, G. M. *Accounts of Chemical Research* **1995**, *28*, 219-226.

(21) Gorman, C. B.; Biebuyck, H. A.; Whitesides, G. M. *Chem. Mat.* **1995**, *7*, 252-254.

(22) Kim, E.; Kumar, A.; Whitesides, G. M. *Journal of the Electrochemical Society* **1995**, *142*, 628-634.

(23) Uchiyama, K.; Etou, H.; Tono, I. In *Jpn. Kokai Tokkyo Koho*; (Toshiba Corp., Japan). Jp, 2003, p 7 pp.

(24) Konry, T.; Novoa, A.; Cosnier, S.; Marks, R. S. *Analytical Chemistry* **2003**, *75*, 2633-2639.

(25) Das, K.; Penelle, J.; Rotello, V. M. *Langmuir* **2003**, *19*, 3921-3925.

(26) Tomonori, H.; Anzai, J. *Kagaku Kogyo* **2002**, *53*, 221-226.

(27) Lahav, M.; Kharitonov, A. B.; Willner, I. *Chemistry--A European Journal* **2001**, *7*, 3992-3997.

(28) Cavallini, M.; Lazzaroni, R.; Zamboni, R.; Biscarini, F.; Timpel, D.; Zerbetto, F.; Clarkson, G. J.; Leigh, D. A. *J. Phys. Chem. B* **2001**, *105*, 10826-10830.

(29) Muguruma, H. *Hyomen* **2001**, *39*, 126-133.

(30) Hwang, B. J.; Yang, J. Y.; Lin, C. W. *Sensors and Actuators, B: Chemical* **2001**, *B75*, 67-75.

(31) Holder, S. J.; Elemans, J. A. A. W.; Donners, J. J. J. M.; Boerakker, M. J.; de Gelder, R.; Barbera, J.; Rowan, A. E.; Nolte, R. J. M. *Journal of Organic Chemistry* **2001**, *66*, 391-399.

(32) *Text of the award for the Nobel Prize in Physics* **1913**.

(33) Simon, R.; Smith, A. *Superconductors: Conquering Technology's New Frontier*; Plenum Press: New York, 1988.

(34) Bednorz, J. G.; Muller, K. A. *Z. Phys. B - Condensed Mattter* **1986**, *64*, 189-193.

(35) Michel, C.; Raveau, B. *Chim. Min.* **1984**, *21*, 407.

(36) Chu, C. W.; Hor, P. H.; Meng, R. L.; Gao, L.; Huang, Z. J.; Wang, Y. Q. *Phys. Rev. Lett.* **1987**, *58*, 405-407.

(37) Wu, M. K.; Ashburn, J. R.; Torng, C. J.; Hor, P. H.; Meng, R. L.; Gao, L.; Huang, Z. J.; Wang, Y. Q.; Chu, C. W. *Phys. Rev. Lett.* **1987**, *58*, 908-910.

(38) Hazen, R. M. *The Breakthrough: The Race for the Supercondcutor*; Summit Books: New York, 1988.

(39) Maeda, H.; Tanaka, Y.; Fukutomi, M.; Asano, T. *Japan. J. Appl. Phys. Lett.* **1988**, *27*, L209-210.

(40) Sheng, Z. Z.; Hermann, A. M. *Nature* **1988**, *332*, 55-58.
(41) Hazen, R. M.; Finger, L. W.; Angel, R. J.; Prewitt, C. T.; Ross, N. L.; Hadidiacos, C. G.; Heaney, P. J.; Veblen, D. R.; Sheng, Z. Z.; Hermann, A. M. *Phys. Rev. Lett.* **1988**, *60*, 1657-1660.
(42) Schilling, A.; Cantoni, M.; Guo, J. D.; Ott, H. R. *Nature* **1993**, *363*, 56-58.
(43) Chu, C. W.; Gao, L.; Chen, F.; Huang, Z. J.; Meng, R. L.; Yue, Y. Y. *Nature* **1993**, *365*.
(44) Nagamatsu, J.; Nakagawa, N.; Muranaka, T.; Zenitani, Y.; Akimitsu, J. *Nature* **2001**, *410*, 63-64.
(45) Canfield, P. C.; Crabtree, G. W. *Physics Today* **2003**, *56*, 34-40.
(46) Poole, C. P.; Farach, H. A.; Creswick, R. J. *Superconductivity*; Academic Press: New York, 1995.
(47) van der Put, P. J. *The Inorganic Chemistry of Materials: How to Make Things Out of Elements*; Plenum Press: New York, 1998.
(48) Yan, M. F.; Barns, R. L.; O'Bryan, H. M.; Gallagher, P. K.; Sherwood, R. C.; Jin, S. *Applied Physics Letters* **1987**, *51*, 532.
(49) Zhou, J.-P.; Savoy, S. M.; Zhao, J.; Riley, D. R.; Zhu, Y. T.; Manthiram, A.; Lo, R.-K.; Borich, D.; McDevitt, J. T. *J. Am. Chem. Soc.* **1994**, *116*, 9389-9390.
(50) Zhou, J.-P.; Savoy, S. M.; Lo, R.-K.; Zhao, J.; Arendt, M.; Zhu, Y. T.; Manthiram, A.; McDevitt, J. T. *Appl. Phys. Lett.* **1995**, *66*, 2900-2902.
(51) Zhou, J.-P.; Zhou, J.-S.; Goodenough, J. B.; McDevitt, J. T. *Journal of Superconductivity* **1995**, *8*, 651-652.
(52) Zhou, J.-P.; Jones, C. E.; McDevitt, J. T.; Talvacchio, J.; Jia, Q. X. In *Advances in Superconductivity X: Procceding of the International Symposium on Superconductivity*; Osamura, K., Hirabayashi, I., Eds.; Springer: Gifu, Japan, 1997; Vol. 1, pp 289-292.
(53) Zhou, J.-P.; Lo, R.-K.; Savoy, S. M.; Arendt, M.; Armstrong, J.; Yang, D.-Y.; Talvacchio, J.; McDevitt, J. T. *Physica C* **1997**, *273*, 223-232.
(54) Zhou, J.-P.; Lo, R.-K.; Savoy, S. M.; Arendt, M.; Armstrong, J.; Yang, D.-Y.; Talvacchio, J.; McDevitt, J. T. *Physica C* **1997**, *273*, 223-232.
(55) Zhou, J.-P.; McDevitt, J. T. *Chem. Mat.* **1992**, *4*, 953-959.
(56) McDevitt, J. T.; Zhou, J.-P.; Zhao, J. In *PCT Int. Appl*; Board of Regents, The University of Texas System: USA, 1996.
(57) McDevitt, J. T.; Zhou, J.-P.; Jones, C. E.; Talvacchio, J. In *Proceedings of the 10th Aniversary HTS Workshop on Physics, Materials, and Applications*; Batlogg, B., Ed.; World Scientific: Houston, Texas, 1996, pp 177-178.
(58) www.amsuper.com, 2003.

(59) Cyrot, M.; Pavuna, D. *Introduction to superconductivity and high-Tc materials*; World Scientific Publishing Co. Pte. Ltd.: River Edge, NJ, 1992.

(60) Riley, D. R.; McDevitt, J. T. *J. Electroanal. Chem.* **1990**, *295*, 373-384.

(61) Riley, D. R.; McDevitt, J. T. *J. Electroanal. Chem.* **1990**, *295*, 373-384.

(62) Riley, D. R.; Manthiram, A.; McDevitt, J. T. *Chem. Mat.* **1992**, *4*, 1176-1181.

(63) Riley, D. R.; Jurbergs, D.; Zhou, J.-P.; Zhao, J.; Markert, J.; McDevitt, J. T. *Solid State Comm.* **1993**, *88*, 431-434.

(64) Riley, D. R. In *Department of Chemistry and Biochemistry*; University of Texas at Austin: Austin, Texas, 1993, p 199.

(65) Bard, A. J.; Faulkner, L. R. *Electrochemical methods: fundamentals and applications*; 2nd ed.; John Wiley & Sons, Inc.: New York, 2001.

(66) Langmuir, I. *J. Am. Chem. Soc.* **1918**, *40*, 1361.

(67) Karpovich, D. S.; Blanchard, G. J. *Langmuir* **1994**, *10*, 3315-3322.

(68) Masel, R. I. *Principles of adsorption and reaction on solid surfaces*; John Wiley & Sons, Inc.: New York, 1996.

(69) Bourdillon, A.; Bourdillon, N. X. T. *High Temperature Superconductors: Processing and Science*; Academic Press, Inc.: New York, 1994.

(70) Hubler, G. K. In *Pulsed Laser Deposition of Thin Films*; Chrisey, D. B., Hubler, G. K., Eds.; John Wiley & Sons, Inc.: New York, 1994, pp 327-355.

(71) Cheung, J. T. In *Pulsed Laser Deposition of Thin Films*; Chrisey, D. B., Hubler, G. K., Eds.; John Wiley & Sons, Inc.: New York, 1994.

(72) Dijkkamp, D.; Venkatesan, T.; Wu, X. D.; Shaheen, S. A.; Jisrawi, N.; Min-Lee, W. L.; McLean, W. L.; Croft, M. *App. Phys. Lett.* **1987**, *51*, 619-621.

(73) Venkatesan, T. In *Pulse Laser Depostion of Thin Films*; Chrisey, D. B., Hubler, G. K., Eds.; John Wiley & Sons, Inc.: New York, 1994, pp 313-323.

(74) Horwitz, J. S.; Sprague, J. A. In *Pulsed Laser Deposition of Thin Films*; Chrisey, D. B., Hubler, G. K., Eds.; John Wiley & Sons, Inc.: New York, 1994, p 229.

(75) Kelly, R.; Miotello, A. In *Pulsed Laser Deposition of Thin Films*; Chrisey, D. B., Hubler, G. K., Eds.; John Wiley & Sons, Inc.: New York, 1994, pp 55-87.

(76) Dreyfus, R. W.; Walkup, R. E.; Kelly, R. *Radiat. eff.* **1986**, *99*, 199.
(77) Dreyfus, R. W.; Kelly, R.; Walkup, R. E. *Nuclear instrumental methods* **1987**, *B23*, 557.
(78) Foltyn, S. R. In *Pulsed Laser Deposition of Thin Films*; Chrisey, D. B., Hubler, G. K., Eds.; John Wiley & Sons, Inc.: New York, 1994.
(79) Geohegan, D. R. In *Pulsed Laser Deposition of Thin Films*; Chrisey, D. B., Hubler, G. K., Eds.; John Wiley & Sons, Inc.: New York, 1994.
(80) Chiba, H.; Murakami, K.; Eryu, O.; Shihoyama, K.; Mochizuki, T.; Masuda, K. *Jpn. J. appl. Phys.* **1991**, *30*, L32.
(81) Koren, G.; Baseman, R. J.; Gupta, A.; Lutwyche, M. I.; Laibowitz, R. B. *Appl. Phys. Lett.* **1990**, *56*, 2144.
(82) Jenkins, R.; Snyder, R. L. *Introduction to x-ray powder diffractometry*; Wiley - Interscience, 1996.
(83) Sands, D. E. *Introduction to Crystallography*; Dover Publications Inc.: New York, 1975.

2. Materials and Methods

In this chapter, the materials and experimental procedures used will be described in detail. Included here in depth will be a description of both bulk and thin film high temperature superconductor fabrication. The second part of this chapter will focus on the experimental techniques used throughout the research process.

2.1 MATERIALS

2.1.1 Bulk High Temperature Superconductors

Ceramic pellets of high temperature superconductors were often used to determine the basic feasibility of a project as they represented a physically robust and easily regenerated surface. The bulk pellets were also used as targets for deposition of thin films using pulse laser deposition. The pulse laser deposition of

thin films of $YBa_2Cu_3O_{7-\delta}$ and $Y_{0.6}Ca_{0.4}Ba_{1.6}La_{0.4}Cu_3O_{7-\delta}$ will be discussed in Chapter 3.

All pellets were fabricated using standard solid-state synthetic methods. In this process, stoichiometric amounts of barium carbonate, yttrium oxide, and copper oxide were combined and ground in an porcelain mortar and pestle until a uniform color and consistency was achieved. Note that great care was taken to avoid scratching the crucible to prevent addition of undesirable alumina contamination of the product. The resulting gray mixture was transferred to an alumina crucible and fired in a box furnace at upwards of 900° C for at least 18 hours. This initial sintering serves both to remove the excess oxides and carbonates as carbon dioxide and to mix further the initial starting components. Further, the initial partial conversion of the starting materials into the complex cuprate material occurs at this time. The black powder was then reground in an agate mortar and pestle and resintered in pressed pellet form at lest twice. Pressing the pellets was performed using machined dies of precision ground hardened stainless steel in a Carver laboratory press (Wabash, IN) at pressures of at least 6 metric tons. The temperature of these sinterings was 925° C, while the duration of the sintering exceeded 18 hours. After the final sintering, the pellets were annealed under flowing oxygen in a tube furnace at 550° C for 12 hours.

The resulting pellets are characterized by X-ray powder diffraction and resistivity vs. temperature measurements. The specifics of both X-ray diffraction and resistivity measurements will be described later. Typical pellets manufactured in the above method yield polycrystalline samples with metallic

behavior. Transition temperatures (T_c) of 92 K have been recorded with narrow (less than 2K) transition widths. The T_c is very dependant upon the oxygen and bulk component stoichiometry. The width of the transition depends upon the grain size and interconnections between them. The larger the grains with numerous connections will have shorter percolation pathways for the electrons and Cooper pairs, thus displaying better superconducting properties. The grain size and fusion between grains depends on the quality of intermixing achieved with both the intermixing and sintering. Pressing of the powder into pellets before sintering increased the grain size by easing intermixing and removing of voids. Shown in Figure 2.1 is the XRD of a typical pellet along with its resistivity vs. temperature plot.

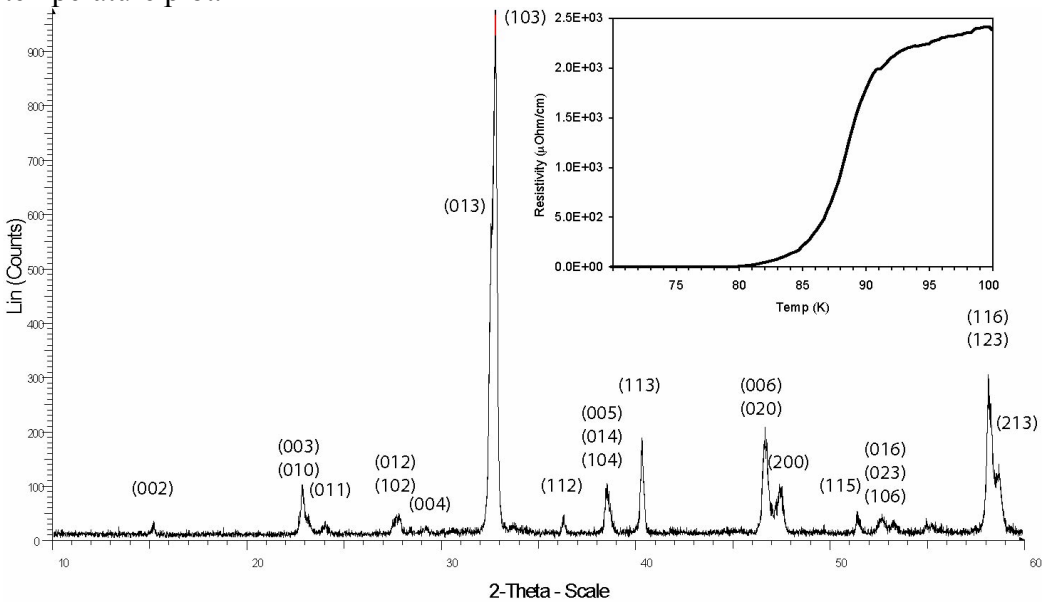

Figure 2.1 X-ray powder diffraction of YBa2Cu3O7 with example resistivity vs. temperature inset

2.1.2 Thin Film Samples

All thin film samples were prepared using pulse laser deposition from bulk targets. Two similar deposition chambers were used, but the deposition conditions described here apply to both systems. The target of bulk ceramic was rotated in the chamber that was first evacuated to a base pressure of 1 x 10^{-6} torr. The substrate to be deposited onto was either silver painted or clipped to the nickel face of the heater (except for load locked films to be described in Chapter 3) and heated to the desired deposition temperature in a flow of oxygen at approximately 200 mtorr. The specifics of both temperature and oxygen pressure and their interrelation will be discussed in the chapter focusing on the deposition of the $Y_{0.6}Ca_{0.4}Ba_{1.6}La_{0.4}Cu_3O_{7-\delta}$. A Lambda Physik Compex 204 KrF excimer laser (Ft. Lauderdale, FL) was focused on the target of ceramic at 45° to the normal of the target. The desired laser spot size of 1mm by 5 mm was maintained by frequently focusing between runs. At this spot size, with a 10 ns pulse width, energy densities of 2 J cm^{-2} at the surface of the target cause the spontaneous evaporation and ionization of the target into a plume of semi spherical shape directed towards the heated substrates. The substrates to target distance was optimized to a distance of ~ 5 cm. The depositions proceeded for varying time scales, dependant upon desired film thickness, but were performed at 8 Hz at approximately 275 mJ energy at the laser to provide an optimal deposition rate of 1Å per pulse without substrate rotation (*vida infra*). Following the deposition the films were slowly cooled to 450°C at an increased oxygen pressure of 450 torr

and held at this temperature for 20 minutes to assure proper oxygen stoichiometry in the resulting films.

In order to control the crystal orientation of the thin films, the oxygen partial pressure as well as the temperature of the substrates during deposition must be controlled. Specifics for the deposition of $Y_{0.6}Ca_{0.4}Ba_{1.6}La_{0.4}Cu_3O_{7-\delta}$ will be given in later chapters, but the general deposition parameters can be summarized here. For a [001] oriented film, the temperature of the nickel plate and the attached substrates in maintained at 760° C in a 200 mtorr oxygen atmosphere. For a mixed [100]-[010] film, 680° C in 200 mtorr oxygen provides the optimal conditions.

All thin films were deposited atop single crystal substrates. Lanthanum aluminate, LaAlO3, or magnesium oxide, MgO, was used. The single crystals were cut and polished along [001] face to assist in the deposition of c-axis films. Prior to use, all substrates were cleaned by multiple 10-minute baths in an ultrasonicator in solutions of 50%(v/v) solution of ammonium hydroxide in nanopure water, nanopure water, ethanol (2x), and finally high purity acetone for 10 minutes. Upon mounting to the heater platens, the films were again rinsed with acetone and blown dry with nitrogen to remove most dust contamination.

The alignment and lattice parameters of the substrate play a crucial role in determining the ordering of the subsequent thin films. Substrate materials such as LaAlO3 and MgO are commonly used in PLD. Both substrates are suitable since their lattice spacing closely matches those of the $YBa_2Cu_3O_{7-\delta}$, $NdBa_2Cu_3O_{7-\delta}$, and $Y_{0.6}Ca_{0.4}Ba_{1.6}La_{0.4}Cu_3O_{7-\delta}$ superconductors. The a-axis lattice parameter of

$YBa_2Cu_3O_{7-\delta}$ is 3.82Å, while the parameters for MgO and $LaAlO_3$ are 4.213Å and 3.793Å respectively. The MgO has an 8% mismatch that leads to angular defects, but is more resistant to shattering than the LaAlO3. Although the mismatch is large compared to other possible substrates, $YBa_2Cu_3O_{7-\delta}$ deposited atop MgO recovers its proper lattice spacing through a misfit strain relaxation.[1] The LaAlO3 also leads to preferential deposition of [100] oriented $YBa_2Cu_3O_{7-\delta}$ films.[2]

2.1.3 Molecular Reagents

Octadecylamine, butylamine, hexylamine, octylamine, hexadecylamine, high purity acetone, and hexanes were obtained from Aldrich (Milwaukee, WI) and, unless otherwise specified, were used as received. Tetrabutylammonium hexafluorophosphate (TBAPF6), electrochemical grade, and high purity ferrocene were purchased from Aldrich. Prior to use, the tetrabutylammonium hexafluorophosphate was dried *in vacuo* at 140° C for at least 24 hours. Spectrophotometric grade hexanes and acetonitrile were obtained from either Fischer (Pittsburgh, PA) or Aldrich. Both were used without modification unless the experiments were conducted in an inert atmosphere glove box. For use in the glove box, the solvents were purged with argon prior to admission to the glove box. Drying over molecular sieves (3Å) was avoided due to contamination of the solvent from minute particles of dust that were subsequently detected in x-ray photoelectron spectroscopy experiments. Distillation of solvents was not performed after the initial purging with argon. No evidence of water was observed in electrochemical experiments performed with a CH660 potentiostat

from CH Instruments (Austin, TX) in the inert atmosphere glove box (MBraun, Stratham, NH).

2.1.4 Electroactive Monolayer Reagent

In chapter 5, measurement of the kinetics of electroactive monolayers atop cuprates is performed. Here the use of ferrocenylethylamine provided a simple way to explore the adsorbate reaction dynamics. The compound was synthesized as follows. Under argon, ferrocenylmethyltrimethylammonium iodide (Strem) was combined with excess potassium cyanide (Aldrich) in a minimum amount of water and refluxed until the formation of red oil and gas evolution was noted. Insoluble potassium iodide precipitates in the bottom of the roundbottom flask. A minimum amount of water is used due to a competing hydrolysis reaction that occurs as the cyanide anion attacks the trimethylammonium iodide leaving group. Refluxing for a further 4 hrs was performed to assure completion of the formation of the ferrocenylmethylnitrile as verified by thin layer chromatography atop reverse phase silica gel 60Å plates (Fisher). The reaction mixture was extracted three times into ether. After drying over sodium carbonate, the ether was removed leaving yellow orange crystals. The crystals were dissolved in ammonia-saturated ethanol. A water Rainey 2800 Nickel solution 50%(v/v) (Aldrich) was added and hydrogen added to the closed pressure vessel. After shaking for 16 hours, the final product was filtered and dried *in vacuo*. The orange oil was then purified by vacuum distillation, collecting the fraction that came over at 80-84° C at 3 mtorr. The product, ferrocenylethylamine, was

verified by proton NMR and GC-MS. The overall yield was 81% of dark orange oil.

For high T_c superconductor pellet synthesis, Y_2O_3, $BaCO_2$, CuO, $CaCO_2$, and La_2O_3 were purchased from Alfa Aesar or Strem with purities greater than 99.99%.

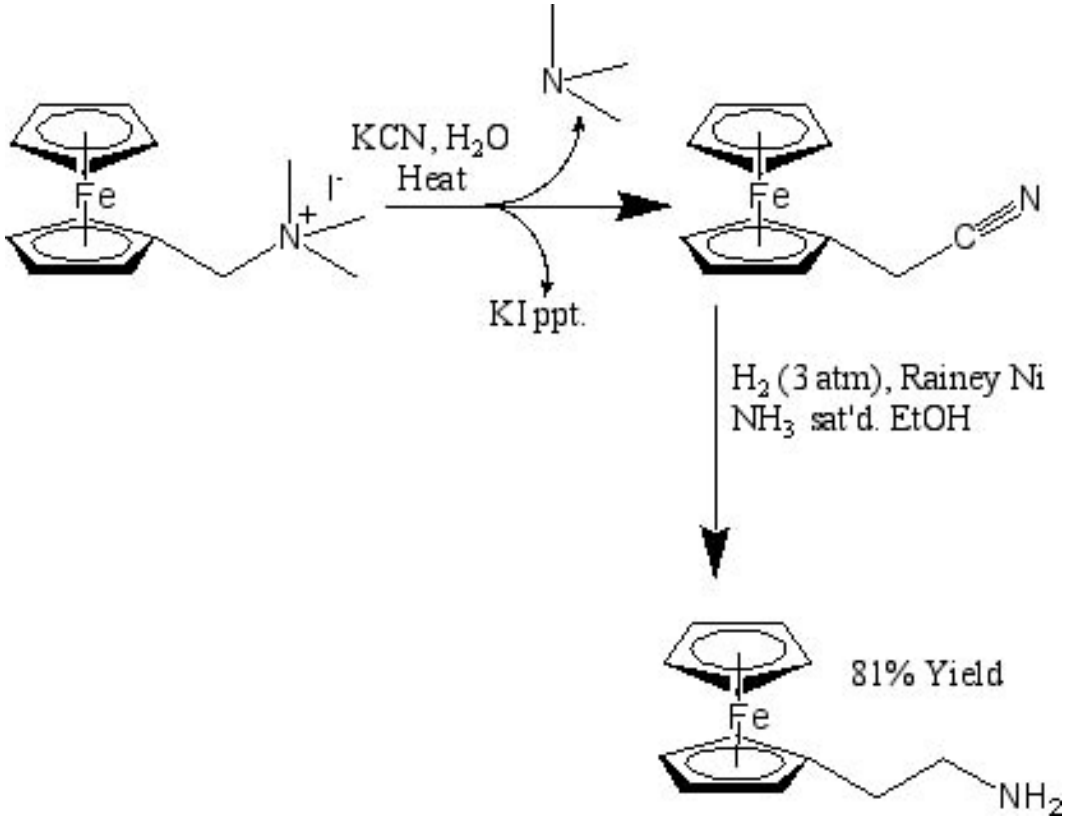

Figure 2.2 Synthesis of ferrocenylethylamine

2.2 METHODS AND PROCEDURES

This section will familiarize the reader with the details of the experimental techniques employed in the research described in this dissertation.

2.2.1 Monolayer Adsorption

For protection of cuprate superconductors, self-assembled monolayers have been show to prevent corrosion. The examination of the formation and kinetics of monolayers is described in chapters 4 and 5, respectively. Monolayer adsorption experiments were performed by soaking the substrates in ~1 mM solutions of the adsorbate of interest in either hexanes unless specifically stated. Monolayer formation proceeded for at least 18 hours. Upon removal from solution, substrates were rinsed by immersion in baths of pure solvent in order to remove any physisorbed reagent. If outside the inert atmosphere box, the films were dried in a stream of dry nitrogen. Analysis was performed immediately afterwards. If the samples were prepared inside the glove box, drying was accomplished by touching the edge of the film with a Kimwipe to allow capillary action to draw the remaining solvent off the film.

2.2.2 X-ray Photoelectron Spectroscopy

In a typical experiment, samples were affixed to the stage using copper clips or an aluminum mask screwed to the sample. This method of attachment provided continuous electrical contact to minimize charging of the film and the resulting shift of the peaks of interest. Any charging that occurred could be neutralized with a beam of argon ions. The reported peak positions are adjusted to place the C (1s) peak at 284.6 eV. Air sensitive samples were transferred

without exposure from either dry box in a special transfer vessel. All experiments were performed in a two-step process. An initial survey scan from 1440 eV to 0 eV was used to look for unusual contamination. A follow-up high-resolution scan was performed to examine peaks of interest.

All samples were measured with the monochromatic aluminum x-ray irradiation (Al Ka 1486.6 eV). For survey scans were performed beginning at 1400 eV and proceeding to 0 eV with a step size of 0.4 eV and integration time of 200 msec. The pass energy, used to retard the photoelectrons to a constant energy, is 93.9 eV. For high resolution scans, the step size is decreased to 0.1 eV and the integration time is increased to 1 sec. The pass energy is lowered to 11.75 eV.

2.2.3 Electrical Measurements

In order to measure the quality of the films deposited in the chamber, the transition temperature of the superconductor must be known. The deposition and characterization of films as determined by the resistivity and transition temperatures will be described in Chapter 3. Resistivity measurements are critical to characterization of the quality of the superconductivity samples. The position and width of the critical temperature transition provides a benchmark of the samples quality. Increases in room temperature resistivity after chemical modification can also indicate damage to the sample.

Electrical measurements were performed using a 4-terminal direct current transport method in either a linear or square geometry. In these measurements, the four terminals are placed an equal distance apart and the voltage measured as

current is applied. In these systems, voltage offsets can occur at the junction of two dissimilar materials. This offset artifact is removed from the measurement by alternating the direction of the current and averaging the measured voltages. These pseudo AC measurements give resistances of the films that are then converted to resistivities, which allow comparison of films of different thicknesses.

For 4 point measurements, a system was built that interfaced a Lakeshore 330 temperature controller, a Keithley 220 programmable current source and a Keithley 182 digital voltmeter. The two current source contacts and two voltage probes were passed to a Keithley 7001 switch system that allowed the geometry of the system to be modified by the controlling computer system. Given 4 fixed electrical contacts to the sample, the system switched which pins were current or voltage (Figure 2.3). The resistivity of the sample is then given by the equation developed by Van der Pauw, where d is the thickness of the film and f is a functional ratio of R1 to R2.

$$\rho = \frac{\Pi d}{\ln 2}\frac{(R_1 + R_2)}{2} f\left(\frac{R_1}{R_2}\right) \qquad \text{Eq 2.1}$$

In practical use, f becomes a correction factor extractable from numerous sources of solid state physics texts. [3-6]

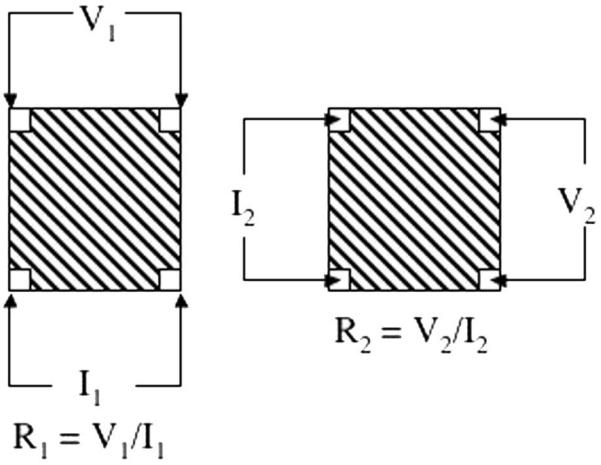

Figure 2.3 Illustration of Van der Pauw geometry for resistivity measurements

2.2.4 Electrochemical Measurements

All electrochemical measurements were performed using a CH Instruments model 660A potentiostat. Platinum wire (99.99% purity, Strem Chemicals) was used as the auxiliary electrode in all experiments. Prior to use, the platinum electrode was prepared by repeatedly cycling the electrode to hydrogen evolution potentials in concentrated sulfuric acid, followed by rinsing in nanopure water and drying in a stream of nitrogen. A silver/silver oxide (Ag/AgO) quasi-reference electrode (99.99% purity, Strem Chemicals) was utilized in all experiments. The Ag/AgO electrode was prepared prior to use by either immersion in concentrated nitric acid or 30% hydrogen peroxide until a whitish-grey layer was visible. The electrode was then rinsed with nanopure water and dried under flowing nitrogen. All electrochemical measurements were performed in a 0.1 M tetrabutylammonium hexafluorophosphate (TBAPF6) supporting

electrolyte in acetonitrile. A dilute ferrocene solution (~0.1 mM) was used to measure the voltage offset of our reference electrode.

2.2.5 X-ray Diffraction Measurements

X-ray diffraction measurements were performed on both bulk and thin film superconductors to study crystal orientation and verify phase purity. Two different diffractometers were used. Earlier studies were conducted using a Philips Electronic Instruments powder diffractometer with Cu K_α illumination. Later experiments were performed on a Bruker-Nonius D8 Advance Theta-2Theta powder diffractometer (Madison, WI). Typical scans, using a Cu source were measured from 10-60° 2Θ in 0.01 steps with 1 second integration time. Example diffraction patterns will be used in chapter 3 to display the crystalline orientation of thin films.

This chapter has described the methods of preparation and examination of high temperature superconductive films used throughout this dissertation. Having explained the methods creating and characterizing bulk and thin film superconductors, the emphasis of this work will shift to the creation and optimization of a pulsed laser deposition system (Chapter3) and the mechanism and kinetics of formation of self-assembled monolayers atop high-T_c cuprates in Chapters 4 and 5, respectively. This chapter serves to summarize the materials and experimental conditions for reference in the more technical sections that follow. The deposition conditions described above describe the ideal settings for the beginning of the PLD optimization. The XPS measurements were used to characterize the surface cleanliness of the thin films analyses in Chapters 3 and 4.

The electrochemical measurements were used to analyze the adsorption kinetics in Chapter 5. Having summarized the methods used, the focus of this work will now shift to the experimental conclusions.

2.3 REFERENCES

(1) Kamigaki, K.; Terauchi, H.; Terashima, T.; Bando, Y.; Iijima, K.; Yamamoto, K.; Hirata, K.; Hayashi, K.; Nakagawa, I.; Tomii, Y. *Journal of Applied Physics* **1990**, *69*, 3653-3662.

(2) Bourdillon, A.; Bourdillon, N. X. T. *High Temperature Superconductors: Processing and Science*; Academic Press, Inc.: New York, 1994.

(3) Kittle, C. *An Introduction to Solid State Physics*; John Wiley & Sons, Inc.: New York, 1976.

(4) Van der Pauw, L. J. *Philips Technical Review* **1958**, *20*, 220-224.

(5) Van der Pauw, L. J. *Philips. Res. Repts* **1958**, *13*, 1-9.

(6) Eom, C.-B.; Murduck, J. M. In *Handbook of Thin Film Devices Volume 3: Superconducting Film Devices*; Francombe, M. H., Ed.; Academic Press: San Diego, 2000, pp 1-33.

(7) Jenkins, R.; Snyder, R. L. *Introduction to x-ray powder diffractometry*; Wiley - Interscience, 1996.

(8) Sands, D. E. *Introduction to Crystallography*; Dover Publications Inc.: New York, 1975.

3 Development of a Novel Pulsed Laser Deposition System

3.1 INTRODUCTION

High quality superconductor devices suitable for use in commercial applications require new processing methods capable of controlling the interfacial properties of these reactive high-T_c systems. Many literature sources now document the corrosion reactivity of the cuprate systems upon exposure to water, CO, CO_2 and acids.[1-22] The McDevitt group has focused on creating a suitable "toolbox" of protective reagents and lattice dopants to control these reactions in the bulk material and at the interfaces on the atomic level.[23-28] In order to understand the effect of these tools, pristine surfaces are required for the surface chemistry and subsequent surface analysis. To generate suitable films for study, a novel pulsed laser deposition system has been built to allow wet chemistry on pristine superconductor surfaces. Although there are literally thousands of PLD systems around the world, the vast majority of these systems do not allow for the transfer of deposited films from the deposition chamber into an inert atmosphere glove box for later analysis. Most other deposition chambers are either opened directly to the atmosphere, or connected to expensive ultra high vacuum systems where the films are transferred between analysis and deposition chambers. The ability to perform typical wet chemistry free of corrosion may be unique to the system here described.

In this chapter, the creation of the required substrate heater and load lock system will be discussed, as will the optimization of film deposition parameters. Both topics are important for research into the interfacial control of high

temperature superconductors. The ability to create high quality films is essential for comparison to bulk materials and eventual incorporation into analytical and electronic devices. The ability to handle these films is essential for the establishment of a clean, corrosion free baseline for the surface studies performed relating to corrosion and the self-assembly mechanism. The first section of the chapter will focus on the development of the PLD system, followed by an analysis of the optimum deposition conditions.

3.2 DEPOSITION AND INERT ATMOSPHERE PROCESSING STATION

The majority of the chamber and attached glove box was purchased from Neocera, Inc. in Beltsville, Maryland in conjunction with MBraun of Stratham, New Hampshire. The 18-inch diameter dual beam chamber is manufactured from SS316 stainless steel with 7 large conflat ports arranged around the equator of the sphere. A fused quartz window for beam access to the target covers one. Another positions the target carousel at a 45° angle to the beam port. Two other ports provide access to the chamber either from the atmosphere or from the glovebox. The remainders of the ports are used as viewports to monitor the deposition. On the top of the chamber a differentially pumped 10-inch rotatable conflat allows positioning of the suspended substrate assembly to face either the target or the other access hatches. The seal at the top of the chamber is viton while all other seals are copper gaskets. A Pfeiffer TMP520 turbo pump for corrosive gas applications is attached to 8-inch rotatable conflat at the bottom of the chamber. Backed by an oil free diaphragm pump, the system base pressure is less than 5×10^{-6} torr. The general layout of the system can be seen in Figure 3.1.

Pressure is measured via a Granville-Philips convectron gauge in the mtorr range, and cold cathode gauge below 10^{-3} torr. Both gauges are capable of handling the corrosive oxygen atmosphere and the particulates generated during the PLD process.

Oxygen is bled into the system through a fine needle valve and a flow meter at rates of 30-40 sccm. The background pressure is fine tuned by varying the speed of the turbo pump between 100-800 Hz. This dual control provides a stable base pressure within 1 mtorr of the desired pressure.

The attached glove box is an Mbraun Unilab model with an oil free pumping system using Varian scroll pumps. The oil free pumps were chosen to allow the entire system to be as clean as possible. The only source of contamination has been particulates from the chamber entering the glovebox during transfer of the deposited films. A 6-inch double-sided conflat port was welded to the back of the glove box to which a connecting tube and access hatch were attached. On the front face of the glove box, a rotary magnetic manipulator from Thermionics Northwest (Port Townsend, WA) was installed allowing a transfer arm to reach into the chamber when the hatch was open.

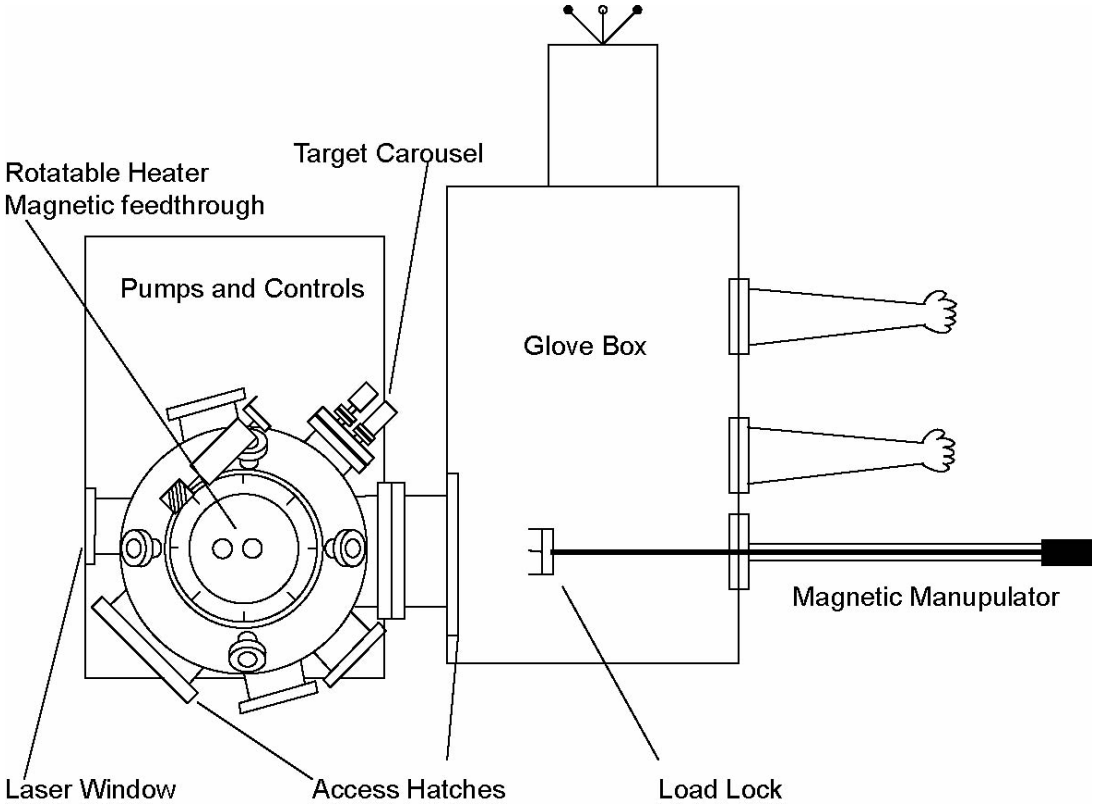

Figure 3.1 Schematic layout of the deposition chamber and attached glovebox

While Neocera provides quality products and is the only known commercial manufacturers of substrate heaters suitable for PLD in an oxygen atmosphere, certain deficiencies exist in the system when load–locking of the substrates is desired. Typical substrate heating is accomplished by attachment to a nickel block brazed to a special Inconel sheathed resistive heater. These heaters provide a uniform temperature across the face of the heater within ±5° C. Atop the heater, the substrates are silver painted to the block for the best heat transfer. Resistive heaters are used due to the high temperatures (>850° C) required to provide sufficient atom mobility for the formation of the HTSC lattice. Most other commercially available heaters are either simple resistive elements, or quartz heating lamps that are unsuitable for our purposes. Most commonly used resistive elements, nichrome, tungsten, or pyrolitic boronitride covered graphite, oxidize rapidly in the partial pressure of oxygen used during deposition. The quartz lamps also commonly used are incapable of providing enough heat to the substrates.

3.2.1 Substrate Heater

As described in the introductory material relating to PLD in Chapter 1, the temperature of the substrate plays a critical role in the quality of the final film. A good substrate heater is essential to provide sufficient thermal motion for the plume species to migrate atop the substrate into the correct lattice position. Because of the repeated failures of the purchased heaters, and the inability of other commercially manufactured heaters to maintain the desired temperature in an oxidizing atmosphere, we have designed and constructed our own heaters from

the same Inconel sheathed resistive elements used by Neocera. The geometry used is different in that no nickel block is brazed to the surface. Our heater relies on radiation to heat the substrates that are attached to a removable nickel platen. The sheathed resistive elements are available from ARI Industries of Addison, Illinois. They consist of a heated section of nickel wire surrounded by 99.4% pure MgO inside an Inconel sheath. Our sheathing is a special formulation of Inconel that allows continuous operating temperatures of 1050° C. This high temperature allows the substrates placed less than 1 cm away to reach surface temperatures in excess of the desired 850°C. From in house measurements, using both attached thermocouples and a pyrometer, the surface of the heater is found to be ~100° less than the temperature of the heating coil depending on the oxygen partial pressure. A model 304 PID controller from Eurotherm runs the ramping and temperature profile of the heater as measured by a stainless steel sheathed K-type thermocouple in contact with the resistive heating element. A second thermocouple stationed behind the element provides a secondary reading to ensure that the heater is not heated past its degradation point. Omega Engineering supplies both thermocouples. As will be seen below, this heater arrangement supplies sufficiently uniform heat to allow precise control of the substrate temperature and in turn deposition of high quality thin films.

3.2.2 Substrate Platen

Rotation of the substrates is useful for the high throughput generation of high quality cuprate films. Prior to this system, our lab produced only two to four films a day using a Neocera flat plate heater. The high thermal mass of the

system provided a very uniform film, but prevented quick cooling of the system (*vide infra*). The fixed geometry required that the positioning of the substrates be directly in the plume of materials in order to achieve the desired stoichiometry. The position is crucial due to the angular distribution of species in the plume due to scattering as mentioned previously. By rotating the substrate, larger numbers of substrates are exposed to the plume as they rotate through. The constant rotation also evens out any inhomogeneity of the plume, since on average, all substrates will sample all sections of the plume as they pass through repeatedly.

The substrate platen rotation is possible since the platen attaches to a "can" that rotates independently of the fixed heater inside, Figure 3.2. This can is supported from the rear on a stainless steel tube held in place by special ceramic bearings in cooled bearing races. The original bearings and housing, as designed by Neocera, were stainless steel microminiaturized assemblies in uncooled raceways. Due to the high temperature of the heating element and the heat flow back through the assembly, the bearings quickly oxidized and failed, usually within 15-20 depositions. To circumvent the bearing failure, a water-cooled bearing raceway was built; and special silicon nitride bearings are used, Figure 3.3 and Figure 3.4. The bearings are available from Champion Bearings of Palm Springs, California. The SiN balls in the bearing assembly are specifically undersized to allow for heat expansion without seizing. They are also specially coated using a titanium implantation process to provide a dry anti-friction surface. The bearings have only been replaced once in the last 3 years since the undersized balls were chosen.

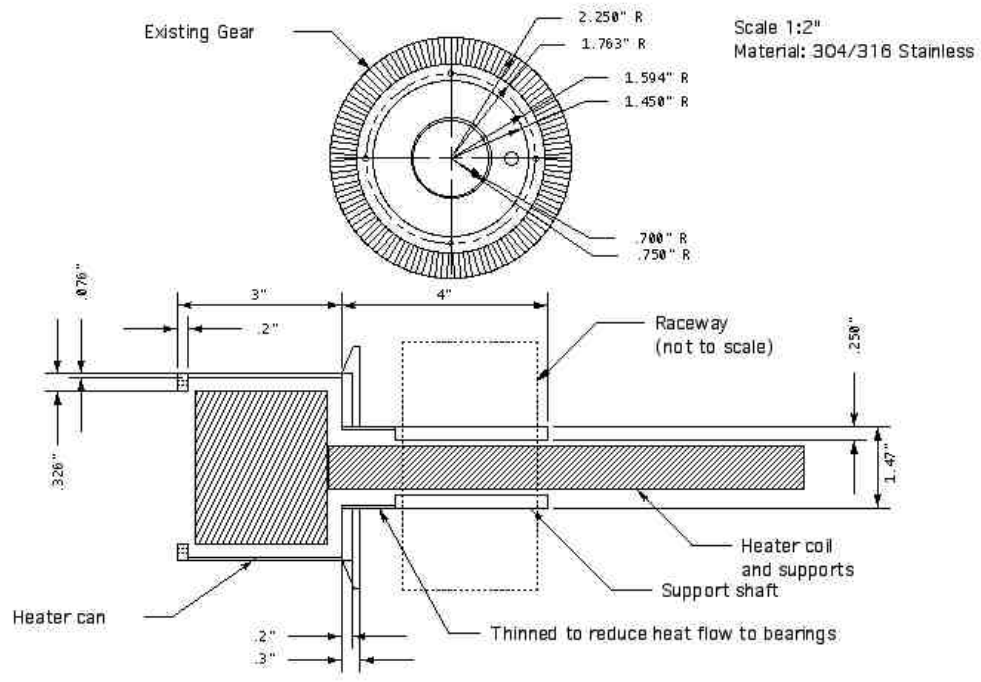

Figure 3.2 Gear driven assembly or "can" used to provide rotation of the substrates through the laser plume

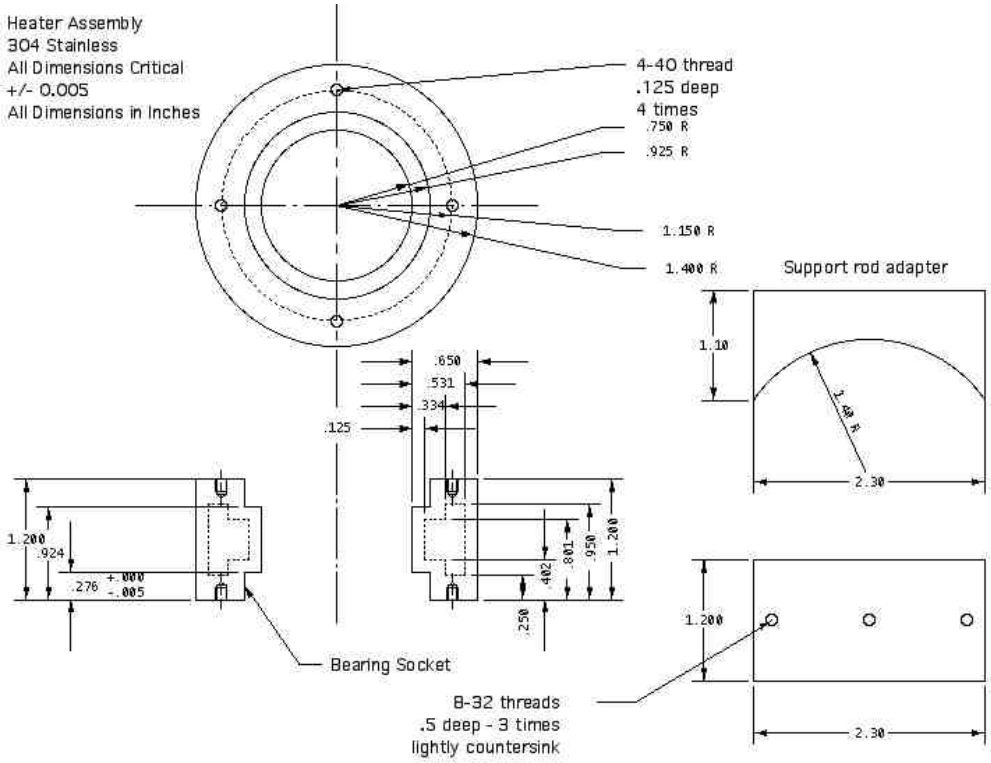

Figure 3.3 General schematic of the cooled raceway built to provide water cooling to the bearings

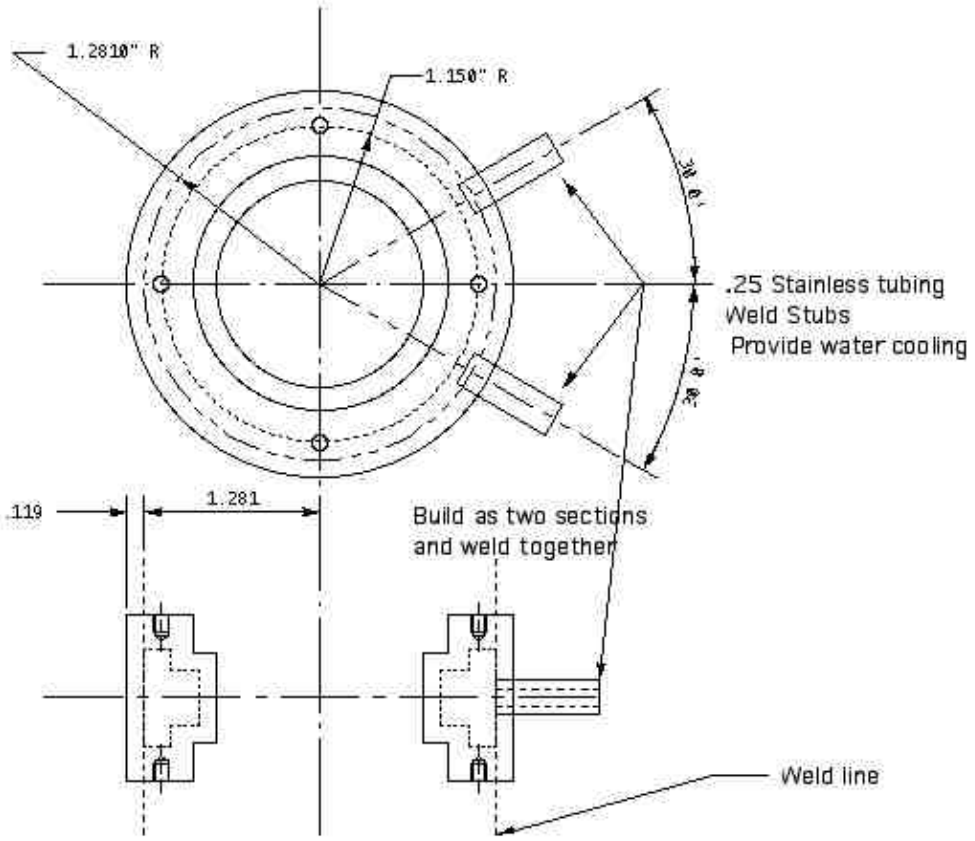

Figure 3.4 Raceway showing position of water inlets for interior cooling

The water-cooling of the raceway housing serves two purposes. First, the cooling helps to extend the life of the bearings in the system. Second, the cooling actively lowers the temperature of the heater assembly after deposition by carrying away heat from the system. This allows for a more rapid cool down after annealing the films and increases the throughput of the system, allowing three deposition cycles to be completed in an 8-hour period.

Rotation is driven through a geared assembly attached to a magnetic rotary motion feedthroughs (Magidrive) built by UHV Designs of England. These feedthroughs were chosen over traditional wobble bar drives due to their ability to slip and their high torque capability. Should the gears seize, as occasionally happened when the ball bearings failed, the feedthrough slips instead of failing, resulting in greater cost savings over the lifetime of the instrument.

Once the rotary motion problems were solved, the ability to load lock films was addressed. The original load lock system consisted of spring steel clips attached to the outside of the rotating can that grip the platen in specially cut grooves. While this system works well for lower temperatures (<250° C) common in most ultra high vacuum systems they failed miserably in our system. The expansion of the spring steel and the weakening of the steel due to repeated thermal cycling resulted in clips that were too pliable. As was often the case, the platens would fall from the heater at deposition temperatures. The author investigated multiple geometries before the final design was built. In this assembly, the platen is attached to a transfer puck that is externally threaded with a coarse 12 turns per inch pitch. A similar internally threaded holder that attaches

to the can was built. Both of the threads are cut deeper than the recommended depths to allow for expansion due to heating during deposition. By allowing for the expansion, the load lock system has yet to freeze together. The schematics of both the male and female load lock parts are shown in Figure 3.5 and Figure 3.6.

After design and construction of this heater, the load lock system, and the removable platen, the necessary modifications to the chamber were complete. The optimization of the deposition conditions was begun to permit the deposition, surface modification and analysis of pristine films of high temperature superconductors.

3.3 OPTIMIZATION OF DEPOSITION CONDITIONS

While the problems of the rotary heater and load lock were being addressed, the deposition parameters of the system were being optimized to provide the best possible films. The conditions within our control are the laser energy density, the oxygen partial pressure, the target to substrate distance and the substrate temperature.[29] All play an important role in the quality of the films.

Research by others suggests that it is possible to deposit large area films atop single substrates by PLD.[30-44] As mentioned previously, rotation of the target is

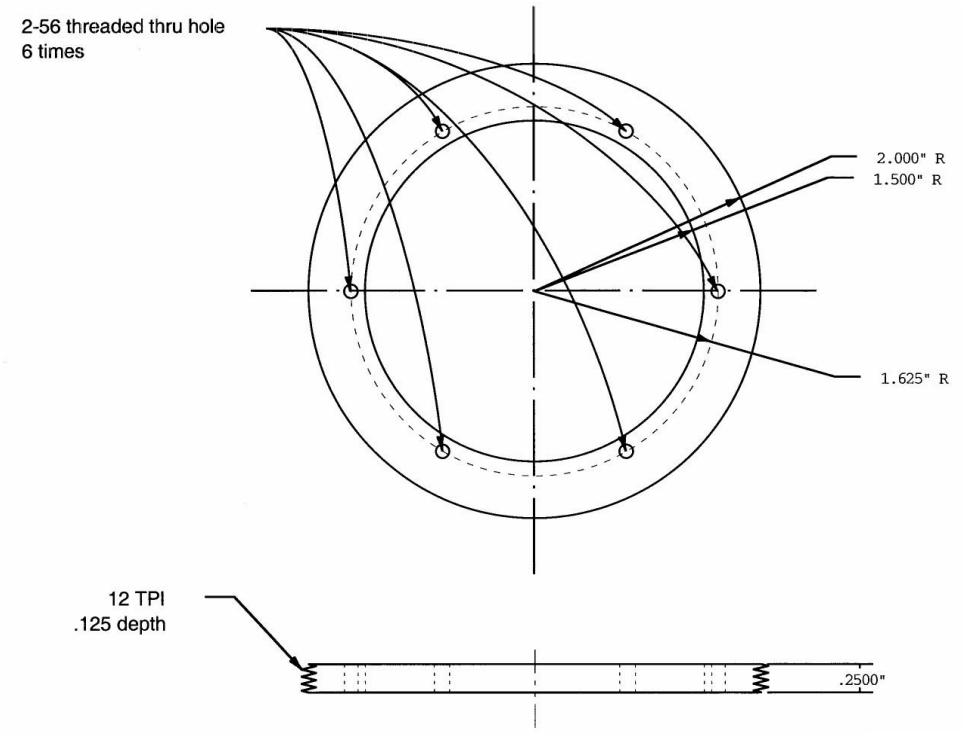

Figure 3.5 Male part of load lock system. Three of the holes are used to mount the sample platen while the remaining three are available for the load lock arm to insert holding pins into for removal from the heater.

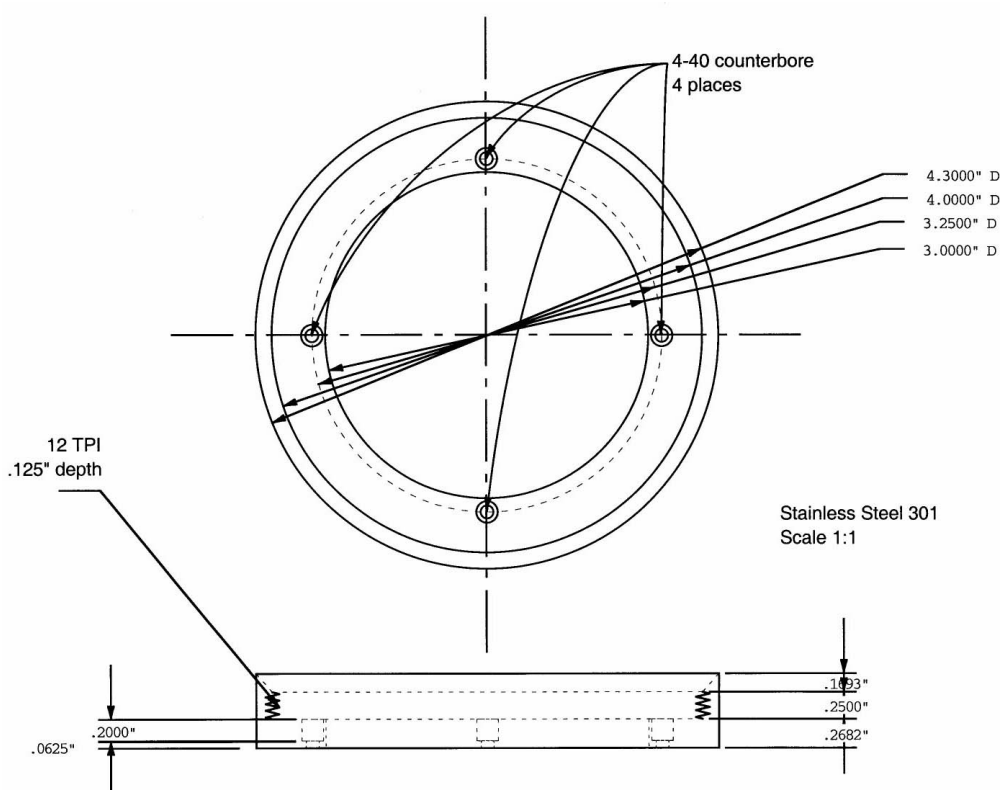

Figure 3.6 Female portion of the load lock system. The four holes are used to mount the load lock portion to four matching holes in the rotatable heater can.

necessary and has been discussed. According to Heinsohn and others, the optimal distance from substrate to target is approximately 10 centimeters for large area substrates[45-47]. In our work we, were unable achieve superconductive films at any distance greater than 5 centimeters. All of the optimization described was conducted at this distance.

Prior work in our lab by Dr. Jiani Zhao, and by other researchers[33,36,37,39,46-49], established a range of starting values for the temperature, oxygen pressure, and laser power to produce ideal films. Literature procedures suggest temperatures between 650°C and 850°C, while the highest T_c and c-axis orientation occur at temperatures higher range of this window. The original *in situ* deposition by Venkatesan suggest a heater temperature of 800°C leading to a substrate temperature of ~700-750°C by their estimation[46,50]. Thus, 750°C was chosen as an initial starting point for the depositions. The same work suggests 250 mtorr as a suitable oxygen pressure. The laser power was not mentioned, but a study of the effects of laser fluence upon $YBa_2Cu_3O_{7-\delta}$ deposition suggest that the lower threshold for ejection of material occurs near 1 J/cm[251]. Increasing the fluence only increases the deposition rate and may lead to increased outgrowths in the film[45]. Accordingly, laser energies near 6 J/cm2 (~200 mJ at the target) were used as starting points.

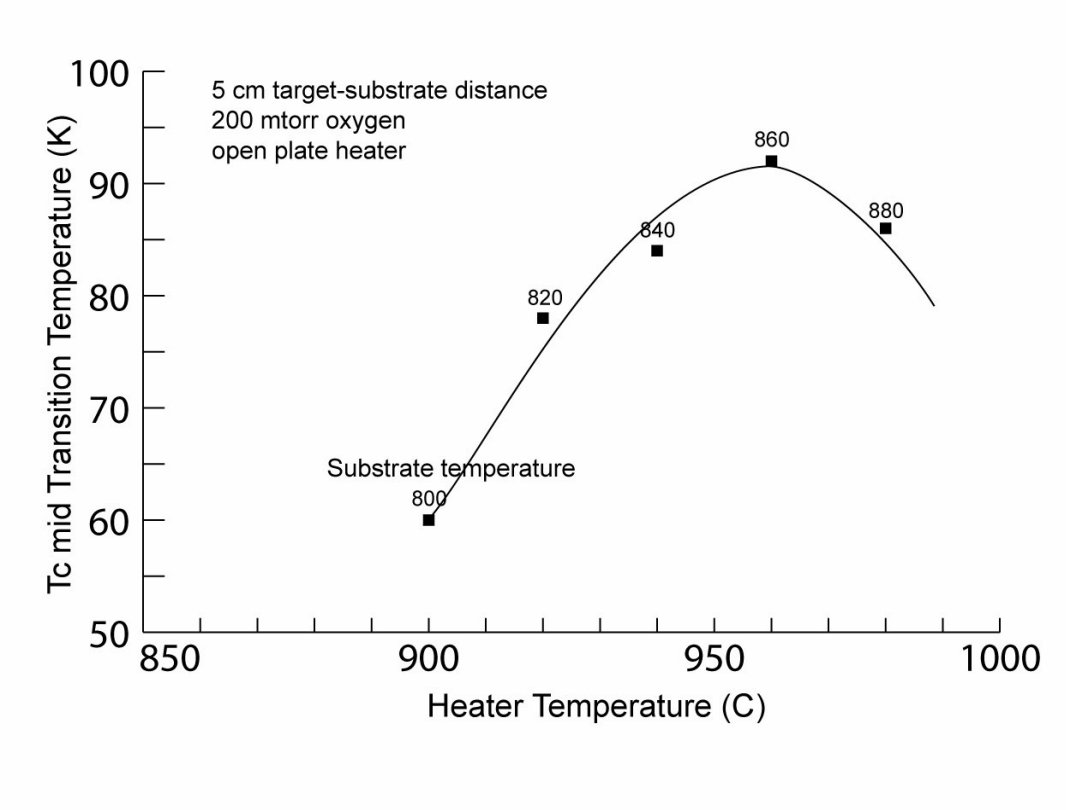

Figure 3.7 Effect of substrate temperature on critical temperature of superconductor. The X-axis is the temperature as set in on the heater controller. The data labels are the temperature of the platen as recorded using an optical pyrometer.

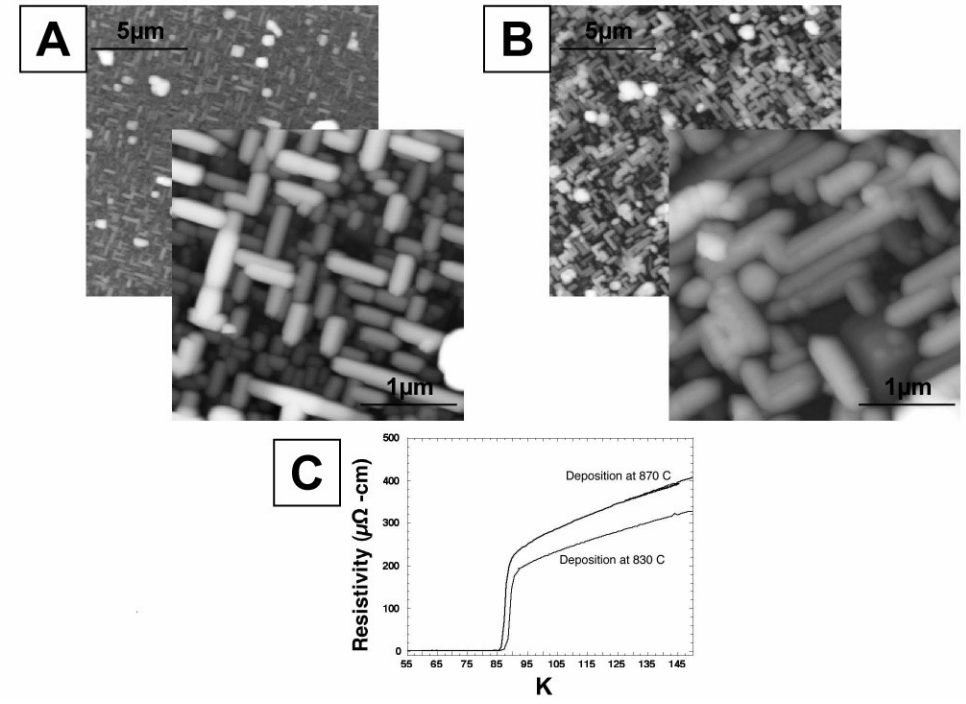

Figure 3.8 Effect of changing temperature on final film quality as visualized by atomic force microscopy. The difference in surface roughness can be seen for the change in temperature as measured by the optical pyrometer from 830°C (A) to 870°C (B). The laser power was 300 mJ with an oxygen pressure of 200 mTorr for both samples. The small change in transition temperature of the films can be seen in (C)

First the laser energy was varied to achieve a plume of the correct dimensions, meaning sizable enough to nearly touch the substrates. This required raising the energy of the laser to near 300 mJ. Subsequent resistivity analysis of the films proved that the substrate temperature was too low, as all the films were semiconducting. Upon raising the heater temperature, superconducting films formed, but with low transition temperatures. Analysis of the proper temperature was conducted; with the best T_c found to be 92 K for a substrate temperature of 800° C as measured by the pyrometer, Figure 3.7. The decrease of T_c at higher temperatures is to be expected given the decrease in supersaturation at the surface and subsequent changes to the structure of the films. Unintended cuprate supercondcutor/substrate interactions also occur at higher temperatures, compromising the properties of the cuprate material, lowering T_c.

Once the optimal deposition temperature window was found, optimization of crystalline orientation began. As can be seen in Figure 3.8, small changes in temperature have large visible effects in the morphology of the films. The herringbone structures in both atomic force microscopy images are characteristic of the a-b axis oriented films. The increase in the amount cross-hatching upon increasing the temperature to 870°C suggests a decrease in the temperature is needed.[36,40,46]

While still staying near the present temperature window, the effect of varying laser power was studied. As can be seen in the two powder XRD's in Figure 3.9, small changes in the energy also affect the crystallinity of the final film. Noticeably absent from the deposition at higher energy (B) are the large

peaks associated with the (010) and (020) reflections. Data acquired here suggest that a change equivalent to 20% of the energy fluence can have a large effect on the final morphology.

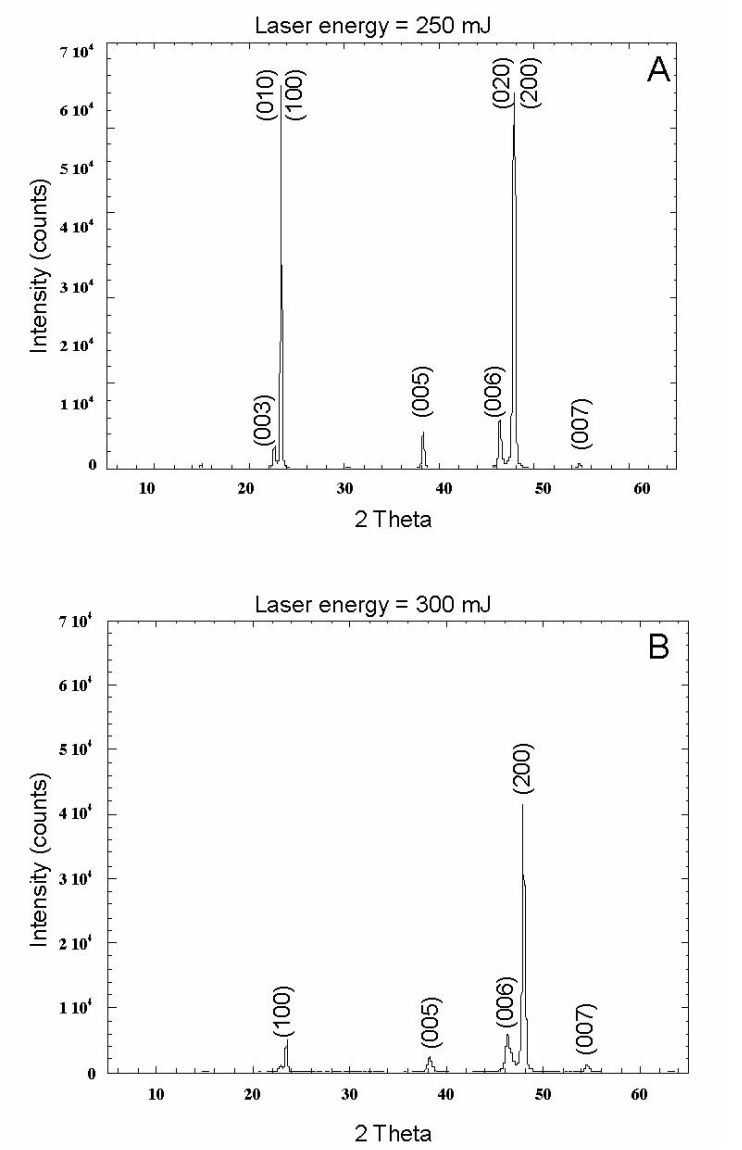

Figure 3.9 Effect of changing laser power on film orientation. For both samples, the deposition temperature was 930°C on the controller and 830°C at the substrate. The oxygen partial pressure was established at 200 mTorr. The samples are the same thickness (1500Å). The only difference between the two sample is in the laser energy used during the deposition. In A, the laser energy was 250 mJ leading to a predominantly a/b axis orientation. In B, the laser energy of 300 mJ leads to a decrease in b-axis orientation.

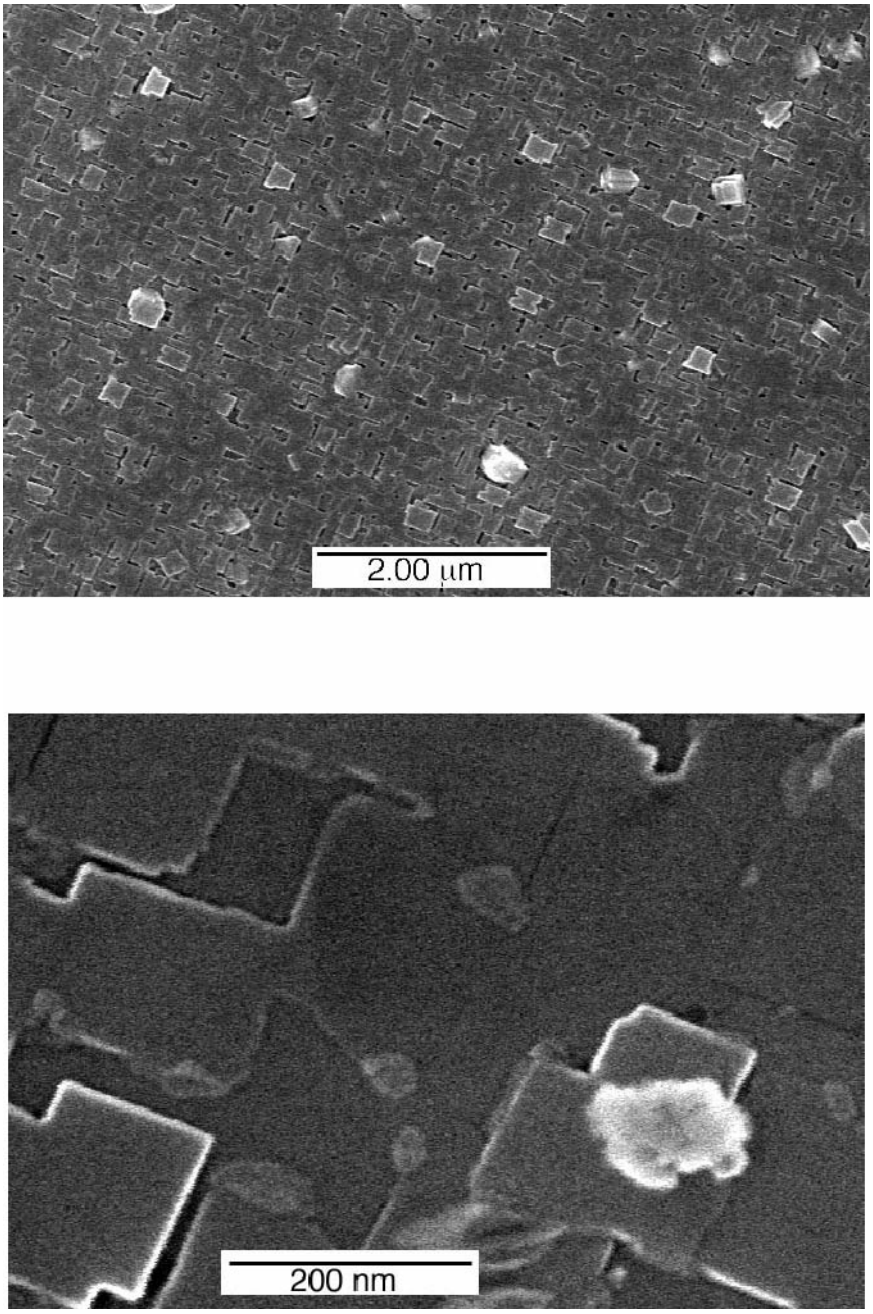

Figure 3.10 Field emitting scanning electron micrographs at both low and high magnification of c-axis $YBa_2Cu_3O_{7-\delta}$

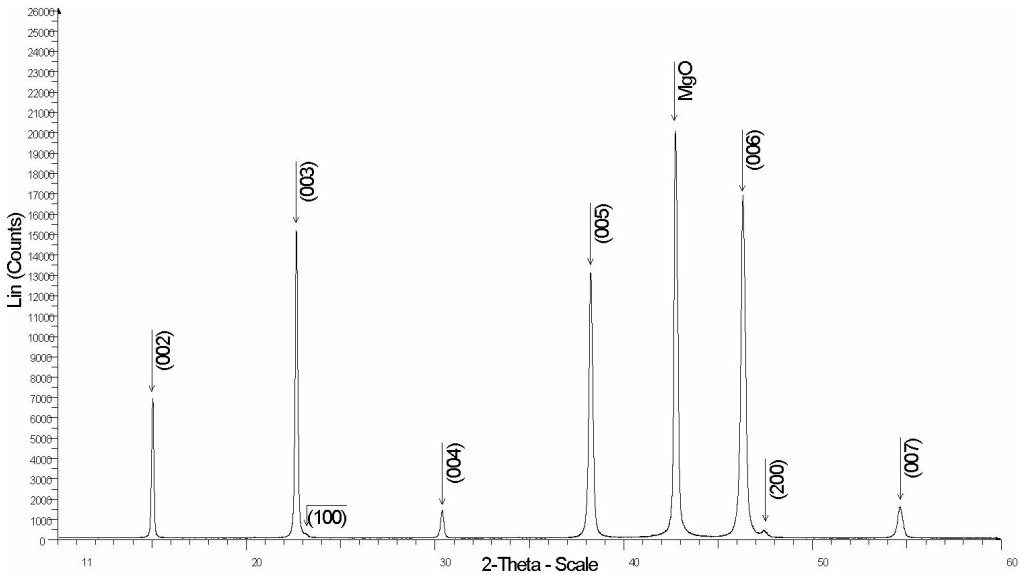

Figure 3.11 Powder x-ray diffraction of c-axis orientation epitaxial $YBa_2Cu_3O_{7-\delta}$ thin film. This film was deposited atop an MgO substrate at 830° C as determined using optical pyrometry. The laser energy was set at 425mJ at 8 Hz, with an oxygen pressure of 200 mTorr.

Continued optimization (actually a requirement after every modification to the heater that involved changing the heater coil) led to the creation of smooth (001) oriented films as verified by XRD and electron microscopy. The transition temperatures of these films approaches the maximum for bulk $YBa_2Cu_3O_{7-\delta}$ materials ranging from 88K to a high of 92K. The electron micrographs for a representative sample of these films are shown in Figure 3.10. None of the (100) and (010) cross-hatching can be seen and only a few odd angled out growths are evident. The deposition conditions for these films follow. The laser power here was set 425 mJ and a repetition rate of 8 Hz. The oxygen pressure was established at 200 mtorr. XRD confirms the c-axis orientation of the films as deposited as shown in Figure 3.11. The (00l) reflections dominate with only a fraction of the (h00) peaks visible. The (0k0) peaks are obscured by the (003) and (006) reflections.

3.4 SURFACE ANALYSIS OF PRISTINE FILMS

In order to test the ability of our system to provide pristine films, we have compared our films to those known to have never been exposed to ambient conditions. Work by Behner and others has demonstrated the XPS signature of pristine and reconstructed $YBa_2Cu_3O_{7-\delta}$ surfaces[52-55]. These indicators are used to gauge qualitatively the amount of surface corrosion. As seen in Table 3.1, the signals different chemical species peaks can be assigned and used to monitor the quality of the surface[53,54].

Table 3.1 Literature XPS peak assignments for $YBa_2Cu_3O_{7-\delta}$ films[53,54]

Core level	Peak Energy	Assignment
Y $3d_{5/2}$	~156 eV	Y in superconducting $YBa_2Cu_3O_{7-\delta}$
Ba $3d_{5/2}$	~780 eV	$YBa_2Cu_3O_{7-\delta}$
	~777 eV	Barium Oxides, Carbonates
C 1s	286.4 eV	Hydrocarbons (Reference peak)
	~288-291 eV	Carbonates
O 1s	~529 eV	O in superconducting $YBa_2Cu_3O_{7-\delta}$
	~ 531 eV	O on surface $YBa_2Cu_3O_{7-\delta}$, Carbonates

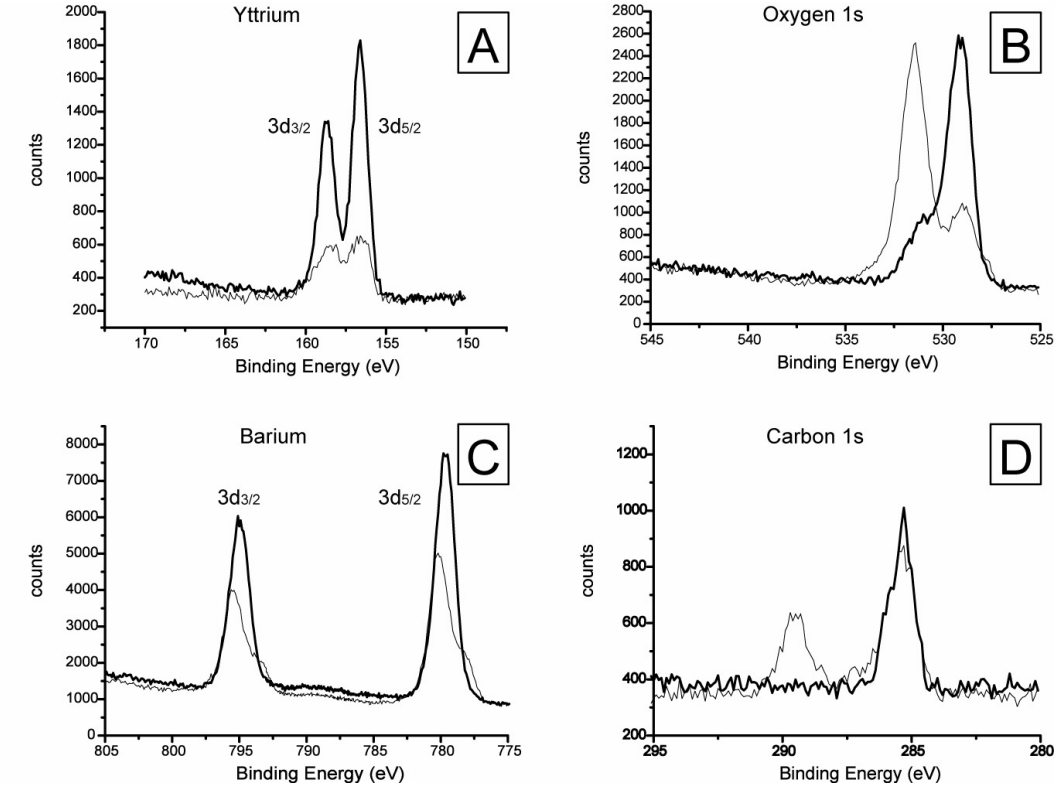

Figure 3.12 XPS spectra of $YBa_2Cu_3O_{7-\delta}$ samples in pristine condition and after 24 hours of exposure to atmosphere. The heavier line is for the pristine sample and the lighter line is for the exposed sample

One of the best ways to gauge the amount of corrosion atop a film is through XPS analysis. For this experiment, films were load-locked directly from the chamber into a nitrogen filled glove box. In this glove box, the films were rapidly transferred into a vacuum transfer vessel for transport to the XPS system and subsequent analysis. After acquiring the spectra for a pristine sample (heavy lines in Figure 3.12) the sample was exposed to ambient atmosphere for a period of 24 hours (fine lines in Figure 3.12). By comparing the pristine spectra to those of the exposed sample, the changes that occur upon exposure are evident. In panel A, the $Y3d_{5/2}$ and $Y3d_{3/2}$ signals indicate only a single chemical environment, with the signal decrease being attributed to covering corrosion. The O 1s signal shift in panel B is indicative of the corrosion of the film. The low energy peak is consistent with bulk oxygen in $YBa_2Cu_3O_{7-\delta}$ and the high-energy peak is assigned to corrosion products and surface species, mostly carbonates, as determined from the literature and reference spectra taken from known corrosion products.[52-55] This increase in surface corrosion is also indicated in the Ba 3d signals in panel C. The low energy shoulder is assigned to carbonates and other barium oxides that form upon corrosion. The shift of the main peak to higher energy is consistent with an increase in surface barium[52]. The formation of carbonates upon exposure is indicated in D, the C 1s signal. The peak at 284.6 is used as the internal reference for the binding energy. This peak is ubiquitous given the oil present in the vacuum system of the XPS system. The tell tale corrosion peak that serves as the best indicator is the carbonate peak at ~290 eV due to the presence of barium carbonates.

The ability of our system to provide pristine thin films has been shown. Comparisons of our spectra to those provided in the literature suggest that this system provides the same quality of surface cleanliness as those formed and manipulated under ultra high vacuum. The films deposited and processed within the described integrated PLD/glove box system yield surface characteristics similar to pristine $YBa_2Cu_3O_{7-\delta}$ films. The peak shapes and positions are identical within a few tenths of an electron volt. Unlike the reference system utilized by Behner, we have the added capability of performing "wet" chemistry atop our films at ambient pressures in an inert atmosphere glove box with minimal exposure to corrosion inducing materials.

3.5 CONCLUSION

By judicious modification of the PLD chamber, a system for deposition and ambient pressure processing of high temperature superconductor thin films has been created. The system is capable of providing corrosion free c-axis films of superconductors. The system in its current state is more mechanically robust and reliable than as purchased. With the ability to create pristine films, the effects of self-assembly and the processes involved can be examined, minimizing the influence of the corrosion overlayer.

3.6 REFERENCES

(1) Rosamilia, J. M.; Miller, B.; Schneemeyer, L. F.; Waszczak, J. V.; O'Bryan, H. M., Jr. *Journal of the Electrochemical Society* **1987**, *134*, 1863-1864.

(2) Bachtler, M.; Lorenz, W. J.; Schindler, W.; Saemann-Ischenko, G. *Modern Physics Letters B* **1988**, *2*, 819-828.

(3) Bachtler, H.; Lorenz, W. J.; Schindler, W.; Saemann-Ischenko, G. *Journal of the Electrochemical Society* **1988**, *135*, 2284-2287.

(4) Dou, S. X.; Liu, H. K.; Bourdillon, A. J.; Tan, N. X.; Zhou, J. P.; Sorrell, C. C.; Easterling, K. E. *Modern Physics Letters B* **1988**, *1*, 363-367.

(5) Kirschner, I.; Trager, T.; Matrai, J.; Porjesz, T.; Gyorgy, J. *Physica C: Superconductivity and Its Applications (Amsterdam, Netherlands)* **1988**, *153-155*, 1419-1420.

(6) Liu, H. K.; Dou, S. X.; Bourdillon, A. J.; Sorrell, C. C. *Superconductor Science and Technology* **1988**, *1*, 194-197.

(7) McDevitt, J. T.; McCarley, R. L.; Dalton, E. F.; Gollmar, R.; Murray, R. W.; Collman, J.; Yee, G. T.; Little, W. A. *ACS Symposium Series* **1988**, *377*, 207-222.

(8) Fitch, L. D.; Burdick, V. L. *Journal of the American Ceramic Society* **1989**, *72*, 2020-2023.

(9) Jandl, S.; Banville, M.; Dufour, P.; Gagnon, R. *Solid State Comm.* **1989**, *70*, 337-340.

(10) Jin, S.; Liu, L.; Zhu, Z.; Huang, Y. *Solid State Comm.* **1989**, *69*, 179-182.

(11) Lyon, S. B.; Lau, H. L.; Newman, R. C.; Thompson, G. E.; Hepburn, B. J.; Alford, N. *Superconductor Science and Technology* **1989**, *2*, 107-110.

(12) Jin, S.; Zhu, Z.; Liu, L.; Huang, Y. *Solid State Comm.* **1990**, *74*, 1087-1090.

(13) Riley, D. R.; McDevitt, J. T. *Journal of Electroanalytical Chemistry and Interfacial Electrochemistry* **1990**, *295*, 373-384.

(14) Barkatt, A.; Hojaji, H.; Michael, K. A. *Corros. Glass, Ceram. Ceram. Supercond.* **1992**, 548-582.

(15) Chandler, G. T. *Corros. Glass, Ceram. Ceram. Supercond.* **1992**, 583-600.

(16) Hepburn, B. J.; Lau, H. L.; Lyon, S. B.; Newman, R. C.; Thompson, G. E.; Alford, N. *Corrosion Science* **1992**, *33*, 515-525.

(17) Zhou, J. P.; McDevitt, J. T. *Chem. Mat.* **1992**, *4*, 953-959.

(18) Goddard, D. T.; Lyon, S. B.; Hepburn, B. J. *Corrosion Science* **1993**, *35*, 761-766.

(19) Zhou, J. P.; Riley, D. R.; McDevitt, J. T. *Chem. Mat.* **1993**, *5*, 361-365.

(20) Desai, V. H.; Sundaram, K. B. *Physica Status Solidi A: Applied Research* **1994**, *143*, 109-116.

(21) Ben Azzouz, F.; M'Chirgui, A.; Ben Salem, M.; Yangui, B.; Nitsche, S.; Lamine, C.; Boulesteix, C. *Superconductor Science and Technology* **2000**, *13*, 1214-1221.

(22) Judge, E.; Markert, J. T. *Physica C: Superconductivity and Its Applications (Amsterdam)* **2000**, *341-348*, 417-420.

(23) McDevitt, J. T.; Mirkin, C. A.; Lo, R.-K.; Chen, K.; Zhou, J.-P.; Xu, F.; Haupt, S. G.; Zhao, J.; Jurbergs, D. *Chem. Mat.* **1996**, *8*, 811-813.

(24) Mirkin, C. A.; Xu, F.; Zhu, J. *Adv. Mat.* **1997**, *9*, 167-172.

(25) Ritchie, J. E.; Wells, C. A.; Zhou, J.-P.; Zhao, J.; McDevitt, J. T.; Ankrum, C. R.; Jean, L.; Kanis, D. R. *J. Am. Chem. Soc.* **1998**, *120*, 2733-2745.

(26) Ritchie, J. E. In *Department of Chemistry and Biochemistry*; University of Texas at Austin: Austin, Texas, 1998, p 166.

(27) Ritchie, J. E.; Murray, W. R.; Kershan, K.; Diaz, V.; Tran, L.; McDevitt, J. T. *J. Am. Chem. Soc.* **1999**, *121*, 7447-7448.

(28) Wells, C. A. In *Department of Chemistry and Biochemistry*; University of Texas at Austin: Austin Texas, 1999, p 176.

(29) Foltyn, S. R.; Muenchausen, R. E.; Dye, R. C.; Wu, X. D.; Luo, L.; Cooke, D. W.; Taber, R. C. *Appl. Phys. Lett.* **1991**, *59*, 1374-1376.

(30) Schey, B.; Bollmeier, T.; Kuhn, M.; Biegel, W.; Stritzker, B. *Review of Scientific Instruments* **1998**, *69*, 474-476.

(31) Tian, Y. J.; Linzen, S.; Schmidl, F.; Cihar, R.; Seidel, P. *Superconductor Science & Technology* **1998**, *11*, 59-62.

(32) Bollmeier, T.; Biegel, W.; Schey, B.; Stritzker, B.; Diete, W.; Kaiser, T.; Mueller, G. *Journal of Alloys and Compounds* **1997**, *251*, 176-178.

(33) Lorenz, M.; Hochmuth, H.; Natusch, D.; Boerner, H.; Lippold, G.; Kreher, K.; Schmitz, W. *App. Phys. Lett.* **1996**, *68*, 3332-3334.

(34) Boerner, H.; Hochmuth, H.; Schurig, T.; Quan, Z.; Lorenz, M. *Fresenius' Journal of Analytical Chemistry* **1995**, *353*, 619-624.

(35) Greer, J. A.; Tabat, M. D. *Journal of Vacuum Science & Technology, A: Vacuum, Surfaces, and Films* **1995**, *13*, 1175-1181.

(36) Lorenz, M.; Hochmuth, H.; Boerner, H.; Natusch, D. *Physica C: Superconductivity (Amsterdam)* **1994**, *235-240*, 639-640.

(37) Lorenz, M.; Hochmuth, H.; Borner, H.; Natusch, D.; Kreher, K. *Mat. Res. Soc. Symp. Proc.* **1994**, *341*, 189-194.

(38) Greer, J. A. *Pulsed Laser Deposition Thin Films* **1994**, 293-311.
(39) Lorenz, M.; Natusch, D.; Boerner, H.; Hochmuth, H.; Unger, K. *Appl. Supercond., [Pap. Eur. Conf.], 1st* **1993**, *1*, 601-604.
(40) Lu, H. B.; Xu, S. F.; Tian, Y. J.; Cui, D. F.; Chen, Z. H.; Zhang, Y. Z.; Li, L.; Yang, G. Z. *Journal of Superconductivity* **1993**, *6*, 335-337.
(41) Greer, J. A. *Journal of Vacuum Science & Technology, A: Vacuum, Surfaces, and Films* **1992**, *10*, 1821-1826.
(42) Muenchausen, R. E.; Cooke, D. W.; Foltyn, S. R.; Wu, X. D.; Nogar, N. S. *Physica C: Superconductivity and Its Applications (Amsterdam, Netherlands)* **1991**, *190*, 46-49.
(43) Foltyn, S. R.; Muenchausen, R. E.; Dye, R. C.; Wu, X. D.; Luo, L.; Cooke, D. W.; Taber, R. C. *App. Phys. Lett.* **1991**, *59*, 1374-1376.
(44) Davis, M. F.; Wosik, J.; Forster, K.; Deshmukh, S. C.; Rampersad, H. R.; Shah, S.; Siemsen, P.; Wolfe, J. C.; Economou, D. J. *Journal of Applied Physics* **1991**, *69*, 7182-7188.
(45) Heinsohn, J.-K.; Reimer, D.; Richter, A.; Subke, K.-O.; Schilling, M. *Physica C* **1998**, *299*, 99-112.
(46) Inam, A.; Rogers, C. T.; Ramesh, R.; Remshnig, K.; Farrow, L.; Hart, D.; Venkatesan, T.; Wilkens, B. *Applied Physics Letters* **1990**, *57*, 2484-2486.
(47) Dijkkamp, D.; Venkatesan, T.; Wu, X. D.; Shaheen, S. A.; Jisrawi, N.; Min-Lee, W. L.; McLean, W. L.; Croft, M. *Applied Physics Letters* **1987**, *51*, 619-621.
(48) Shokoohi, F. K.; Schiavone, L. M.; Rogers, C. T.; Inam, A.; Wu, X. D.; Nazar, L.; Venkatesan, T. *Appl. Phys. Lett.* **1989**, *55*, 2661-2663.
(49) Zhao, J.; Jurbergs, D.; Yamasi, B.; McDevitt, J. T. *J. Am. Chem. Soc.* **1992**, *114*, 2737-2738.
(50) Pique, A.; Harshavardan, K. S.; Moses, J.; Mathur, M.; Venkatesan, T.; Brasunas, J. C.; Lakew, B. *Applied Physics Letters* **1995**, *67*, 1920.
(51) Foltyn, S. R.; Muenchausen, R. E.; Estler, R. C.; Peterson, E.; Hutchinson, W. B.; Ott, K. C.; Nogar, N. S.; Hubbard, K. M.; Dye, R. C.; Wu, X. D. *Materials Research Society Symposium Proceedings* **1990**, *191*, 205.
(52) Aarnink, W. A. M.; Gao, J.; Rogalla, H.; van Silfhout, A. *Applied Surface Science* **1992**, *55*, 117-133.
(53) Behner, H.; Ruhrnschopf, K.; Rauch, W.; Wedler, G. *Applied Surface Science* **1993**, *68*, 179-188.
(54) Behner, H.; Ruhrnschopf, K.; Wedler, G.; Rauch, W. *Physica C* **1993**, *208*, 419-424.

(55) Frank, G.; Zeigler, C.; Gopel, W. *Physical Review B* **1991**, *43*, 2828-2834.

4 Alkyl amine self-assembly atop superconductors: surface etching and monolayer formation

4.1 INTRODUCTION

The development of monolayer adsorption chemistry becomes increasing important for a number of practical and fundamental reasons. As commercialization of high-T_c materials occurs, the modification of these corrosion prone materials using "soft chemical" methods becomes increasingly important. While the adsorption chemistry is well understood for many metal, semiconductor and insulator materials, expansion into the realm of superconductors has not been elucidated to the same degree. Prior work by the McDevitt group at the University of Texas and the Mirkin group at Northwestern University has shown that amine containing reagents form monolayers that exhibit a high degree of conformational order on c-axis oriented $YBa_2Cu_3O_{7-\delta}$ films.[1-7]

Monolayers atop superconductors are interesting for many reasons. They provide a means to prevent corrosion of the material[1-3,8], and also allow the development of new molecular based superconductor devices[9-13]. However, while much is known about the resulting order and properties of these monolayers[5], little is understood about the mechanism of adsorption, especially atop superconductors that have been exposed to ambient conditions.

In this chapter, amine adsorbate molecules will be studied in their role to alter the exterior region of the prototypical cuprate, $YBa_2Cu_3O_{7-\delta}$. Both surface sensitive methods such as XPS and electrochemistry along with solution phase

measurements are exploited to study the interaction between amine moieties and the high temperature superconductor lattice. In order to exploit the chemistry of self-assembly, the mechanism of adsorption needs to be better understood. The two main theories for the formation of $YBa_2Cu_3O_{7-\delta}$ / alkyl amine structures will be examined and evidence for the removal of corrosion products will be presented.

4.2 SELF-ASSEMBLY ATOP SUPERCONDUCTORS

The key elements of these spontaneous adsorptions as described earlier, are the head group interaction with the substrate ($YBa_2Cu_3O_{7-\delta}$) and the Van der Waals attraction of the long alkyl chains. The chemisorption of the head group will be discussed first.

The head group interaction provides the majority of the driving force for the formation of the monolayer. Energetically, the pinning of the SAM molecule to a specific site in the lattice results is the most exothermic process. The chemical bond that forms can range from purely ionic in the case of carboxylic acids attached to silver, to the covalent, as in the case of Si-O bonds formed from silanes attached to silicon surfaces. The most studied interaction, that of thiols on gold, yields a slightly polar covalent bond with energies on the scale of ~40-45 kcal/mol[14,15]. This exothermic adsorption process leads to the molecules trying to maximize coverage by binding to all accessible binding sites, forcing already adsorbed molecules together on the surface.[16]

The head group interaction in alkylamine/superconductor structures mimics the traditional Werner complexes in that a lone pair from the alkyl amine

"ligand" donates electron density to the copper sites in the $YBa_2Cu_3O_{7-\delta}$ lattice. This dative bond is formed exothermically according to modeling[7] and the energies have yet to be measured. Attempts at measuring the energy of adsorption have been performed using thermogravimetric analysis (TGA), but the alkyl amine reagents decompose prior to desorption[6].

Once the materials are chemisorbed to the substrate, the molecules are close enough that van der Waals forces act to crystallize the monolayer. These exothermic attractive forces are generally less than 10 kcal/mol, but can be greater when polar groups are embedded in the chains leading to electrostatic attraction[16]. Computational studies by Cyndi Wells in the McDevitt group estimated that the van der Waals forces are expected to be about –8.8 kcal/mol in the ideal geometry atop $YBa_2Cu_3O_{7-\delta}$.[5]

Experimentally, the McDevitt group has shown that effective persistent monolayer structures adsorb onto numerous phases of high temperature superconductors including: $YBa_2Cu_3O_{7-\delta}$, $Y_{0.6}Ca_{0.4}Ba_{1.6}La_{0.4}Cu_3O_{7-\delta}$, and $Tl_{1.4}Ba_2CaCu_3O_{7-\delta}$. Molecular reagents with reactive functional groups were electrochemically tagged to determine which reactive groups spontaneously adsorb atop superconductors.[1,2,8] Amine and amide groups were found to be more persistent than the tested thiols, hydroxides, and phospines. The amine reactivity towards the surface was found to be dependant upon the degree of substitution around the amine nitrogen, with primary amines adsorbing better than secondary and tertiary amines. This ordering is assumed to be a result of the closer head group packing atop the cuprate superconductor minimizing steric interference. In

work done by Ritchie and Wells, the ordering of the monolayer was experimentally and computationally determined. From the calculations, a $\sqrt{2}x\sqrt{2}$ R45° overlayer structure was found to provide the lowest energy for the adsorbed structure. An organized monolayer motif has been been experimentally confirmed using grazing angle FTIR spectroscopy on thin films[5], and the intermolecular distance confirmed by atomic force measurements atop single crystal samples[17]. The expected structure can be seen in Figure 4.1.

The basic features of the packing of the adsorbate monolayers has been shown previously to be independent of the solvent used (hexanes, ethanol, acetonitrile, hexadecane).[6,7] However, this observation says nothing of the mechanism of adsorbate layer formation. Rather, this FTIR data shows that the final structures of the monolayers are similar, not that the process of formation is similar. Important thermodynamic differences that influence the mechanism may exist and require further study to determine this issue more carefully. With this caveat in mind, the following experiments were undertaken in hexanes, and the process may or may not occur in a similar manner in other solvents.

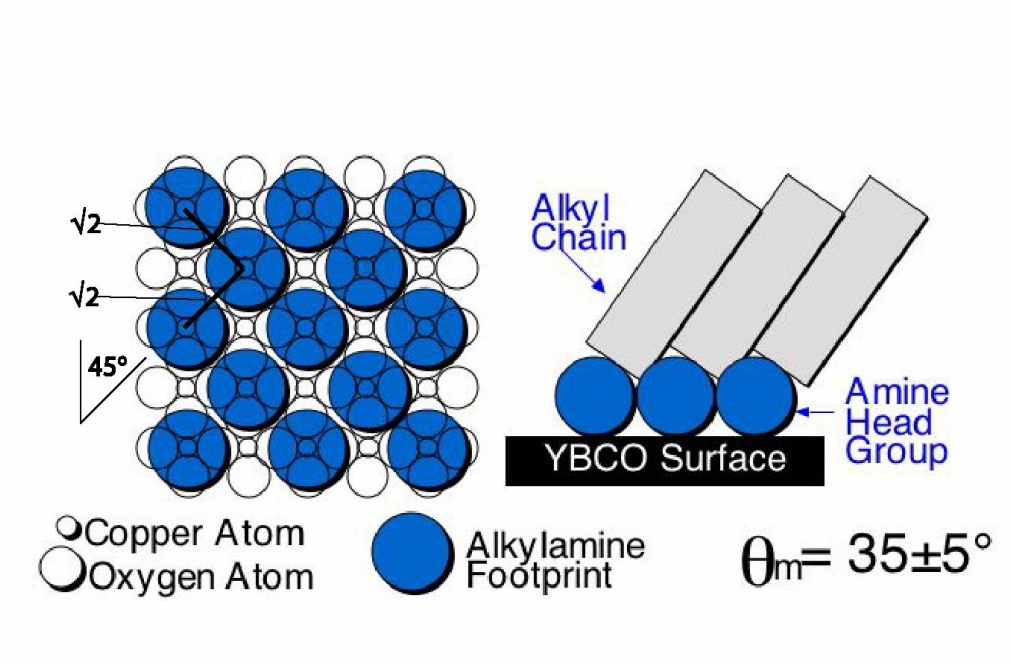

Figure 4.1 Alkylamine adsorption atop $YBa_2Cu_3O_{7-\delta}$. The $\sqrt{2}x\sqrt{2}$ distance of the amines can be seen, as well as the 45° rotation of the overlayer with respect to the $YBa_2Cu_3O_{7-\delta}$ lattice. The θ_m angle of 35±5° refers to the lowest energy tilt angle of the alkyl tails normal to the surface.

4.3 MECHANISM OF ADSORPTION

While much is known about the ordering of monolayers atop cuprate superconductors, little of the mechanism of formation is understood. Assuming a pristine surface, it is reasonable to expect that the nitrogen lone pairs of the amine would have no problem donating to the vacant copper sites. This idealized model would result in no noticeable change in the surface of the superconductor or the electrical properties of thin films.

Mirkin and co-workers at Northwestern have proposed a mechanism involving the oxidation of the amines to imines prior to deposition as shown in

Figure 4.2 A and B. In addition it is proposed that the surface region of the superconductor becomes reduced due to the oxidation of the alkylamines (Figure 4.2 C). The resulting oxygen deficient layer becomes the substrate for further amine monolayer formation (Figure 4.2 D). The evidence given by Mirkin for this mechanism was based on the mass spectra evidence of imines in the solution used to form the SAM originally.[18,19]

Absent from the Mirkin proposal is the role of surface damage of the reactive cuprate compound prior to amine exposure. Indeed, given the highly reactive nature of the films, the absence of corrosion products atop the films is difficult to achieve. As explained previously, the surface of superconductors corrodes rapidly upon exposure to ambient conditions leading to the tell tale signature of barium carbonate crystals. Due to this rapid corrosion, we propose here an alternate mechanism of SAM formation. According to our new model, the alkyl amines serve two chemically distinct roles. In the initial step, the degraded superconductor is etched away with the help of the amine reagent, (Figure 4.2 M). The etching process proceeds until a fresh superconductor film is presented for the assembly of the monolayer. The amine reagents aid this etching process by acting as ligands for the removed species, assisting the dissolution of corrosion species. (Figure 4.2, N, O). Once the surface is clean, the assembly of the monolayer proceeds to a point where the energetics of the monolayer are such that the process self-passivates, (Figure 4.2 P).

Evidence for the etching process and the self-passivation of the films will be presented below.

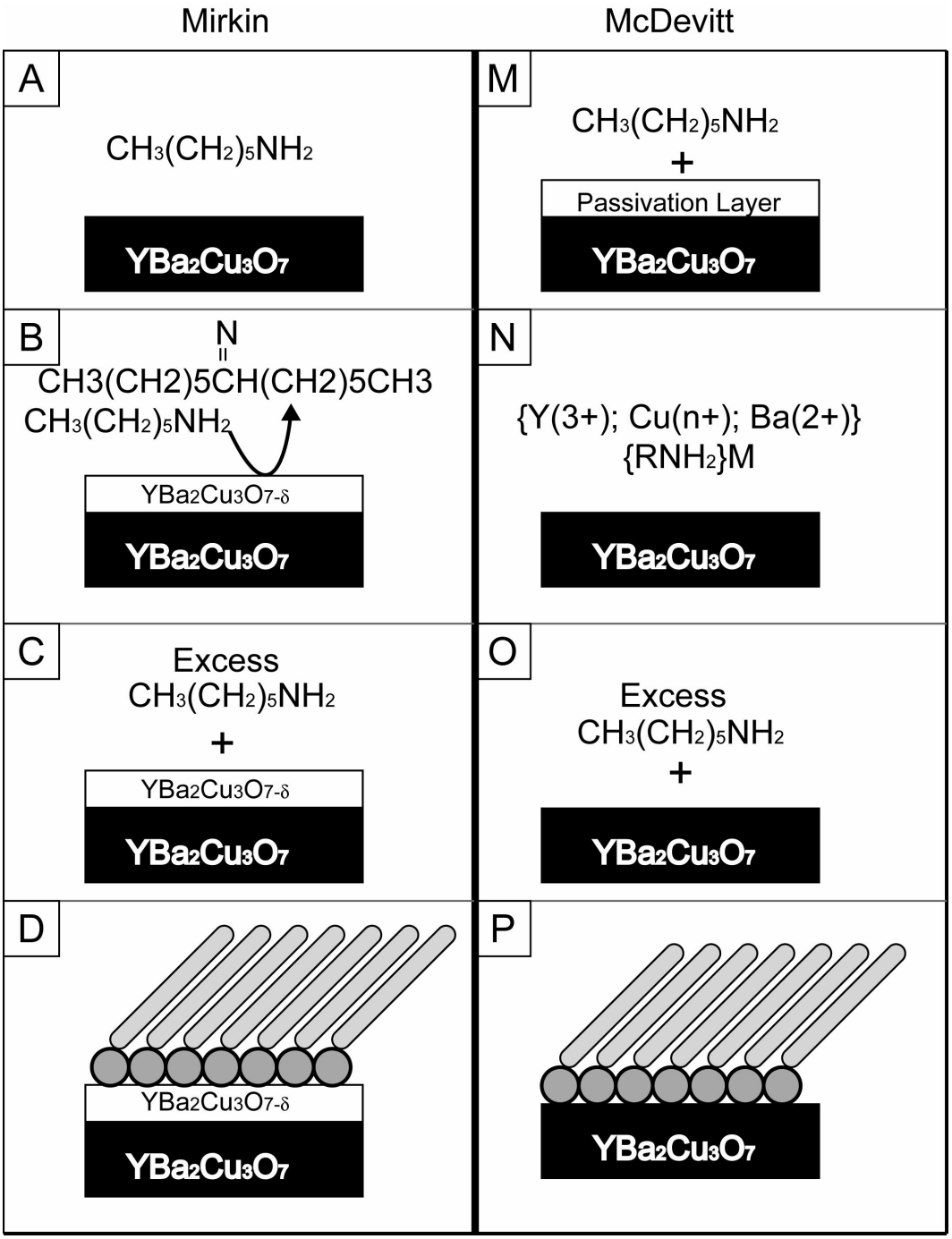

Figure 4.2 Mechanism of SAM adsorption atop YBCO. See text for explanation of individual steps.

4.4 EVIDENCE OF SURFACE CLEANING

The effect of alkylamine reagents to the surface of superconductive material is examined. Resistivity measurements indicate an increase in room temperature resistance and a decrease in the critical current suggesting that 5-10% of the material is removed from the samples.[20] These measurements hint at the processes involved and the removal of material from the surface, but direct evidence of the mechanism is desirable.

4.4.1 X-ray photoelectron spectroscopy

Numerous studies have described the chemical damage that occurs upon short atmospheric exposures[21-26]. These signals appear after as little as 2 minutes of exposure to atmosphere. Likewise, any plausible mechanism must take into account the corrosion of the surface. This degradation layer appears in the spectra in multiple ways, Figure 4.3 B. The corrosion is manifest as a broad multiplet in the Y (3d) region, the low energy humps attributed to $BaCO_3$ on the main peaks in the Ba (3d) area, and the carbonate peaks in the O (1s) and C (1s) spectra at ~531 eV and ~291 eV respectively. These spectral features are absent on pristine films where great care has been taken to prevent exposure (*vide supra*). Treatment with amine reagents

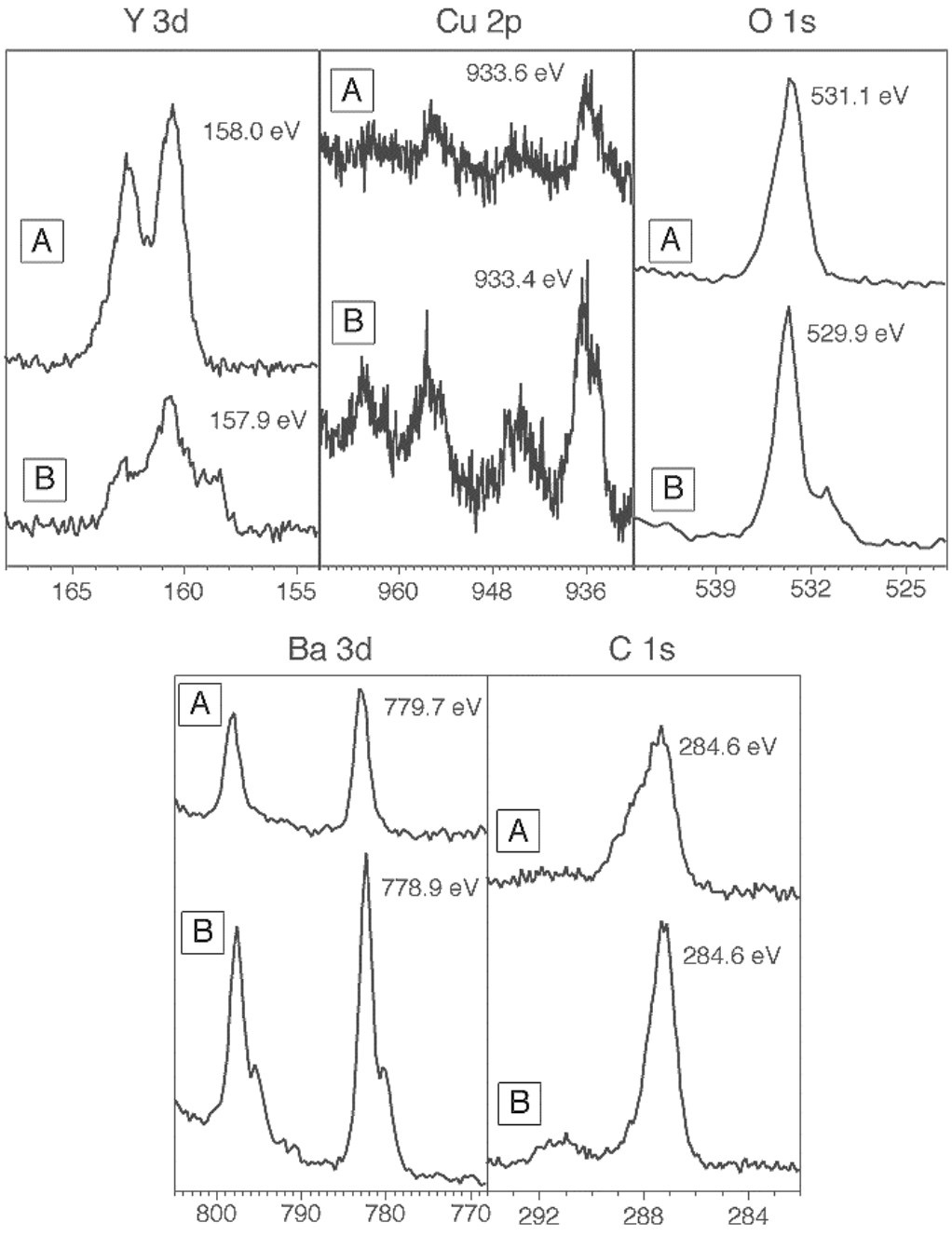

Figure 4.3 Demonstration of etching of $YBa_2Cu_3O_{7-\delta}$. Shown are the XPS spectra of the $YBa_2Cu_3O_{7-\delta}$ thin film before (B) and after (A) exposure to butylamine solution. In spectra (B), the degradation products before exposure can be noted on the film.

leads to a cleaner signal as shown in Figure 4.3 A. The "dirty" films from above were exposed to 2mM solutions of butylamine in hexanes for 12 hours. Noticeably, the Y (3d) area of the film has been returned to a doublet structure matching the pristine films described in the earlier chapter. In addition, the amine exposure removes most of the carbonate signature apparent in the Ba (3d), O (1s), and C (1s) spectra, Figure 4.3 A. These results suggest that even carefully prepared films are initially coated with corrosion products, and that after sufficient amine exposure; the amine reagent removes the majority of the surface layer.

The copper signal is also important in that is provides an indication of an overlayer. The satellite peaks on the high-energy side of the main Cu (2p) peaks are reduced upon self-assembly. The satellites are often called shake-up satellites and the result of multi-electron transitions[27]. The satellites are a result of the valence reorganization that occurs after the ejection of a core electron. Often a valence electron will be promoted to a higher unfilled level (the "shake-up") and then interact with another photoelectron to give the high-energy peak.

In some transition metals and rare earths, strong shake-ups occur as a result of the unpaired electrons in 3d and 4f orbitals. The explanation for these shake ups of greater than usual intensity is based on the final state of the atom and the ligand to metal charge transfer that occurs. In effect, after the photoelectron is ejected the metal atom extracts an electron from the ligand to close its shell compared to the original state. Literature uses this explanation to elucidate why a closed-shell system like a Cu^{2+} system ($3d^{10}$) does not have any shake up satellites

while an open-shell system like Cu^{1+} ($3d^9$) does. This would also work for the nominal Cu^{3+} ($3d^8$) used to justify the non-integer stoichiometry of the $YBa_2Cu_3O_{7-\delta}$[28], Figure 4.4 A.

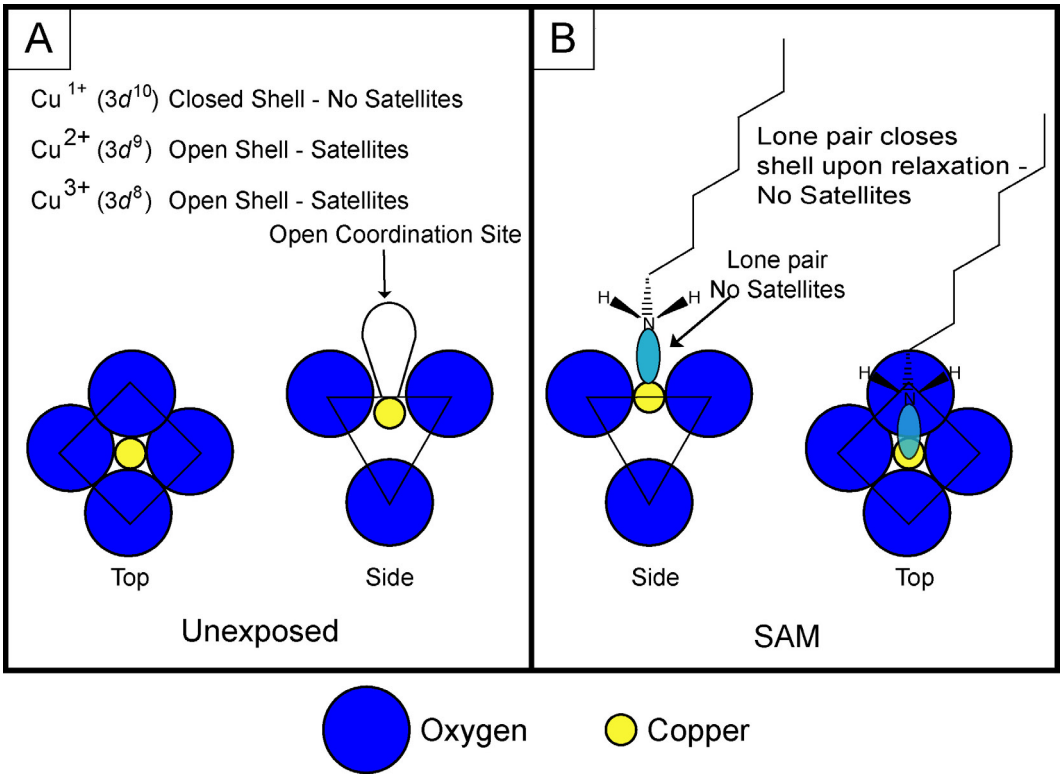

Figure 4.4 Schematic of amine bonding to copper site in $YBa_2Cu_3O_{7-\delta}$. Upon relaxation after ejection of the photoelectron, the closed shell systems are less likely to eject a second photoelectron, leading to fewer shake-up peaks. The amine-covered sites donate electron density to the copper in the final state effectively closing the shell.

Examining the Cu 2p spectra in Figure 4.3, it is reasonable to assume that the decrease in shake-up lines after exposure to amine solutions is a result of the adsorption of the amine reagent. Although not looking at the 3d shell, the entire system undergoes reorganization, so shake up peaks are expected. The amine acts

as a ligand and the lone pair of the nitrogen provides an extractable electron to close the shell of the copper after the initial excitation (Figure 4.4 B). This ligand is not present in the initial peak (Figure 4.3 Cu 2p spectra curve B), thus the increased intensity of the shake up. By ratioing the area of the satellite peak to the corresponding main peak a decrease of 18% is measured. While not a complete absence of shake-up peaks, the decrease is significant.

Presence of the alkylamine reagent is also shown with XPS spectra of the nitrogen 1s region, Figure 4.5. The dashed curve is the exposed film prior to self-assembly while the lighter solid curve is the nitrogen signal from the alkylamine monolayer. The nitrogen peak is a result of the amine adsorption, with the peak at ~399 eV attributable to amine nitrogen.

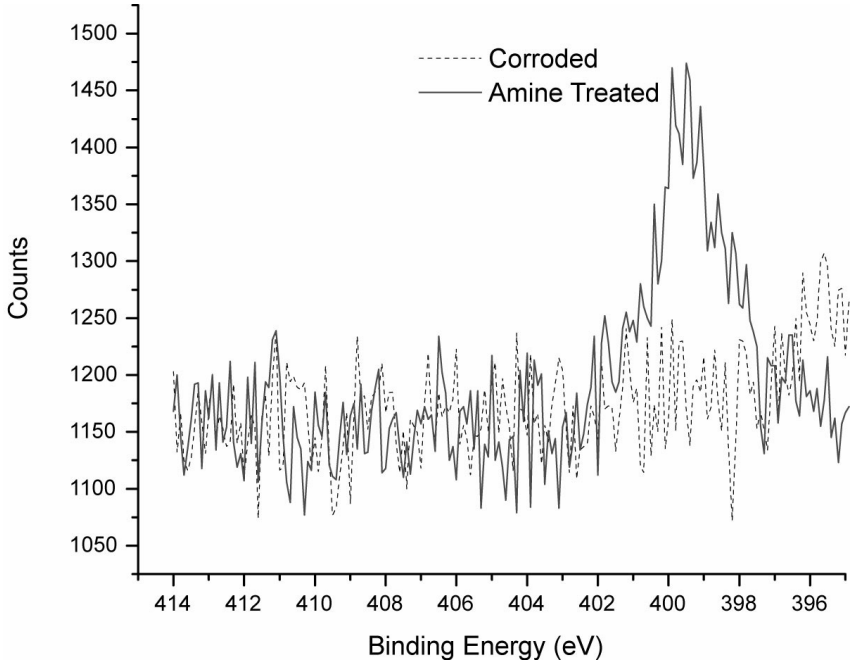

Figure 4.5 XPS spectra of the nitrogen 1s region of a corroded film and after monolayer self-assembly. In this sample, the $YBa_2Cu_3O_{7-\delta}$ film was immersed in 2mM solutions of butylamine for 12 hours

4.4.2 Atomic Absorption Spectroscopy

A series of atomic absorption spectroscopy (AAS) experiments was undertaken to search for dissolved corrosion product in the solution used for self-assembly as shown in Figure 4.6. In these experiments, freshly annealed $YBa_2Cu_3O_{7-\delta}$ powder was exposed to a 1mM solution of hexylamine in hexanes. Aliquots of this solution were extracted at regular intervals and examined using a flame AA.

A significant amount of copper was detected in this method, an interesting result not totally unexpected given the frequent bluish tint observed in other SAM studies. The dissolved copper is presumed to be in a coordination complex with

the alkylamines. However, no copper was detected by AAS after long duration exposure to non-polar solvents like hexanes, although solvents like acetonitrile and tetrahydrofuran have formed complexes and leech copper from the superconductors without amine reagents present.

For the time dependant AAS studies, the aliquots of hexylamine in hexanes were washed with aqueous tetrasodium ethylenediamenetetraacetic acid solutions to transfer the copper over to the aqueous phase. This transfer avoids problems with using organic solvents in flame AA.

The resulting time resolved etching studies show that after about 20 minutes, no further increase in the amount of dissolved copper occurs. This leveling off of the copper concentration suggests a surface passivation. Calculations performed here suggest that approximately 2 unit cells of $YBa_2Cu_3O_{7-\delta}$ are removed from the surface of the powder particles.[6]

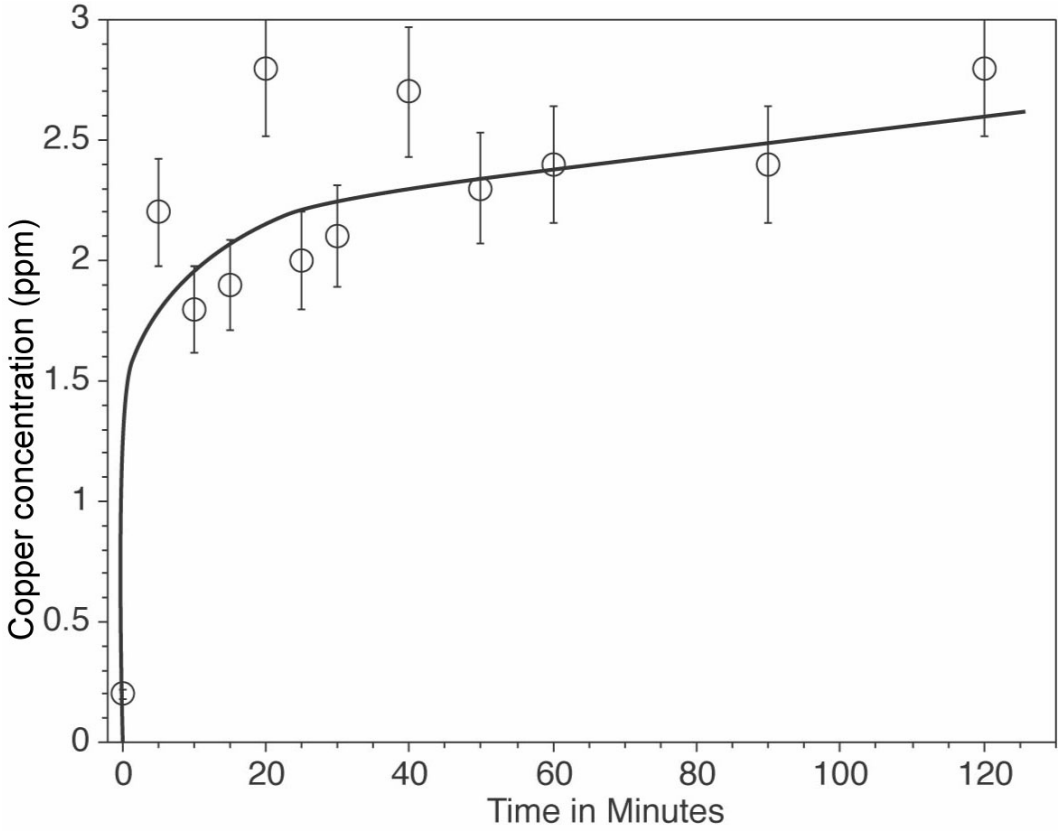

Figure 4.6 Time dependence of copper etching by hexylamine in hexanes. For this data, 3 g of YBCO was exposed to 250 mL of 2%(V/V) of hexylamine in dry hexanes. Aliquots were removed, filtered and extracted into an aqueous phase for AA analysis.

Collectively the XPS, atomic adsorption and resistivity measurements support a plausible new mechanism for monolayer formation atop cuprate superconductors, in which the alkylamine serves two distinct roles. First, the removal of corroded material from the surface of the superconductor occurs. Second the amine reagents adsorb in a persistent manner atop cuprate materials. Once the amines are anchored and the etching process ceases, the adsorbate layer is attached to a conductive exterior region. Unlike the majority of other processing techniques for cuprate superconductors, this amine monolayer formation simultaneously creates and preserves a pristine interface.

4.5 SURFACE MORPHOLOGY CHANGES BY SCANNING ELECTRON MICROSCOPY

Recently, more direct evidence of the etching of superconductors by alkyl amine reagents has been acquired. Examination of micrographs obtained by field emitting scanning electron microscopy clearly shows the removal of material from the surface of the thin films. In this series of electron micrographs, duplicate films of $Y_{0.6}Ca_{0.4}Ba_{1.6}La_{0.4}Cu_3O_{7-\delta}$ deposited simultaneously, are given three different treatments for the same duration (18 hrs). One is exposed to atmosphere (Figure 4.7 A); one was exposed to the electrolyte solution (0.1 mM *tert*-butylamine hexafluorophosphate in acetonitrile) (Figure 4.7 B); and one was exposed to an amine reagent (1mM ferrocenylethylamine in acetonitrile) (Figure 4.7 C). Although originally performed as part an electrochemical study (see Chapter 5), the self-assembled sample clearly shows the planarization of the thin films. The first two films (Figure 4.7 A and B) exhibit the surface structures

characteristic of (001) oriented thin films, with no noticeable etching. The last film (Figure 4.7 C) shows the removal of these large units until a smoother base plane is achieved allowing for better self-assembly due to improved tail group interaction. Interestingly, the non-stoichiometric outgrowth remain after self-assembly, suggesting a preferential etching of the film.

The etching observed in the films exposed to an electroactive amine reagent has not been previously noted. This unusual observation is most likely a result of the different reagent structure. The long linear hydrocarbons are know to passivate the surface, and the increased interactions between the hydrocarbon groups most likely slow the desorption process necessary for the removal of the corroded cuprate material. The shorter chains used here lack the inter-chain interactions and also have a bulkier tail group. Further experiments are underway to identify the best short chain reagent for use in planarization and etching experiments.

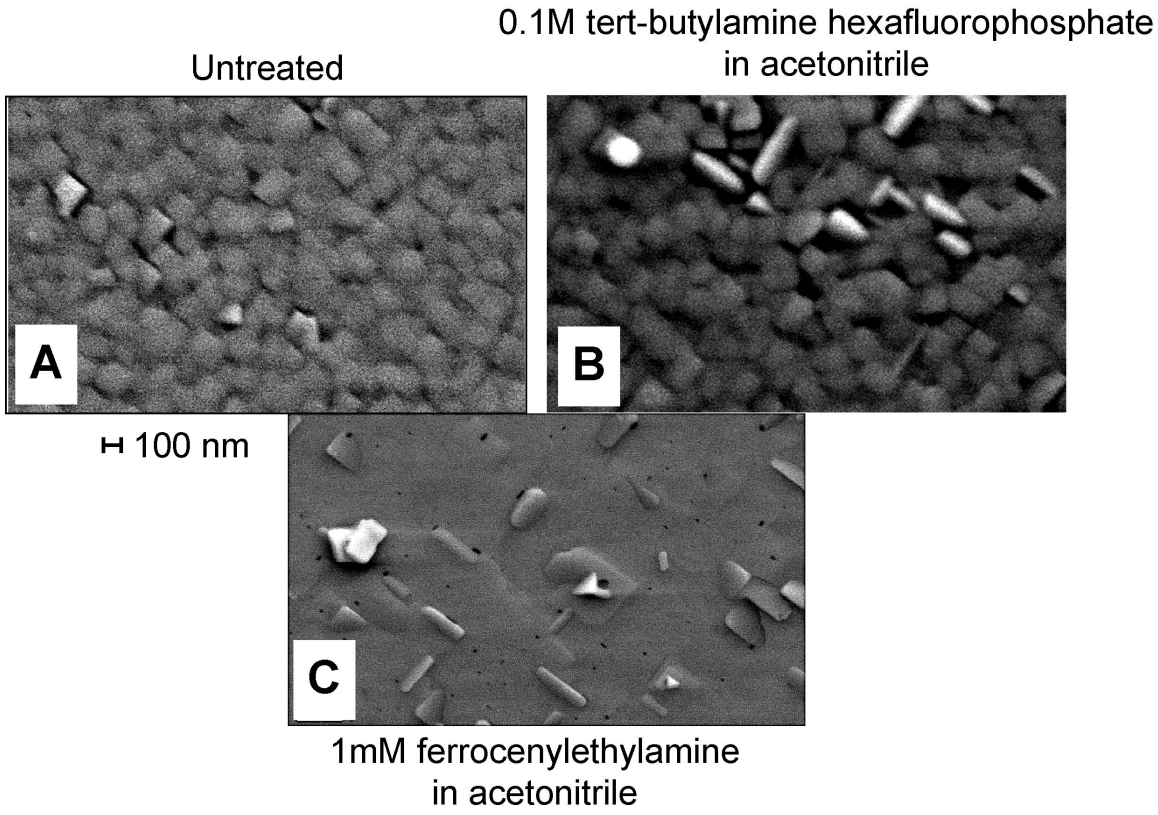

Figure 4.7 Etching of $Y_{0.6}Ca_{0.4}Ba_{1.6}La_{0.4}Cu_3O_{7-\delta}$ by self-assembling amine reagents. These films were all deposited at the same time and treated simultaneously for 24 hours. The untreated film (A) and the film soaked in electrolyte solution (B) display no visible difference, where as the film exposed to the electroactive self-assembly reagent (C) shows significant smoothing.

In order to better understand this process, consider the forces involved in self-assembly. The tail group interactions provide additional stability to the monolayer structure, usually only after an initial layer of adsorbate has bound to the surface.[16] Prior to and during this formation, the adsorbate is dynamically exchanging between the solution and the surface of the film. Atomic adsorption

spectroscopy has shown that for amines atop cuprate superconductors, copper will be extracted into solution. Anywhere there is a defect site or edge the amine reagent would be expected to desorb differently than for a flat terrace since there are fewer tail group interactions. Similar behavior has been shown for thiols atop gold where formation of stable islands occurs first on terraces and then later at defects.[29,30]

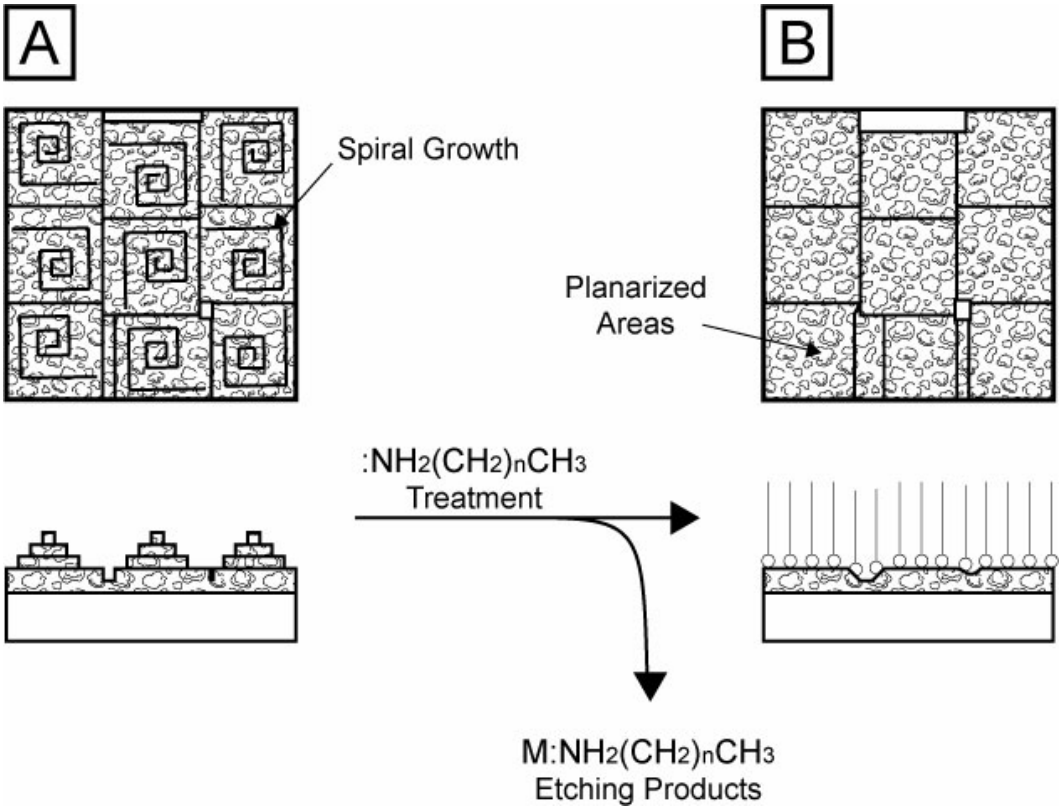

Figure 4.8 Schematic of planarization occurring during formation of self-assembled monolayers atop superconductors. As the monolayer forms, the spirals and islands in (A) are etched away and subsequent terraces are nucleation sites for the formation of stable monolayers (B).

A scheme for the etching and adsorption of amine atop cuprates is shown in Figure 4.8. The spiral or island growths common in deposition of c-axis oriented films provide an uneven surface for the formation of stable monolayers. The top few layers are also known to be porous and subject to rapid etching in chelating solutions of ethylenediamenetetraacetic acid (EDTA).[31,32] As seen in part A, the spirals and islands protrude from the surface, providing edges for the amine to attack the cuprate. As the edges are removed and the etch products are removed into solution, larger terraces are formed, and the monolayer can form close packed structures as shown in B. Similar effects have been noted for adsorption of octadecylthiol adsorbed atop copper films with a native oxide surface. The formation of robust films were found to vary with the solvent used, but a smoothing of the surface was measured with AFM.[33] In similar studies on intentionally oxidized films of gold, the gold oxide was trapped beneath the monolayer formed without subsequent smoothing.[34]

Another important aspect of this process is the self-termination that occurs with the formation of a stable monolayer. With close packing of the tail groups, the etching of the superconductor is reduced. The rate of these described etching and self-passivation steps is the subject of Chapter 5.

4.6 CONCLUSION

The new mechanism of formation of alkylamine monolayers atop cuprate superconductors has been proposed along with the acquisition of evidence supportive to this hypothesis. The process requires the solution phase etching of corrosion products followed by subsequent adsorption of the amine reagent. This

process differs from those of the thiol gold systems, in that the gold oxide is not removed during the formation of thiol monolayers as occurs for the copper amine systems.

This etching process opens the possibility a fascinating strategy for the molecular level planarization of cuprate thin films. By selecting c-axis films and appropriate amine reagents, the porous and corroded outer layer of the films can be removed, while protecting the underlying film from further damage, spontaneously packaging the cuprates. Typically, ~50Å of material is removed in the pre-etching step, as evidenced by the atomic adsorption measurements and resistivity studies. The removal of corrosion products has been demonstrated, resulting in films with XPS signatures similar to those obtained from *in situ* analysis, even when starting with dirty samples. Likewise, careful choice of adsorbate reagents will provide a "chemically soft" approach for packaging oxide superconductor materials.

4.7 REFERENCES

(1) Chen, K.; Mirkin, C. A.; Lo, R.-K.; Zhao, J.; McDevitt, J. T. *J. Am. Chem. Soc.* **1995**, *117*, 6374-6375.

(2) Chen, K.; Xu, F.; Mirkin, C. A.; Lo, R.-K.; Nanjundaswamy, K. S.; Zhou, J.-P.; McDevitt, J. T. *Langmuir* **1996**, *12*, 2622-2624.

(3) McDevitt, J. T.; Mirkin, C. A.; Lo, R.-K.; Chen, K.; Zhou, J.-P.; Xu, F.; Haupt, S. G.; Zhao, J.; Jurbergs, D. *Chem. Mat.* **1996**, *8*, 811-813.

(4) Mirkin, C. A.; Xu, F.; Zhu, J. *Adv. Mat.* **1997**, *9*, 167-172.

(5) Ritchie, J. E.; Wells, C. A.; Zhou, J.-P.; Zhao, J.; McDevitt, J. T.; Ankrum, C. R.; Jean, L.; Kanis, D. R. *J. Am. Chem. Soc.* **1998**, *120*, 2733-2745.

(6) Ritchie, J. E. In *Department of Chemistry and Biochemistry*; University of Texas at Austin: Austin, Texas, 1998, p 166.

(7) Wells, C. A. In *Department of Chemistry and Biochemistry*; University of Texas at Austin: Austin Texas, 1999, p 176.

(8) Lo, R.-K.; Ritchie, J. E.; Zhou, J.-P.; Zhao, J.; McDevitt, J. T.; Xu, F.; Mirkin, C. A. *Journal of the American Chemical Society* **1996**, *118*, 11295-11296.

(9) Zhao, J.; Jurbergs, D.; Yamasi, B.; McDevitt, J. T. *Journal of the American Chemical Society* **1992**, *114*, 2737-2738.

(10) Haupt, S. G.; Riley, D. R.; Jones, C. T.; Zhao, J.; McDevitt, J. T. *Journal of the American Chemical Society* **1993**, *115*, 1196-1198.

(11) Haupt, S. G.; Riley, D. R.; Grassi, J.; Lo, R.-K.; Zhao, J.; Zhou, J.-P.; McDevitt, J. T. *Journal of the American Chemical Society* **1994**, *116*, 9979-9986.

(12) Clevenger, M. B.; Zhao, J.; McDevitt, J. T. *Chemistry of Materials* **1996**, *8*, 2693-2696.

(13) Jurbergs, D.; Savoy, S. M.; Zhao, J.; Eames, S. J.; McDevitt, J. T. *Chemistry of Materials* **1997**, *9*, 1377-1384.

(14) Dubois, L. H.; Nuzzo, R. G. *Annual Review of Physical Chemistry* **1992**, *43*, 437-463.

(15) Dubois, L. H.; Zegarski, B. R.; Nuzzo, R. G. *Journal of the American Chemical Society* **1990**, *112*, 270-579.

(16) Ulman, A. *An introduction to ultrathin organic films: from Langmuir-Blodgett to self-assembly*; Academic Press: San Diego, CA, 1991.

(17) Schougaard, S. B.; Bjornholm, T.; Markert, J.; McDevitt, J. T., Manuscript in preparation for Chemistry fo Materials.

(18) Zhu, J.; Mirkin, C. A.; Braun, R. M.; Winograd, N. *Journal of the American Chemical Society* **1998**, *120*, 5126-5127.
(19) Xu, F.; Zhu, J.; Mirkin, C. A. *Langmuir* **2000**, *16*, 2169-2176.
(20) Ritchie, J. E.; Murray, W. R.; Kershan, K.; Diaz, V.; Tran, L.; McDevitt, J. T. *Journal of the American Chemical Society* **1999**, *121*, 7447-7448.
(21) Riley, D. R.; McDevitt, J. T. *Journal of Electroanalytical Chemistry* **1990**, *295*, 373-384.
(22) Riley, D. R.; Jurbergs, D.; Zhou, J.-P.; Zhao, J.; Markert, J.; McDevitt, J. T. *Solid State Communications* **1993**, *88*, 431-434.
(23) Zhou, J.-P.; McDevitt, J. T. *Chem. Mat.* **1992**, *4*, 953-959.
(24) Zhou, J.-P.; Riley, D. R.; McDevitt, J. T. *Chem. Mat.* **1993**, *5*, 361-365.
(25) Zhou, J.-P.; Savoy, S. M.; Zhao, J.; Lo, R.-K.; Borich, D.; McDevitt, J. T. *Journal of the American Chemical Society* **1994**, *116*, 9389-9390.
(26) Zhou, J.-P.; Lo, R.-K.; Savoy, S. M.; Arendt, M.; Armstrong, J.; Yang, D.-Y.; Talvacchio, J.; McDevitt, J. T. *Physica C* **1997**, *273*, 223-232.
(27) Olefjord, I. In *Surface Characterization: A User's Sourcebook*; Hunderi, O., Ed.; Wiley-VCH: New York, 1997, pp 291-319.
(28) Briggs, D.; Riviere, J. C. In *Practical Surface Analysis*; 2nd ed.; Seah, M. P., Ed.; John Wiley & Sons, Inc.: New York, 1990; Vol. 1. Auger and X-ray photoelectron spectroscopy, pp 85-142.
(29) Strong, L.; Whitesides, G. M. *Langmuir* **1988**, *4*, 546-558.
(30) Poirier, G. E.; Plyant, E. D. *Science* **1996**, *272*, 1145-1148.
(31) Shokoohi, F. K.; Schiavone, L. M.; Rogers, C. T.; Inam, A.; Wu, X. D.; Nazar, L.; Venkatesan, T. *Appl. Phys. Lett.* **1989**, *55*, 2661-2663.
(32) Dam, B.; Koeman, N. J.; Rector, J. H.; Stäuble-Pümpin, B.; Poppe, U.; Griessen, R. *Physica C* **1996**, *261*, 1-11.
(33) Ron, H.; Cohen, H.; Matlis, S.; Rappaport, M.; Rubinstein, I. *J. Phys. Chem. B* **1998**, *102*, 9861-9869.
(34) Ron, H.; Rubinstein, I. *Langmuir* **1994**, *10*, 4566-4573.

5 Kinetics of self- assembly atop thin film high temperature superconductors

5.1 INTRODUCTION

While much attention has been placed on the discovery of new high-T_c phases with the goal of increasing transition temperature, thin film deposition methods and device fabrication, less information is available regarding chemical routes for controlling high temperature superconductor surface decomposition reactions. As described in the introductory chapter, prior work of the McDevitt and Mirkin groups has led to discovery of amine adsorbate reactions that can be used to control interfacial properties of cuprate compounds. Self-assembled monolayers have been used extensively for numerous applications for a variety of metals, oxides and semiconductor systems. Here sensors, resist, corrosion passivation, optoelectronic applications have been demonstrated.[1,2] By understanding the dynamics of the adsorption of amines atop cuprate superconductors, we can further exploit the monolayer–superconductor structure for useful purposes, such as improved device manufacture and better corrosion protection.

This chapter examines conditions necessary for formation of full coverage monolayers and the rates of the reactions involved. Here electroactive amine compounds are utilized as a convenient vehicle in conjunction with standard electrochemical methods to explore the dynamics of cuprate adsorption processes. A short review of the electrochemistry of superconductors will be followed by the details of the experiments to derive the rate constant for SAM adsorption and desorption.

5.2 ELECTROCHEMISTRY ATOP SUPERCONDUCTORS

One of the pioneering foci of the McDevitt group has been the determination of the surface chemistry of $YBa_2Cu_3O_{7-\delta}$ and related compounds.[3-10] Electrochemistry is an ambient pressure, surface sensitive technique that avoids many of the problems associated with other surface science techniques involving $YBa_2Cu_3O_{7-\delta}$, namely oxygen loss and the presence of impurities. Early work performed by Miller and co-workers measured the rate of corrosion for bulk electrodes in aqueous solutions using rotating ring disk electrodes. Later work by McDevitt and co-workers employed cyclic voltammetry to determine the surface quality of the bulk electrodes.[5,6,9,10] In these prior University of Texas studies, superconductor pellets are encapsulated in epoxy and used as the working electrode to measure the electrochemistry of dissolved redox species. The peak splitting (ΔE_p) was used to diagnose the surface quality of the bulk superconductor. Values close to 59/n mV were reported in the absence of the thin layer of corrosion products that readily forms upon exposure to corrosive reagents (i.e. moisture, protic solvents, atmospheric CO_2, etc.). As the electrode corrodes, the ΔE_p widens yielding a broad cyclic voltammograms. This broadening is accounted for by the slow heterogeneous electron exchange as described by Nicholson and Shain[11].

Other studies have been carried out to assess the stability of samples engineered to prevent this corrosion.[12-21] A detailed examination of various superconductive phases points to the doped superconductor, $Bi_2(Sr_{1.5}Ca_{0.5})Ca_{0.75}Y_{0.25}Cu_2O_{8.24}$ as being less sensitive to corrosion than the other phases tested; $La_{2-x}Sr_xCuO_4$, $YBa_2Cu_3O_{7-\delta}$. $Bi_2Sr_2Ca_{n-1}Cu_nO_{2n+4+y}$, $Tl_2Ba_2Ca_{n-}$

$_{11}Cu_nO_{2n+4+y}$, and $TlBa_2Ca_{n-11}Cu_nO_{2n+3+y}$[10]. These investigations lead to the development of other corrosion resistant phases, most notably $Y_{0.6}Ca_{0.4}Ba_{1.6}La_{0.4}Cu_3O_{7-\delta}$[19], (*vide supra*). While the material characteristics and bulk properties of electrochemistry of $Y_{0.6}Ca_{0.4}Ba_{1.6}La_{0.4}Cu_3O_{7-\delta}$ are understood, little electrochemistry has been documented using $Y_{0.6}Ca_{0.4}Ba_{1.6}La_{0.4}Cu_3O_{7-\delta}$.

The development of self-assembly methods atop superconductors provides new ways to analyze the interface of superconductors with solutions. Following the multitude of studies based on the gold-thiol systems, the McDevitt and Mirkin groups undertook the electrochemical investigation of redox active superconductive self-assembled structures.[3,4,22] The initial work used linear hydrocarbon chains terminated at one end with thiols, hydroxides, phosphines, selenols, and amines; ferrocene carboxylate was anchored at the other end $[Fe(CP)_2C(O)N(CH_2)_nR]$.[3,4,22,23] Once amines were identified as having the best coverage electrochemically, cuprate SAM research has focused there almost exclusively. Early work has measured the surface coverages of $Fe(CP)_2C(O)NH(CH_2)_2NH_2$ at 4×10^{-9} mol/cm^2 and 2×10^{-9} mol/cm^2 atop ceramic and thin films respectively[3]. These values are reasonably close to those of ferrocenyl alkanethiols on noble metal thin films. The ceramic values are approximately 10 times the expected value, but consistent with the increased surface area of a rough and porous material. Prior work here only provided rough estimates of coverage due to uncertainties of sample roughness values. More careful understanding of coverage atop high-temperature superconductors is highly

desirable en route to obtaining a molecular-level understanding of cuprate adsorbate chemistry.

Once the electrochemistry of fully formed amine monolayers was understood, methods to measure the rate of adsorption were untaken. Prior work of Ritchie in the McDevitt lab targeted time and concentration dependant adsorption experiments to examine the thermodynamics and kinetics of alkylamine monolayer formation.[7,24] This work was based on grazing angle FTIR spectroscopy of steady state samples, examined *ex situ*. The fractional coverage was measured based on peak height instead of area, but results obtained here are consistent with the literature for gold thiol systems to validate the method. Difficulties arose when attempts were made to measure the fractional coverage of the reaction with $YBa_2Cu_3O_{7-\delta}$, however. From these studies, it was possible to estimate values for ΔG_{ads} of −7.2 kcal/mol for the alkylamine cuprate superconductor system.

Recent work by Xu at Northwestern University, has explored the monolayer growth and exchange rates for alkylamines on $YBa_2Cu_3O_{7-\delta}$ electrochemically, in an effort to understand the monolayer formation process[25]. In this work, the previously used compound, $Fe(CP)_2C(O)NH(CH_2)_2NH_2$(1) and a newly synthesized 6-aminohexylferrocene, $Fe(CP)(CH_2)_6NH_2$(2) were adsorbed onto epoxy encapsulated ceramic electrodes and measured using cyclic voltammetry. The two ferrocenyl reagents are sufficiently different that two peaks appear separated by ~220 mV in the voltammograms. In the concentration dependant adsorption of (1) on the $YBa_2Cu_3O_{7-\delta}$ electrode, the different concentrations approach different total coverage asymptotes.

Complications from prior works in terms of surface roughness, multiple crystal orientations, unknown surface cleanliness, and other factors have prevented a detailed understanding of high temperature superconductor processes to evolve.

5.3 Electrochemical Probes for the Study of High Temperature Superconductor Adsorbate Chemistry

Electrochemistry provides a convenient method for probing the kinetics and dynamics of adsorbate processes. Here we use an adaptation of the methods used to study thiol-gold systems to examine relevant surface reactions of the cuprate-amine system. Using electrochemistry we will probe here the monolayer formation atop two different cuprate materials. These experiments will show the influence of material choice and exposure history upon surface coverage, rate and persistence of an electroactive monolayer. Changes in surface roughness will be explored as well.

Using cyclic voltammetry to determine surface concentration, the fractional coverage of the surface of c-axis thin films can be determined. Plotting the coverage as a function of time will allow the examination of the reaction kinetics of the assembly of a redox reactive amine monolayer.

For these experiments, a ferrocenylethylamine, $Fc(CH_2)_2NH_2$ (**3**), was synthesized as described previously in Chapter 2. The short two carbon chain has the advantage of being able to remove the corrosion products that form atop the films and also the advantage of not interacting strongly with neighboring adatoms. Both of these characteristics will be important later. The amine is also different enough from the regular straight chain amines that a new packing order may be less dense than those previously recorded. The cross sectional area of the straight chain

amines is assumed to be 63.6Å^2 or 4.5Å in radius. This is considerably larger than the 2.5Å radius (~20Å^2) of the alkyl chains. Evaluation of simple space filling models suggest that the densest packing arrangement for the ferrocenylethylamine would be a 2×2 overlayer, since other logical packing arrangements are either too closely packed or too diffuse to minimize the surface energy, Figure 5.1.

Assuming a 2×2 overlayer, calculation suggests that the overall coverage should be on the order of ~2.9x10^{-10} mol/cm^2. This coverage is in line with those calculated for other ferrocene containing monolayers[25]. These calculations assume a perfectly flat surface, free of debris from the ablation process used in deposition.

In these studies, both $Y_{0.6}Ca_{0.4}Ba_{1.6}La_{0.4}Cu_3O_{7-\delta}$ and $YBa_2Cu_3O_{7-\delta}$ were used as substrates for adsorption. The ferrocenylethylamine was used for monolayer formation to provide an electrochemical signature. Unless otherwise noted, the ferrocene-amine concentration was 0.1mM in dry acetonitrile for the adsorbate reaction process. All monolayer growth was performed inside an inert atmosphere dry box. Electrochemical measurements were performed in 0.1M-tetrabutylamino hexafluorophosphate (TBAPF6) in dry acetonitrile within the dry box as well. Cyclic voltammetry was performed, limiting the potentials to between 0V and 1.4V versus an Ag/AgOx quasi-reference electrode in order to minimize damage to the superconductor. Unless specified, the scan rate was 100mV/s.

In these experiments, the films were exposed for measured time periods ~10 minutes in duration to a 1mM solution of **3** in acetonitrile, followed by subsequent rinsing with ~50ml of pure acetonitrile. The films were held in a custom made cell so that the geometric area of examination was a constant 0.062 cm^2 as determined

by the teflon o-ring, Figure 5.2. The platinum counter electrode and Ag/AgOx quasi-reference electrode were press fit through undersized holes in the block of teflon opposite the film. The volume of the electrolyte/SAM reservoir was ~0.5 ml. All measurements were carried out in an inert atmosphere glove box to limit corrosion damage to the films.

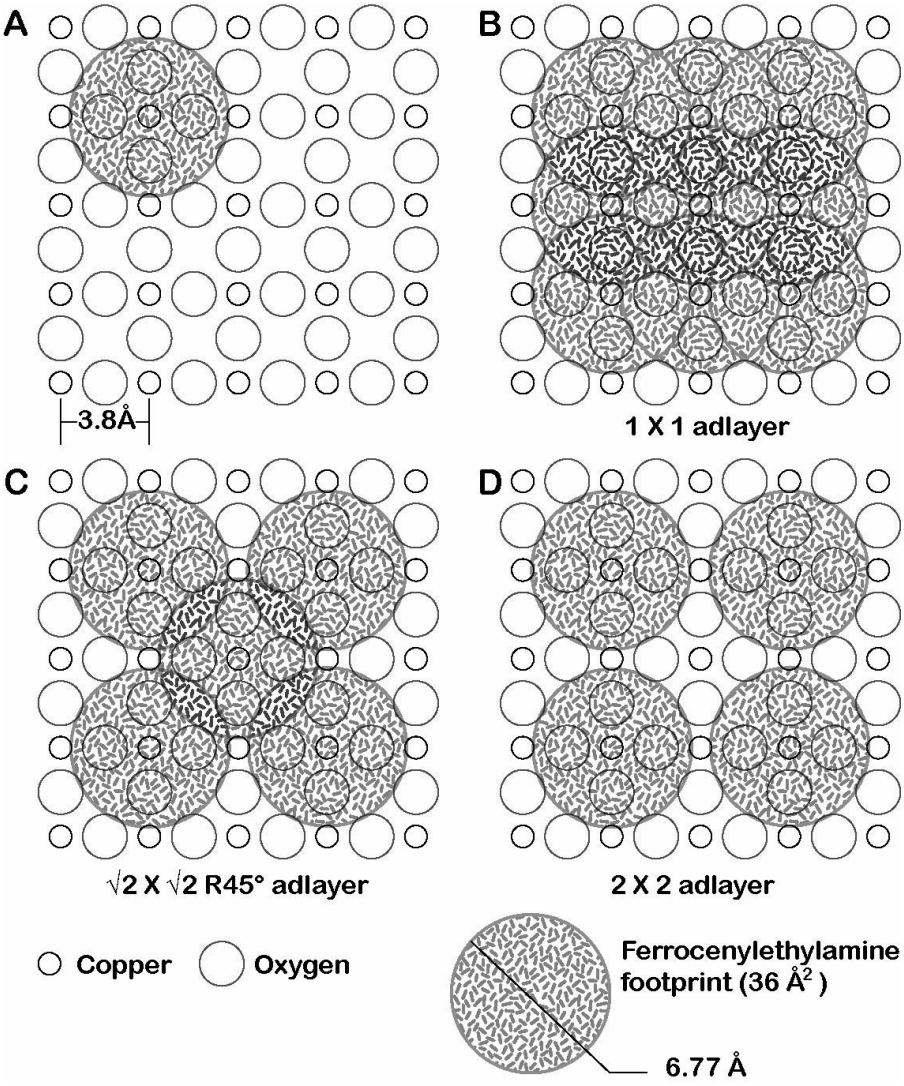

Figure 5.1 Possible packing arrangements atop (001) oriented $YBa_2Cu_3O_{7-\delta}$. Figure A shows the relative scale of the copper oxide sheets to the ferrocenylethylamine footprint. The closest packed 1x1 overlayer is shown in B. The normal alkylamine packing scheme is shown in C. The suggested overlayer structure is shown in C. Any other overlayers are more diffuse than those shown and are not considered.

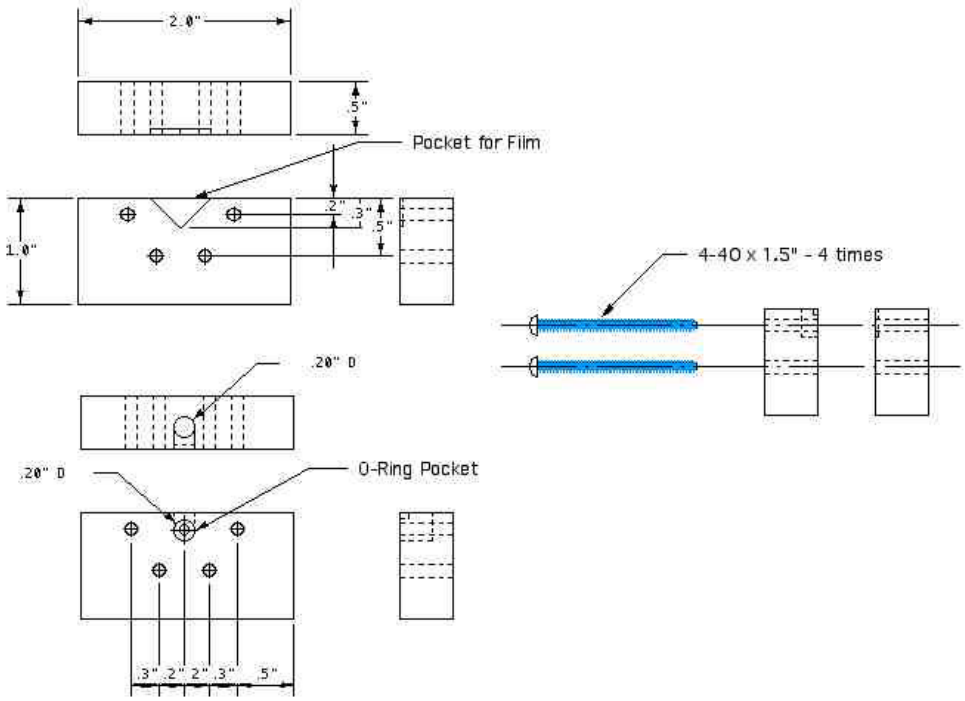

Figure 5.2 Schematic of the custom teflon electrochemical cell. The teflon cell and o-ring provide a constant geometric surface area of .75 cm^2. In this geometry the film is sandwiched between the two halves for the cell and held in place by 4 #4-40 bolts. The platinum counter electrode and Ag/AgOx reference electrodes are press fit through undersized holes in the block opposite the film.

5.4 ELECTROCHEMISTRY ON $Y_{0.6}Ca_{0.4}Ba_{1.6}La_{0.4}Cu_3O_{7-\delta}$

Due to it's increased corrosion resistance, $Y_{0.6}Ca_{0.4}Ba_{1.6}La_{0.4}Cu_3O_{7-\delta}$ was chosen for the majority of the kinetic experiments[12-17,19]. By minimizing the corrosion layer atop the thin films in this study, more ideal electrochemistry studies ccan be achieved. It was hoped that the kinetics of the adsorption could be decoupled from the aforementioned etching process using such stable cuprate phases.

The $Y_{0.6}Ca_{0.4}Ba_{1.6}La_{0.4}Cu_3O_{7-\delta}$ films used in this series of experiments were deposited in the same PLD chamber described in Chapter 3. The deposition conditions used are similar to those for $YBa_2Cu_3O_{7-\delta}$. The exact deposition temperature for $Y_{0.6}Ca_{0.4}Ba_{1.6}La_{0.4}Cu_3O_{7-\delta}$ was 925° C with the controller in 200 mTorr oxygen. The laser energy was set at 275 mJ with an 8 hz repition rate. The transition temperatures of the films were within ±3 degrees of average transition temperature of 68 Kelvin. A representative resistance versus temperature plot is show in Figure 5.3. The X-ray diffraction data acquired for such films reveals a predominantly c-axis orientation as shown in Figure 5.4.

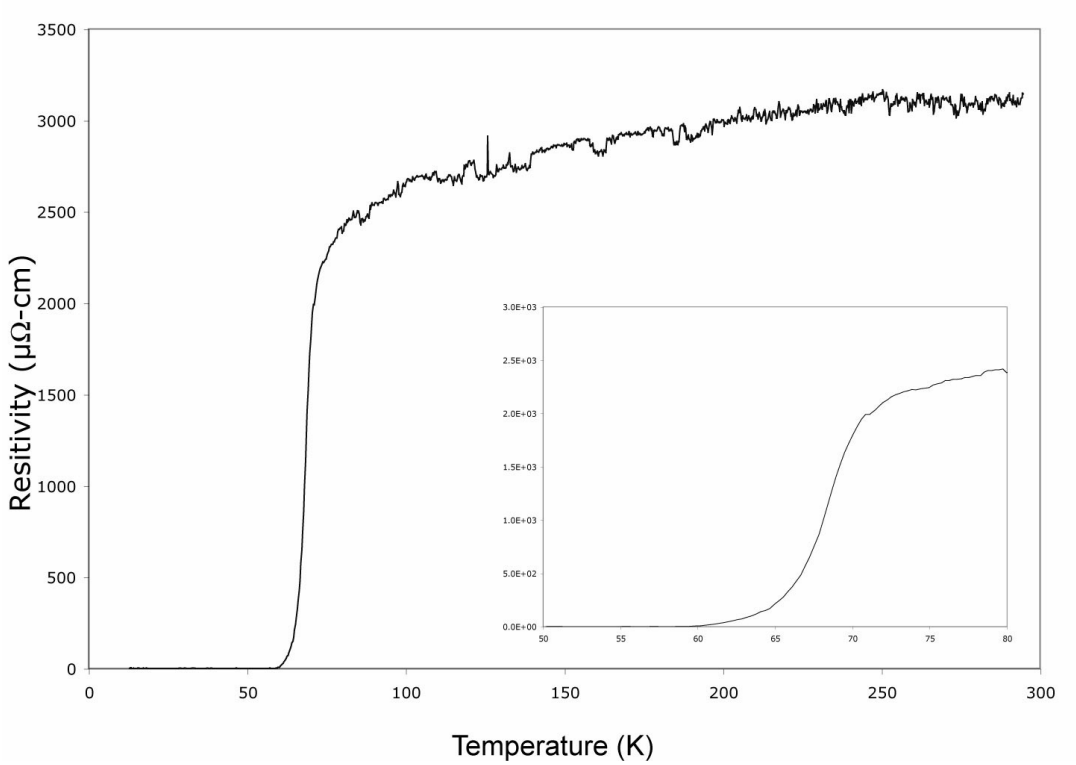

Figure 5.3 Representative resistance versus temperature curve for $Y_{0.6}Ca_{0.4}Ba_{1.6}La_{0.4}Cu_3O_{7-\delta}$ thin film. The inset is an enlargement of the transition temperature region.

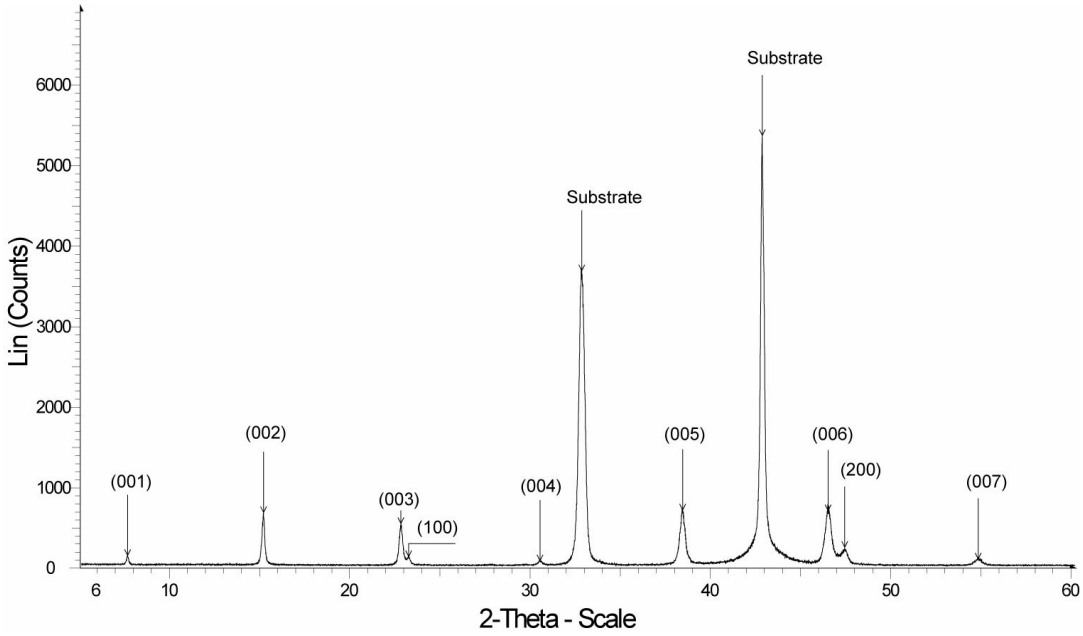

Figure 5.4 Representative X-ray diffraction measurement of a $Y_{0.6}Ca_{0.4}Ba_{1.6}La_{0.4}Cu_3O_{7-\delta}$ thin film. The films are majority c-axis (00l) with some a-axis (h00) grains apparent.

5.4.1 Electrochemistry of $Y_{0.6}Ca_{0.4}Ba_{1.6}La_{0.4}Cu_3O_{7-\delta}$ with Redox Couples in Solution

While prior attempts have been made to use $YBa_2Cu_3O_{7-\delta}$ films for the study of solution dissolved redox couples, the rapid decomposition of their surfaces has made these measurements quite difficult. Interestingly, the combination of inert atmosphere processing and stable material here results in well-defined electrochemical responses. Prior $YBa_2Cu_3O_{7-\delta}$ ambient exposure revealed little Faradaic electrochemistry for redox couples like ferrocene and TCNQ in acetonitrile.[5,9,26]

A sample of the electrochemical response is shown below in Figure 5.5. This data provides the first documentation of the electrochemical response of thin

films of $Y_{0.6}Ca_{0.4}Ba_{1.6}La_{0.4}Cu_3O_{7-\delta}$. For this test, a pristine film was immersed in ~1 ml of 10mM ferrocene in 5 ml of 0.1 M $TBAPF_6$. The peak splitting is larger than the 59 mV expected for single electron reversible "Nernstian" processes, but this behavior is observed commonly with non-aqueous processes and has been determined previously to be a result of uncompensated resistance in the acetonitrile-superconductor system[11,27,28]. These results also compare favorably with response of freshly prepared $YBa_2Cu_3O_{7-\delta}$ pellets, surfaced to expose the uncorroded interior. Corrosion would manifest itself as a broader, less resolved cathodic wave when compared to the anodic wave. This behavior is common in p-type conductors such as $YBa_2Cu_3O_{7-\delta}$. The p-type superconductors, with a majority of hole carriers, favor oxidative electron transfers.[28]

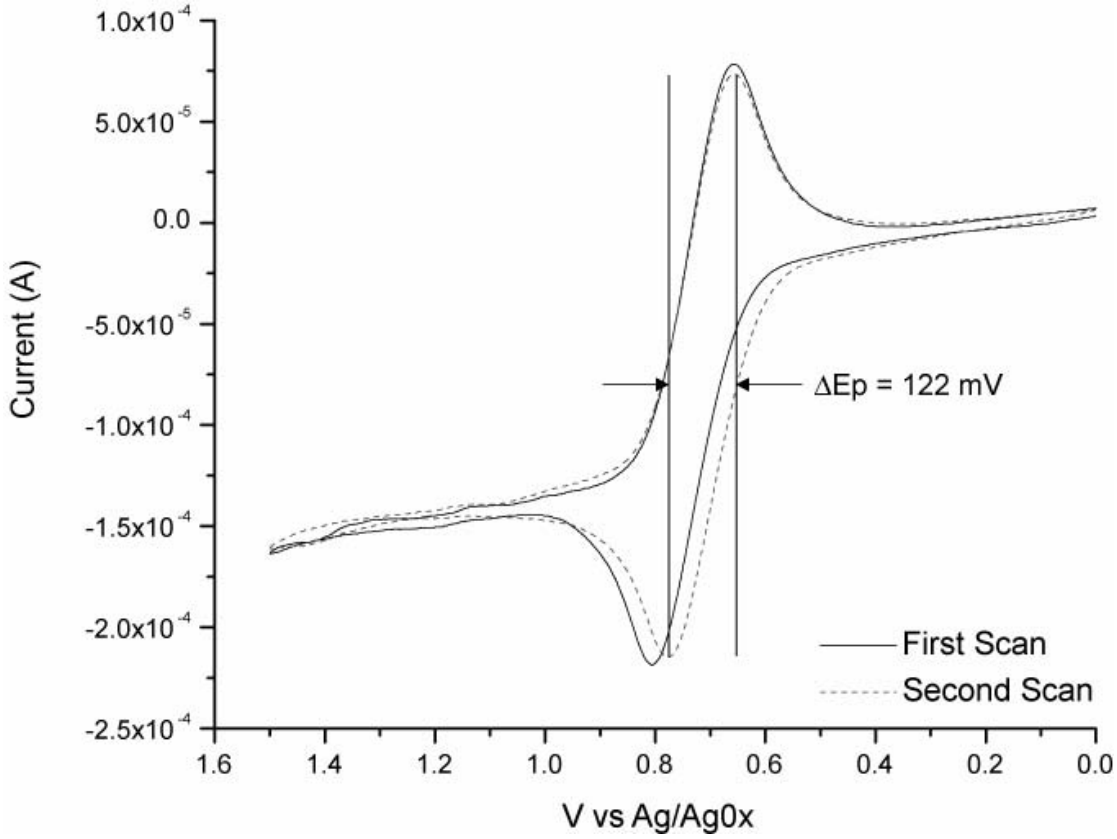

Figure 5.5 Electrochemical response of ferrocene solution at a pristine $Y_{0.6}Ca_{0.4}Ba_{1.6}La_{0.4}Cu_3O_{7-\delta}$ electrode. The ferrocene concentration was ~1 ml 10 mM Ferrocene in 5 ml $TBAPF_6$. The large peak splitting (ΔE_p) is not unusual in non-aqueous solutions.

5.4.2 Short term adsorption isotherms

Having demonstrated that $Y_{0.6}Ca_{0.4}Ba_{1.6}La_{0.4}Cu_3O_{7-\delta}$ films can be prepared and manipulated to yield ideal electrochemistry within inert atmospheres, the next series of experiments were completed in an attempt to explore surface localized redox active monolayer formation dynamics. For these studies, thin films of $Y_{0.6}Ca_{0.4}Ba_{1.6}La_{0.4}Cu_3O_{7-\delta}$ were synthesized as described previously and exposed to timed baths in ferrocenylethylamine in dry acetonitrile. The films were then rinsed with dry acetonitrile and the cyclic voltammetry recorded in 0.1 M $TBAPF_6$. A representative cyclic voltammograms is shown in Figure 5.6. In this sample, a pristine $Y_{0.6}Ca_{0.4}Ba_{1.6}La_{0.4}Cu_3O_{7-\delta}$ film has been exposed to 1mM ferrocenylethylamine in CH_3CN for a total of 100 minutes with interspersed sampling CV's. The initial background scan is also shown here for reference. While the peak splitting of ~66mV is somewhat larger than expected for an idealized attached redox couple, this is most likely due to the uncompensated resistance of the solution, and also the presence of small amounts of corrosion products.

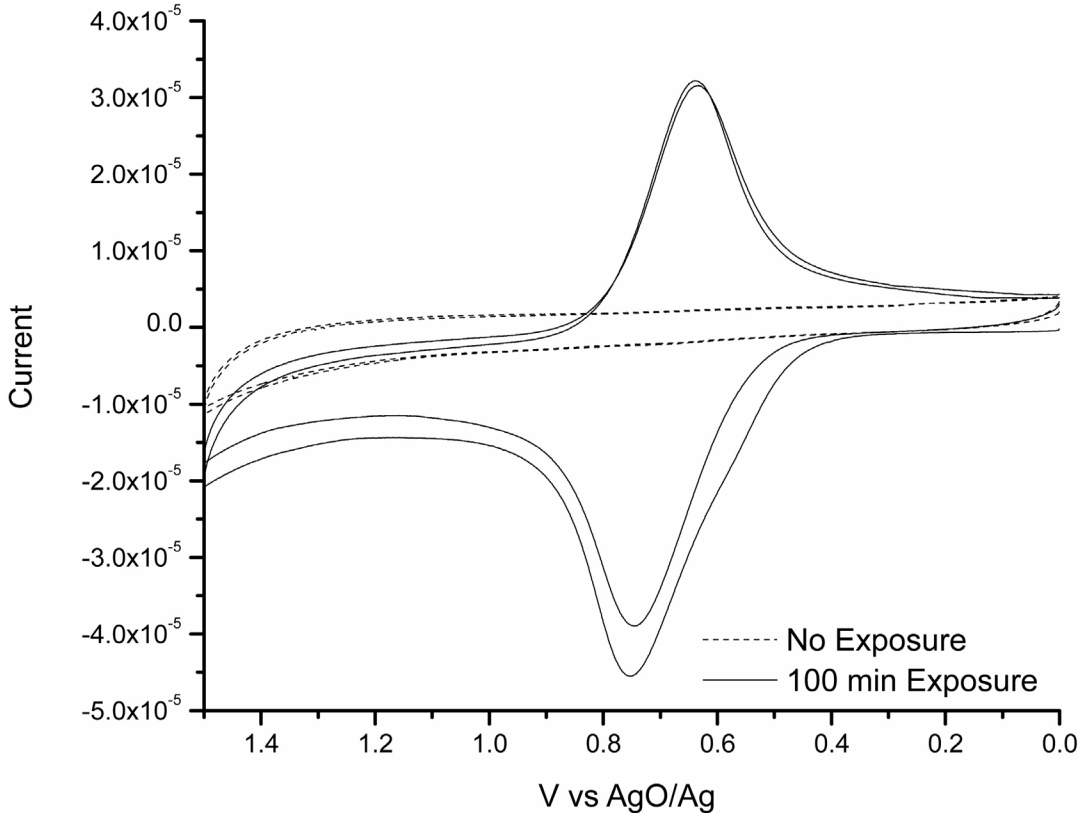

Figure 5.6 Cyclic voltammogram of $Y_{0.6}Ca_{0.4}Ba_{1.6}La_{0.4}Cu_3O_{7-\delta}$ after 100 min exposure to 1mM ferrocenylethylamine in CH_3CN. A background scan of the same electrode prior to exposure is shown for reference.

For the adsorption experiments involving electroactive amines atop cuprate films, the following conditions were used initially. The length of exposure of the films to the ferrocene-amine reagent was a measured 10 minutes, followed by rinsing with copious acetonitrile. The electrochemistry was then performed. In each case, the aforementioned Teflon o-ring maintained the geometric area. Attempts to measure the electroactive area of the electrode with other reagents in the electrolyte solution were unsuccessful. An example of the increase in ferrocene-amine coverage can be seen in Figure 5.7. These results are for a film freshly made and transported to the dry box without exposure to ambient conditions.

In order to convert the cyclic voltammograms to monolayer coverage the curves were fit to a Gaussian shape and the peak heights measured. A modified form of the Cottrell equation as described below, derived to account for specific adsorption of the electroactive species, is used to determine the coverage[29].

$$i_p = \frac{n^2F^2}{4RT}\upsilon A\Gamma_O^* \qquad \text{Eq 5.1}$$

This simple treatment assumes an ideal case where the only adsorbed ferrocene amine exists and adsorption or desorption does not occur during the potential sweep. The coverage (Γ) is also assumed to be independent of the potential during the scan. To minimize the possible effect of potential upon the monolayer, cycling to excessive anodic and cathodic potentials were avoided, minimizing damage to the films and subsequent monolayers.

The preceding experiments were only performed for a maximum of 180 minutes, sampling every 10 minutes. Plotting the coverage as a function of time yields information related to the observed rate of adsorption atop the

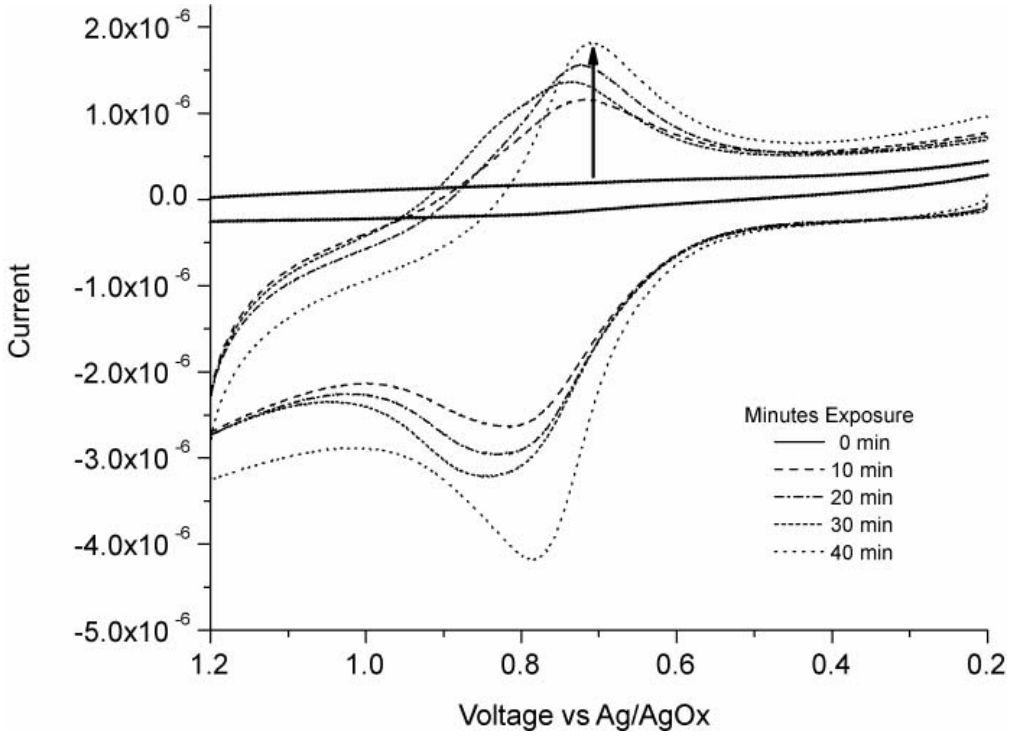

Figure 5.7 Raw cyclic voltammograms for adsorption of ferrocenylethylamine atop $Y_{0.6}Ca_{0.4}Ba_{1.6}La_{0.4}Cu_3O_{7-\delta}$. In this series, the $Y_{0.6}Ca_{0.4}Ba_{1.6}La_{0.4}Cu_3O_{7-\delta}$ was exposed to 1mM ferrocene amine in CH_3CN, followed by subsequent rinsing with CH_3CN, and electrochemical measurements in 0.1 M $TBAPF_6$ in CH_3CN.

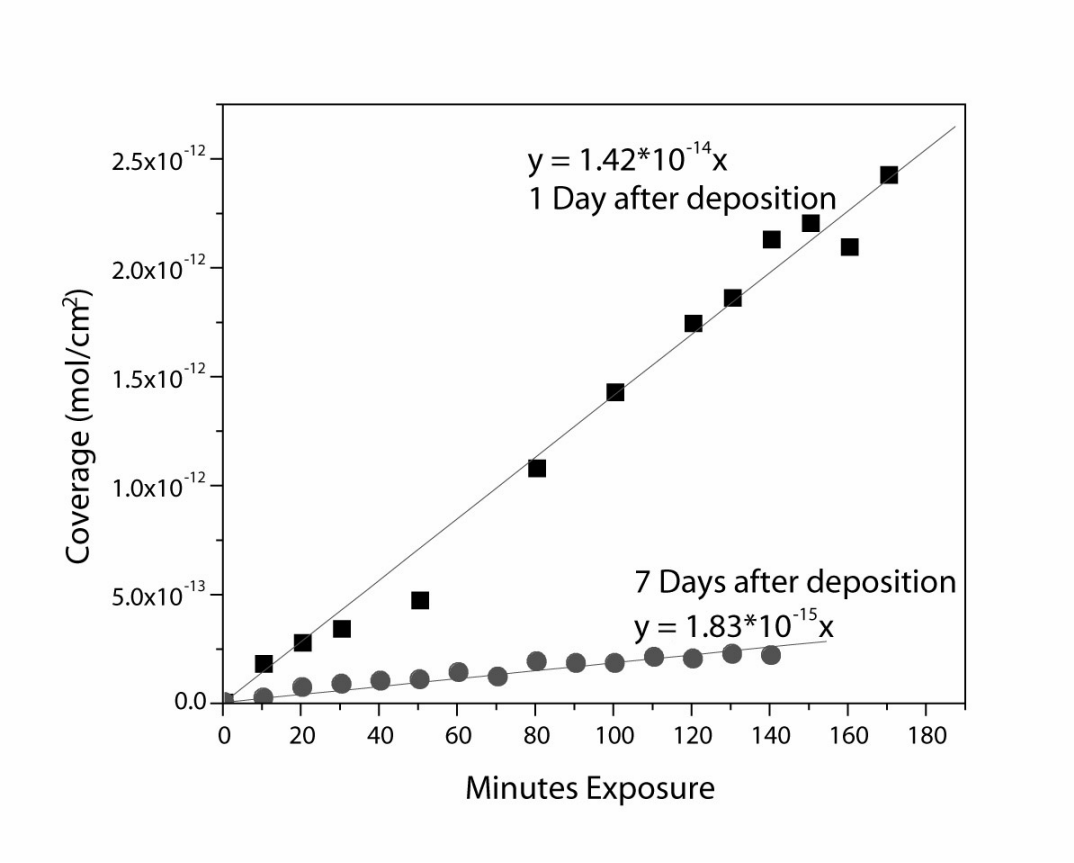

Figure 5.8 Linear adsorption of 1mM ferrocenylethylamine atop $Y_{0.6}Ca_{0.4}Ba_{1.6}La_{0.4}Cu_3O_{7-\delta}$. For pristine films the rate of adsorption is greater than the rate atop aged films.

superconductor, Figure 5.8. Not surprisingly, for films that have aged in the glove box at less than 1 ppb oxygen content**,** the rate of adsorption is decreased presumably due to the accumulation of a corrosive barrier. Interestingly, the exposed sample of $Y_{0.6}Ca_{0.4}Ba_{1.6}La_{0.4}Cu_3O_{7-\delta}$ still adsorbs the ferrocene amine reagent, but at a rate approximately 7 times slower than the pristine film. This decrease is attributed to the presence of a corrosion layer that must be removed for a stable SAM to form. It is expected from previous studies on the mechanism of amine adsorption that that two processes need to occur. At first, the amine reagent must remove the corrosion products from the surface of the film. Only after cleaning can the amine adsorb atop the film forming stable monolayers. More mechanistic details were provided in Chapter 4 of this dissertation. Further aging for a total of 14 days in the inert atmosphere glove box results in a completely passivated film, showing no Faradaic electrochemical response with either adsorbed or solution dissolved redox species. (Data not shown)

5.4.3 Long term adsorption to establish full coverage

For an adsorption isotherm to be useful, the total coverage of the monolayer must be determined. Knowing the total coverage of the surface will aid also in distinguishing the adsorbate structure and provide information about the fraction of the surface involved in the adsorption process. Total coverage will also enable comparison between different experiments by providing a normalization point.

To assess the total coverage and the overall adsorption isotherm, longer-term adsorption experiments were conducted. In this series, thin films were examined in a more concentrated solution of the ferrocenylethylamine than used

previously. This 22mM concentration was chosen to ensure a rapid rise in the overall coverage and to ensure that sufficient material for the rapid removal of any impurity layer on the superconductor. The film was exposed to the SAM reagent in a closed vessel to prevent the evaporation of the CH_3CN over the extended times used in this study. Prior to each electrochemical measurement, the films was removed from the container, rinsed repeatedly in fresh CH_3CN (~50 ml), and then placed in the same electrochemical cell described previously. The repeated alignment of the film was assured by placing the same corner of the film into the cell every time. Sample cyclic voltammograms are shown for the initial and final scans in Figure 5.9. The peak splitting in these samples in only 66 mV, significantly smaller than the 122 mV typically observed for free ferrocene in solution, but not the ideal 0 mV of a bound electroactive reagent (*vide supra*). A comparison of the bound ferrocene response to that of solution ferrocene is shown in Figure 5.10 for reference.

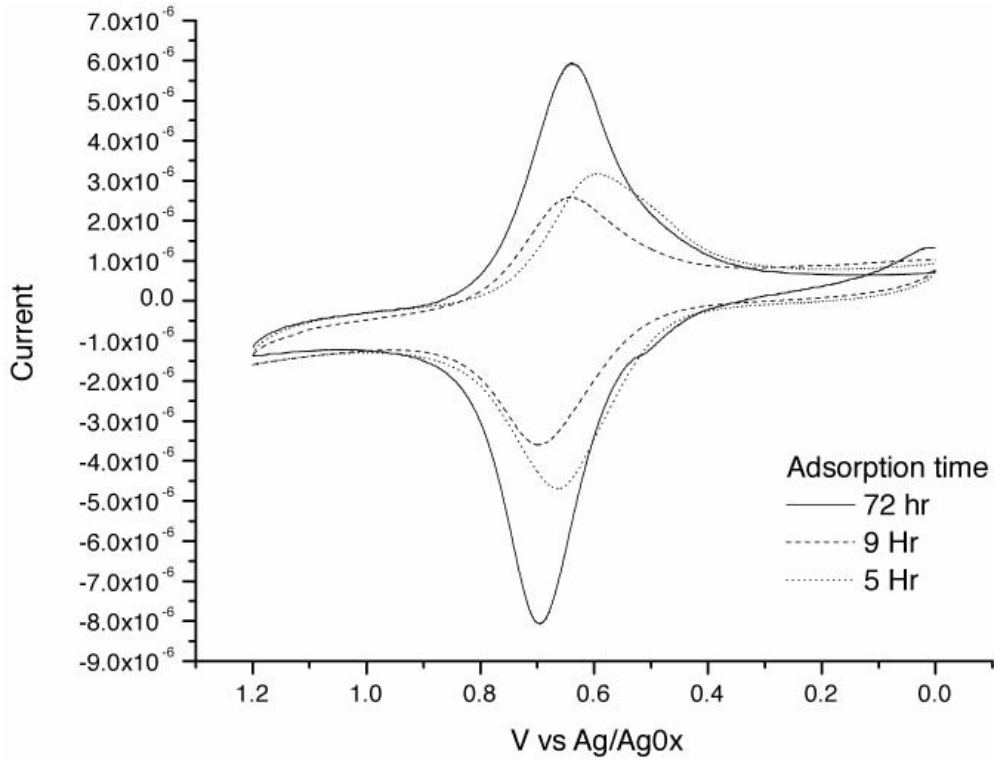

Figure 5.9 Example CV's of ferrocenylethylamine adsorbed atop $Y_{0.6}Ca_{0.4}Ba_{1.6}La_{0.4}Cu_3O_{7-\delta}$ from 22 mM ferrocenylethylamine solution in acetonitrile.

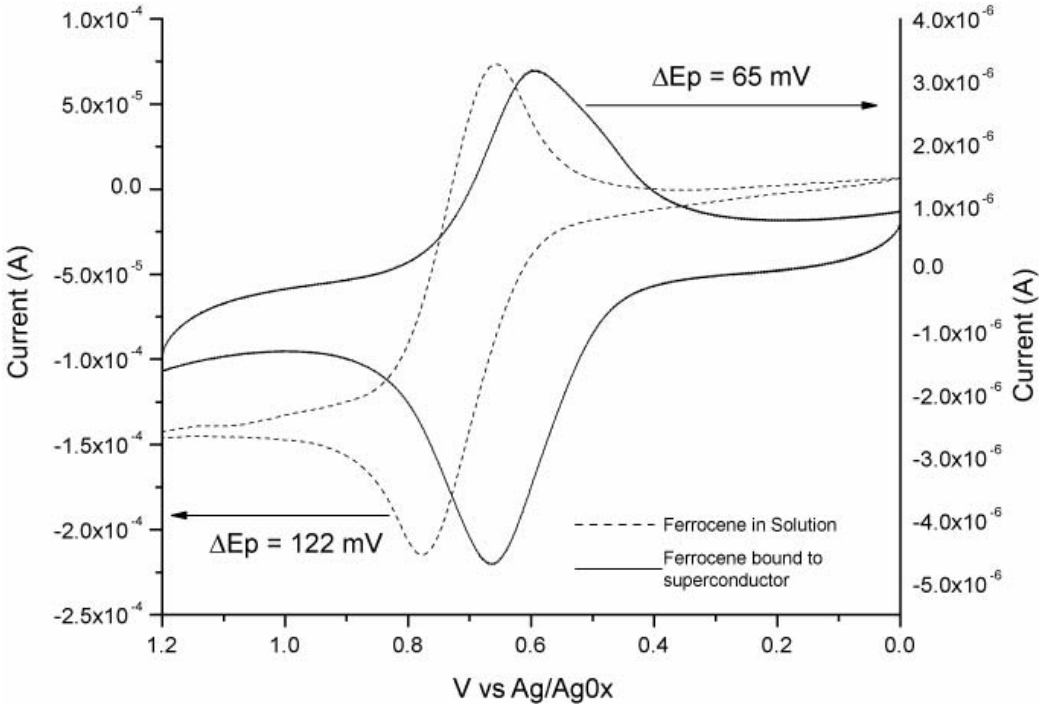

Figure 5.10 The difference in the peak splitting of bound and free ferrocene reagents can clearly be seen in the above voltammograms. The solid curve is for a full monolayer of ferrocenylethylamine bound to the surface of a $Y_{0.6}Ca_{0.4}Ba_{1.6}La_{0.4}Cu_3O_{7-\delta}$ film. The dashed curve is for a solution on ferrocene in CH_3CN with a $Y_{0.6}Ca_{0.4}Ba_{1.6}La_{0.4}Cu_3O_{7-\delta}$ working electrode. For the voltammograms, a Pt counter electrode and Ag/AgOx pseudo-reference electrode were used.

The adsorption isotherm for the 22 mM ferrocenylethylamine atop $Y_{0.6}Ca_{0.4}Ba_{1.6}La_{0.4}Cu_3O_{7-\delta}$ is shown in Figure 5.11. This is the first reported adsorption isotherm atop a thin film superconductor electrode. The total measured coverage measured at the end of exposure of the ferrocene amine atop the superconductor was calculated to be 2.6×10^{-10} mol/cm^2. This compares favorably with the predicted value of ~2.9×10^{-10} mol/cm^2. Not accounting for the roughness of the films, this value suggests that the predicted 2×2 overlayer structure is correct and that nearly the entire area of the film is electroactive.

Based on the fit of a Langmuir isotherm, the observed rate constant for self-assembly from a 22mM solution is $0.12\pm0.02 s^{-1}$. This value is the k_{obs} in Eq 5.12 and represents the combined rate of pre-etching and adsorption/desorption of the ferrocenylethylamine on the $Y_{0.6}La_{0.4}Ba_{1.6}Ca_{0.4}Cu_3O_{7-\delta}$. A value of K′ is also obtained from the fit data. This value is related to the equilibrium parameter of the adsorption process. Given that the K′ is related to the rates of adsorption and desorption in the derivation of the Langmuir isotherm, substitution of K′ = 0.933 into $K'=C/(C+(k_d/k_a))$ where C=0.022M yields a k_d/k_a=0.0667. This value is the inverse of the overall rate constant for the reaction $K_{RXN}=(k_a/k_d)$. The measured rate of reaction is therefore $1/(k_d/k_a)$=1/0.0667 or 15.0 mol/s.

Compared to the rates of adsorption of thiols atop gold, this initial value for the observed rate suggests that the adsorption of amines is approximately 1/10th that of the thiol gold system as measured by adsorption atop a quartz crystal microbalance.[30] Comparison with numerous other rates of adsorption in the

literature also shows the adsorption of amines to copper to be much slower than the gold thiol and related systems.[31-38]

The present examination of the amine rate of adsorption assumes a pseudo-first order rate of reaction as was done for the early work atop gold-thiols. However, careful study of the other experiments reveals a two step process for formation of monolayers atop gold. In the thiol system, initial adsorption is assumed to occur with the hydrocarbon chains laying down across the surface of the film and then later being propped up into the densely packed structure. The speed at which this evolution occurred was directly related to the chain length and final stability of the monolayer.[31,38] This increase in speed and stability is expected, given that longer hydrocarbon chains have greater van der Waals interactions. This increased attraction should also lead to a lower rate of desorption, further enhancing the observed rate of formation.

Given the early stage of this work, a pseudo-first order reaction is not an untenable assumption. The short length of the ferrocene amine used in this study lower the interaction energy between the individual molecules and would increase the rate of desorption from the surface relative to longer chain molecules. The requirement that corrosion products be removed from the surface would also mask any ability to differentiate possible structural changes occurring during the deposition.

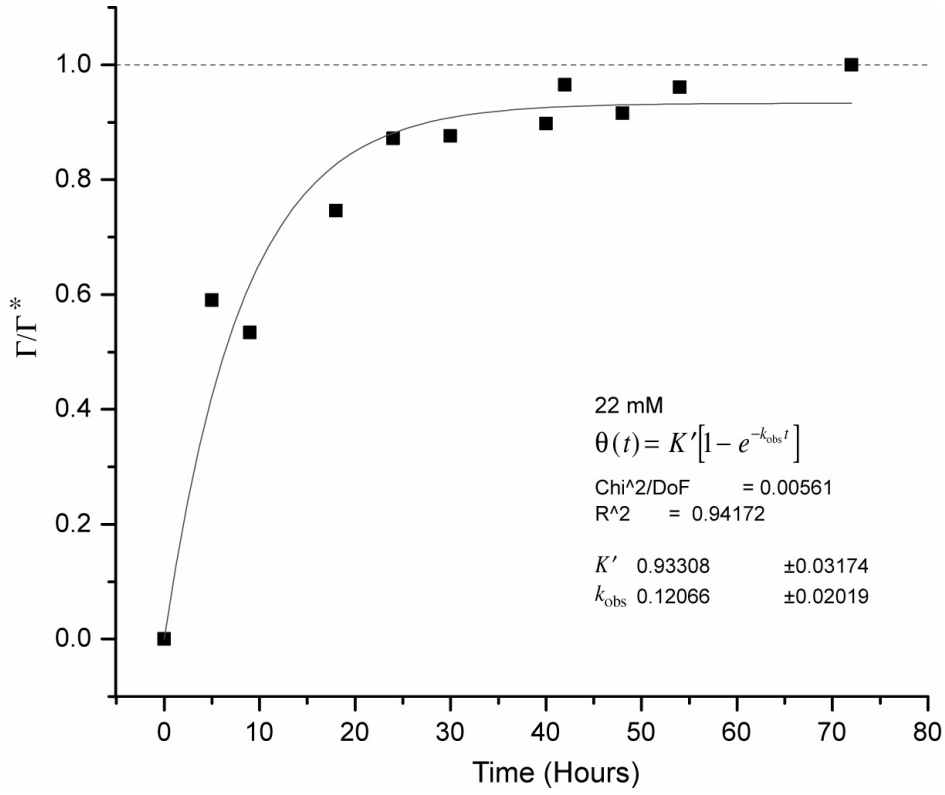

Figure 5.11 Adsorption isotherm for 22mM ferrocenylethylamine in acetonitrile atop $Y_{0.6}Ca_{0.4}Ba_{1.6}La_{0.4}Cu_3O_{7-\delta}$. The cyclic voltammograms were performed in 0.1M $TBAPF_6$ using a Pt counter electrode and Ag/AgOx quasi-reference electrode. The peak heights were converted into the coverage using Eq 5.14 and normalized against the coverage at 72 hrs.

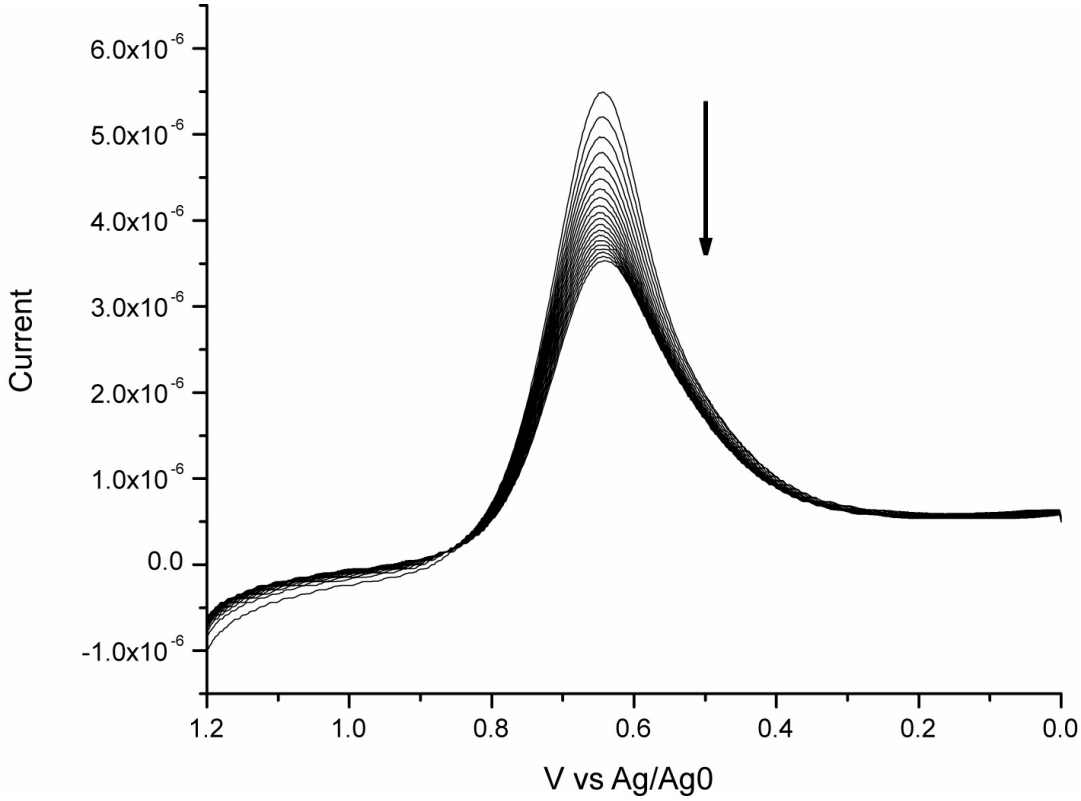

Figure 5.12 Raw data showing the cathodic peaks for a series of 20 cyclic voltammograms performed concurrently. The uppermost peak is the first scan of the monolayer of ferrocenylethylamine adsorbed atop $Y_{0.6}Ca_{0.4}Ba_{1.6}La_{0.4}Cu_3O_{7-\delta}$. The peak height ($\propto$ coverage) decreases in a regular manner until the experiments were stopped after 20 scans.

The presence of a passivation corrosion layer is assumed to hinder the deposition as well, as demonstrated in the short adsorption time studies described in the previous section. Removal of the barrier by the etching action of the amine also slows the observed rate constant. From the fit of the ferrocene-amine adsorption, the free energy of adsorption may be estimated.

The fit of a Langmuir isotherm to the adsorption data is shown in Figure 5.11. This fit provides two values, K′ and k_{obs}, which can be used to calculate the rates of adsorption and desorption, k_a and k_d. Using the following relations, defined in the derivation of the Langmuir isotherm:

$$K' = \frac{C}{C + \left[k_d / k_a \right]} \qquad \text{Eq 5.2}$$

$$k_{obs} = k_a C + k_d \qquad \text{Eq 5.3}$$

and given the fit values of K′ =0.93 and k_{obs}=0.12 when the concentration C is 0.022M, the $k_a = 1.4\ M^{-1}s^{-1}$ and $k_d = 0.09\ s^{-1}$. These data can be used to calculate the equilibrium constant K_{eq} and thus the Gibbs free energy of adsorption, ΔG_{ads}, for the adsorption reaction.

$$K_{eq} = K_a / K_d \qquad \text{Eq 5.4}$$

$$\Delta G_{ads} = -RT \ln K_{eq} \qquad \text{Eq 5.5}$$

The calculated ΔG_{ads} is –6.8kJ/mol or –1.6kcal/mol. This value is approximately 30% of the values reported for longer chain thiols on gold and 15% of the value for long chain alkyl amines atop $YBa_2Cu_3O_{7-\delta}$. The values are tabulated in Table 5.1. Possible reasons for the lower observed free energy are many. The monolayer would not be expected to be as stable since the chain length

is shorter and the ferrocene is a bulky tail group. This different reagent structure limits the stronger lateral intermolecular forces found in the straight chain alkylamine systems. The reduced hydrophobic effect of the polar ferrocenylethylamine in acetonitrile may also lower the stability of the monolayer. The hydrophobic effect arises when a polar(non-polar) solvent which self-associates (i.e. water or methanol), excludes the non-polar(polar) portion of a molecule from the solvent resulting in a net energy gain. This hydrophobic effect increases linearly as function of the number of carbon atoms. As the hydrocarbon chain gets longer, the energy of the adsorption is lowered, as shown in the following equation:[39,40]

$$\Delta G_{ads} \cong A - 1.4RTN_C \qquad \text{Eq 5.6}$$

where A is a constant dependant on the nature of the polar headgroup, the headgroup-surface interaction and the solvent. The constant A may be either positive or negative but is generally on the order of a few kilocalories per mole. The term $-1.4RTN_C$ accounts for the energy change associated with an increase in the number of carbons in the alkyl chain, through both an increase in the lateral intermolecular forces and the increase in the hydrophobic effect of excluding the non-polar regions from a polar solvent. In the case of the ferrocenylethylamine, which is very soluble in acetonitrile, the hydrophobic effect is expected to be minimal. Further experiments are required to define more precisely the various contributions to the thermodynamic content of the adsorbate monolayer formation process.

Interestingly, the Gibbs free energy of adsorption for ferrocenylethylamine atop cuprates is almost half of that for a comparably short alkyl thiol on gold. This difference suggests the amine-cuprate lattice association is considerably smaller than the alkyl thiol–gold case. The relatively small head-group interaction strength is consistent with surface mobility of amine adsorbents, which allows for annealing into more organized motifs. In a different set of experiments, Xu *et al.* performed monolayer exchange studies of longer chain ferrocenylamines and noted that 30% of the original C4 amide coupled ferrocene was replaced in only 2 hours by a C5 monolayer. They specifically noted that the electrochemical peaks did not broaden with coverage, suggesting a loose packing due to the bulk of the ferrocene end group.[25]

Table 5.1 Selected Results of Adsorption Isotherm Studies

System	Method	ΔG_{ads} (kcal/mol)	Reference
C_8SH/Au terrace	Electrochemistry	-5.5	Walczak *et. al*[41]
C_8SH/Au defect	Electrochemistry	-11	Walczak *et. al*[41]
$C_{18}SH$/Au	QCM	-5.5	Karpovich *et. al*[33]
$C_{18}SH$/Au	Radioactive	-5.5	Schlenoff *et. al*[42]
RS^-/Ag	Electrochemistry	-22.8	Hatchett *et. al*[43]
$C_{18}COOH/Al_2O_3/Al$	ATR FTIR	-9.2	Chen *et. al*[44]
$C_{18}COOH/SiO_2$	ATR FTIR	-7.3	Chen *et. al*[44]
$C_{18}NH_2/YBa_2Cu_3O_{7-\delta}$	RAIRS	-7.2	Ritchie[24]
$C_{18}NH_2$/Au	RAIRS	-8.4	Ritchie[24]
$C_{18}NH_2$/Au defects	Resistivity	-9.9	Ritchie[24]

A series of repetitive cyclic voltammograms was obtained after 72 hours of total adsorption in order to judge the stability of the monolayer. The decrease in peak height and subsequent decrease in coverage is shown in Figure 5.12, leveling off at approximately 37% of the original coverage. There are three possible reasons for the observed decrease in signal. The monolayer may be desorbing into the fresh electrolyte solution, as would be expected for any labile structure where an

equilibrium needs to be established. The electroactive area of the electrode may be decreasing, as evidenced by the obvious etching shown in Chapter 4. Or finally, the ferrocene may be degrading. A method for determination of the mechanism causing the observed decrease in signal will be discussed after all three possibilities have been considered.

If the monolayer were desorbing, the calculation of a k_d would be possible. The electrochemical shape would be different, however, given that a fraction of the electroactive material is diffusing out into the solution. The peak splitting would be expected to increase over time, approaching the free ferrocene splitting observed earlier in Figure 5.10. Another possibility is that the desorbing molecules are lost to the large sample volume of solution and that the peak splitting may decrease due to the loss of surface interactions causing charge broadening.

If the decrease in coverage is a result of the etching of the surface, the surface roughness of the film should also change. This reduction in roughness would be a result of the amine reagent solublizing $Y_{0.6}La_{0.4}Ba_{1.6}Ca_{0.4}Cu_3O_{7-\delta}$ components and carrying them into the solution. The majority of the components are not electroactive in the range of the cyclic voltammograms performed with the exception of the expected Cu^{2+} and Cu^{1+} species.

Previous work by R. W. Murray, M. Porter and others has shown that ferrocene covalently bound to surfaces degrades over time. The work performed by Porter's group was performed on thiol/gold assemblies in aqueous solutions.[41,45] In work performed in Murray's lab, the decomposition kinetics of ferrocene reagents tethered to platinum electrodes was measured in acetonitrile solutions.[46] In

those studies, the ferrocinium was found to be susceptible to degradation due to attacks from nucleophiles in solution. In the reduced state, the ferrocene was stable for long periods as evidenced by repeated washings in acetonitrile followed by measurement of the iron signal using XPS. It is probable that the ferrocene group is degrading as a result of attack from the supporting electrolyte to the oxidized ferrocinium.

In order to determine the mechanism of desorption, additional studies are needed. The best method to determine the mechanism would be a bi-potentiostatic measurement with two different working electrodes. A ring of platinum around the $Y_{0.6}La_{0.4}Ba_{1.6}Ca_{0.4}Cu_3O_{7-\delta}$ main electrode would allow greater variation of voltages outside the region of $Y_{0.6}La_{0.4}Ba_{1.6}Ca_{0.4}Cu_3O_{7-\delta}$ stability. Using the alternate platinum electrode, the presence of a Cu^{2+} reduction peak at +0.21 V positive of the ferrocinium-ferrocene reduction would indicate that etching was occurring at the surface. The absence of the Cu reduction, but the presence of an iron couple – 0.72 V from the ferrocene couple would represent a decomposition of the ferrocene as observed by Murray and others. The presence of only a ferrocene couple would represent simple desorption. This work will be carried out in further studies.

5.5 ELECTROCHEMISTRY ON $YBa_2Cu_3O_{7-\delta}$

In order to estimate the influence of surface corrosion on the adsorption process, experiments similar to those described in the previous section were performed atop $YBa_2Cu_3O_{7-\delta}$. This cuprate superconductor is the parent compound of $Y_{0.6}La_{0.4}Ba_{1.6}Ca_{0.4}Cu_3O_{7-\delta}$ possessing a similar unit cell, but without the stabilization dopants added to the lattice. Previous studies have show that the

$Y_{0.6}La_{0.4}Ba_{1.6}Ca_{0.4}Cu_3O_{7-\delta}$ is approximately 100 times more stable in than $YBa_2Cu_3O_{7-\delta}$ in ambient conditions.[12,14-16,19] It would then be expected that the $YBa_2Cu_3O_{7-\delta}$ would have a greater amount of corrosion atop the film, slowing the rate of adsorption as displayed in the comparison of pristine and aged $Y_{0.6}La_{0.4}Ba_{1.6}Ca_{0.4}Cu_3O_{7-\delta}$. Thus, the study of adsorption atop $YBa_2Cu_3O_{7-\delta}$ vs. $Y_{0.6}La_{0.4}Ba_{1.6}Ca_{0.4}Cu_3O_{7-\delta}$ may provide information regarding the role of surface corrosion on monolayer processes.

The films used in these experiments are essentially the same as those described in Chapter 3 where the optimization of the deposition conditions is described at length.

The identical short-term adsorption experiments were conducted atop thin films of $YBa_2Cu_3O_{7-\delta}$. While not providing useful kinetic data, the experiments helped to elucidate the mechanism of the adsorption and highlight the importance of corrosion resistivity for thin films.

Like the previous series of short-term adsorption studies, the films were encased in the custom electrochemical cell and exposed to 1mM ferrocenylethylamine in CH_3CN in 15 minute increments. After each exposure period, the films were washed in copious amounts of CH_3CN equivalent to 100 times the volume of the cell (total wash volume ~ 50 ml). The same 0.1 M $TBAPF_6$ electrolyte solution was used for the cyclic voltammetry. Examination of Figure 5.13 shows the decrease in coverage with increased exposure to the self-assembly reagent.

This unusual result is easily explained upon examination of the electron micrographs of the films. In Figure 5.14, three electron micrographs of the same batch of $YBa_2Cu_3O_{7-\delta}$ thin films used for the electrochemical experiments are shown. In A and B, the pristine film and the film exposed to electrolyte show typical c-axis orientation with no signs of pitting or etching. In C, the section of the film that was

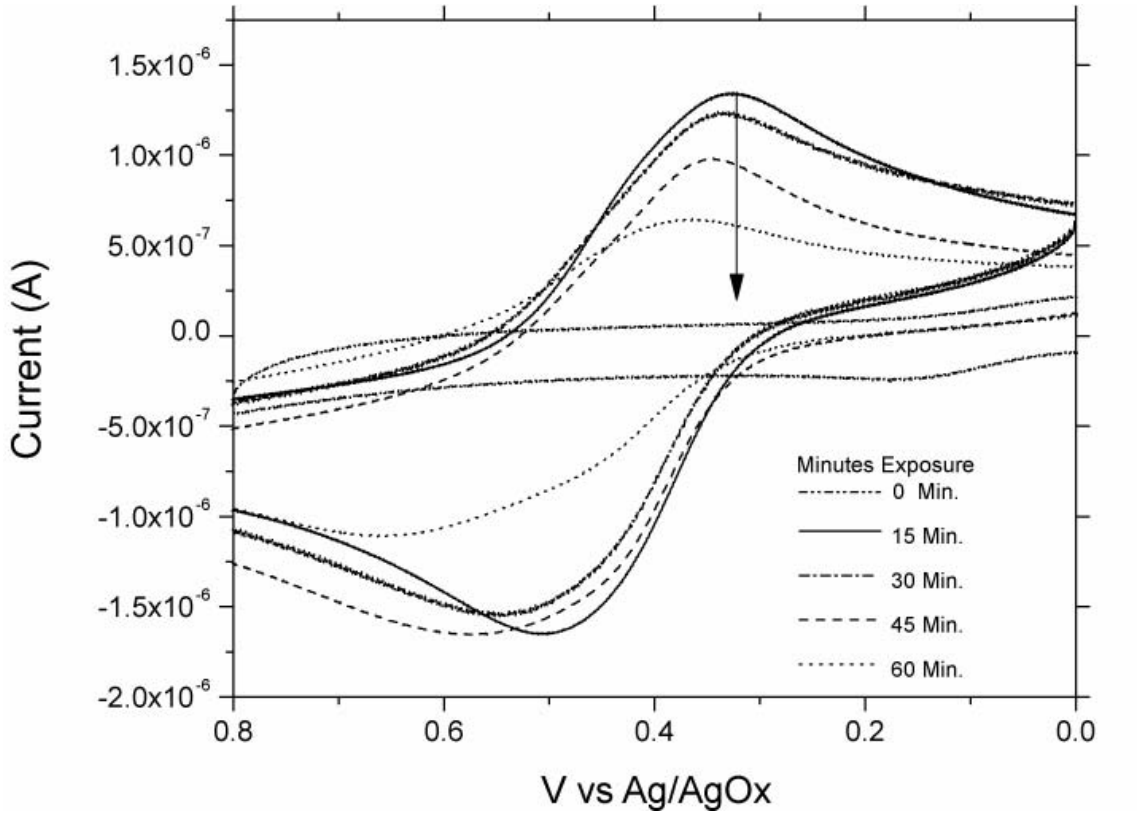

Figure 5.13 Cyclic voltammetry of ferrocenylethylamine atop $YBa_2Cu_3O_{7-\delta}$. Surprisingly, increased exposure leads to decreased coverage and visible etching of the film.

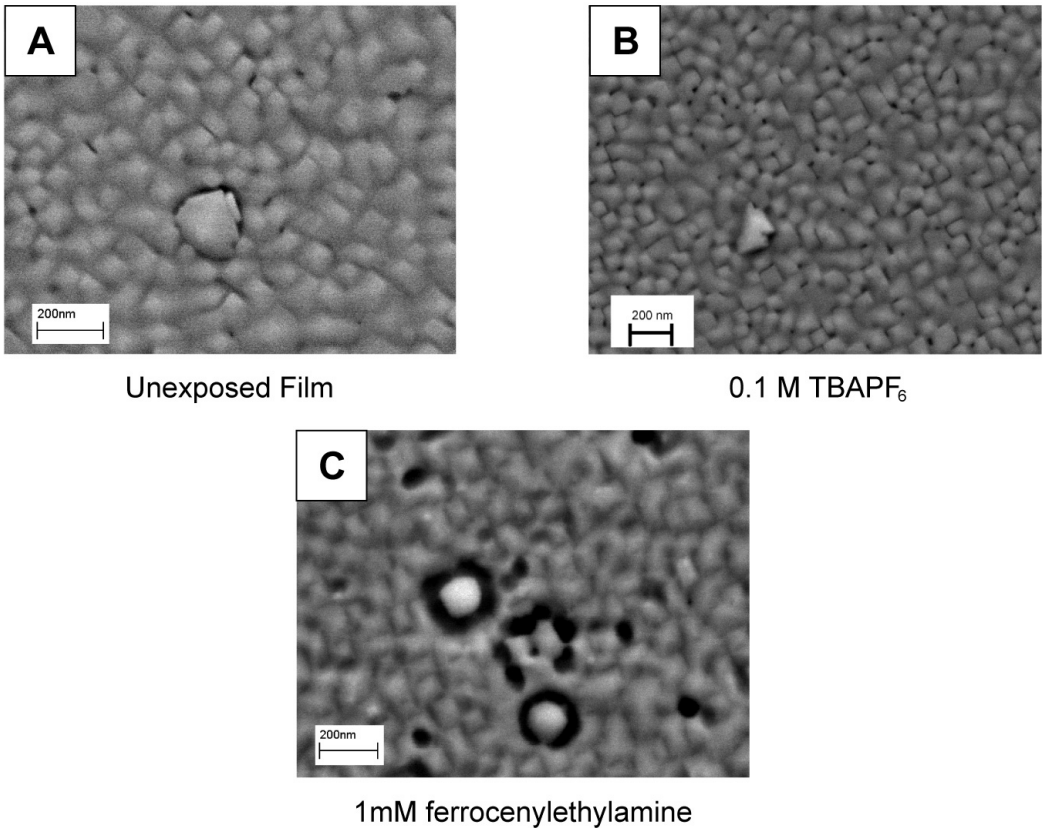

Figure 5.14 Scanning electron micrographs of $YBa_2Cu_3O_{7-\delta}$ films showing the etching that occurs with self-assembly. The micrograph of the pristine film (A) and the film exposed to electrolyte (B) show typical c-axis orientation. The film that was exposed to 1mM ferrocenylethylamine (C) shows significant etch pits after only 1 hour of total exposure time.

exposed to a 1mM ferrocenylethylamine for a total of 1 hr, pitting and etching are noted at pinholes and around laser droplets. As stated previously, the nature of the adsorbent molecule hinders the ability to form monolayers. The proposed larger inter-atomic distances and the large footprint of the ferrocene prevent formation of the normal van der Waals attractions that helps to stabilize the monolayer. This poor packing should lead to a higher rate of desorption and also etching until a smooth surface is achieved that allows the closest packing possible. In effect, the monolayer reagent is planarizing the film until it reaches a suitable level of flatness and self-passivates. It is also important to note that for this sample, the repeated washing and replacement of solution also helps to drive the etching. The repeated solution exchanges create a non-equilibrium situation that should favor desorption into the electrolyte, and more aggressive etching every time fresh SAM solution is introduced. Other members of the McDevitt group have recent micrographs showing similar effects with medium length alkylamine reagents ($CH_3(CH_2)_xNH_2$ where x=4,6,8).

The decrease in the monolayer coverage can be explained by the changing the electroactive surface area of the film. In addition to loosing surface area, optical micrographs show the overall thinning of the area exposed to the SAM reagent, with large pinholes evident around the periphery of the exposed area, Figure 5.15. Recall from Chapter 4 that etching is a vital part of the mechanism of adsorption. Interestingly, etching of $YBa_2Cu_3O_{7-\delta}$ is more noticeable than for the corrosion resistant $Y_{0.6}Ca_{0.4}Ba_{1.6}La_{0.4}Cu_3O_{7-\delta}$ samples of the previous chapter.

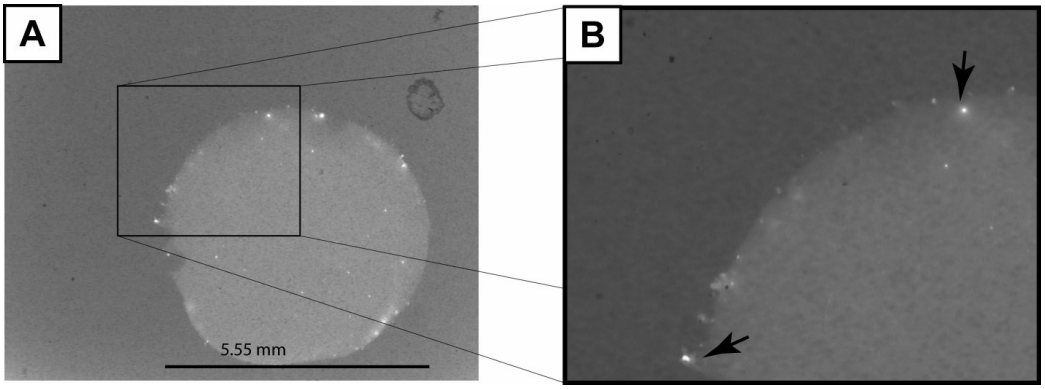

Figure 5.15 Optical micrograph of etched $YBa_2Cu_3O_{7-\delta}$ thin film showing the exposed area (A) and pinholes formed by the etching process (arrows in B)

5.6 CONCLUSION

The first reported determination of the kinetics of adsorption of electroactive monolayers atop high temperature superconductors has been presented. While rough, the method shows promise given a judicious choice of concentrations and reagents. The effect of surface cleanliness on the rate of adsorption is also noted. Importantly, further evidence of the ability of the amine reagents to planarize the surface of thin films has been presented.

In this chapter, three important effects of monolayer adsorption have been defined. Firstly, the requirement for stable films has been shown through a comparison of the etching behavior atop $YBa_2Cu_3O_{7-\delta}$ and the more corrosion resistant $Y_{0.6}La_{0.4}Ba_{1.6}Ca_{0.4}Cu_3O_{7-\delta}$. The $YBa_2Cu_3O_{7-\delta}$ is shown to be too sensitive to corrosion for the determination of adsorption kinetics. This result suggests that any further monolayer work occur using the corrosion resistant phases of the cuprate superconductors. Secondly, the measurements of adsorption

kinetics atop superconductor thin films have been shown for the first time. The development of this technique will aid in the assembly of more robust monolayers affording better protection. Thirdly, the labile nature of the monolayer atop superconductors has been shown,

5.7 DISSERTATION SUMMARY

The goal of this dissertation was to examine the mechanism and kinetics of formation of self-assembled amine monolayers atop cuprate superconductors. In order to examine these phenomena, a new pulsed laser deposition system capable of generating larger quantities of pristine thin film superconductors was built and optimized. Experimental evidence for the removal of previously exposed corroded material by the alkyl amine monolayer reagent has been provided using x-ray photoelectron spectroscopy, atomic absorption spectroscopy, and scanning electron micrography. Evidence of the alkylamines role in planarizing the superconductors is also provided. The kinetics of adsorption have been examined using a redox active monolayer reagent, providing the first documentation of adsorption isotherms atop cuprate thin films.

This information is useful because it suggests that "soft chemical" routes can be used to control the interfaces of cuprate superconductors. Ambient pressure methods can be used to process cuprate films and devices. Further development of the monolayer chemistry and associated chemistry of adsorption may lead to reduction of the problems associated with decomposition of the cuprate during photolithographic processing.

An interesting two step etching/adsorption mechanism is seen for amine monolayer formation. Remarkably, dirty superconductor samples can be cleaned through exposure to judiciously chosen amine adsorbate.

Molecular level details of adsorbate processes from a thermodynamic prospective show surface adsorbate interactions in the amine/cuprate systems are less energetic than comparable gold/thiol systems. The amine/cuprate systems is more amenable to exchange with the solution as needed for creation of ordered systems. Further longer times are required to form monolayers atop high temperature superconductors, with the surface binding becoming even slower if corrosive damage must be removed in a pre-etching step.

Finally, an interesting molecular approach for planarization of cuprate superconductor films has been discovered. Planar films and well-defined interfaces have been important for the high-T_c device community where poor yields and lack of uniform device characteristics have been problematic. Further work in this area is warranted in attempts to aid the device fabrication area.

5.8 REFERENCES

(1) Whitesides, G. M.; Ferguson, G. S.; Allara, D.; Scherson, D.; Speaker, L.; Ulman, A. *Critical Reviews in Surface Chemistry* **1993**, *3*, 49-65.

(2) Isaacs, L.; Chin, D. N.; Bowden, N.; Xia, Y.; Whitesides, G. M. *Perspectives in Supramolecular Chemistry* **1999**, *4*, 1-46.

(3) Chen, K.; Mirkin, C. A.; Lo, R.-K.; Zhao, J.; McDevitt, J. T. *J. Am. Chem. Soc.* **1995**, *117*, 6374-6375.

(4) Chen, K.; Xu, F.; Mirkin, C. A.; Lo, R.-K.; Nanjundaswamy, K. S.; Zhou, J.-P.; McDevitt, J. T. *Langmuir* **1996**, *12*, 2622-2624.

(5) Riley, D. R.; McDevitt, J. T. *J. Electroanal. Chem.* **1990**, *295*, 373-384.

(6) Riley, D. R.; Jurbergs, D.; Zhou, J.-P.; Zhao, J.; Markert, J.; McDevitt, J. T. *Solid State Comm.* **1993**, *88*, 431-434.

(7) Ritchie, J. E.; Wells, C. A.; Zhou, J.-P.; Zhao, J.; McDevitt, J. T.; Ankrum, C. R.; Jean, L.; Kanis, D. R. *J. Am. Chem. Soc.* **1998**, *120*, 2733-2745.

(8) Ritchie, J. E.; Murray, W. R.; Kershan, K.; Diaz, V.; Tran, L.; McDevitt, J. T. *J. Am. Chem. Soc.* **1999**, *121*, 7447-7448.

(9) Riley, D. R.; McDevitt, J. T. *J. Electroanal. Chem.* **1990**, *295*, 373-384.

(10) Riley, D. R.; Manthiram, A.; McDevitt, J. T. *Chem. Mat.* **1992**, *4*, 1176-1181.

(11) Nicholson, R. S.; Shain, I. *Analytical Chemistry* **1964**, *36*, 706-723.

(12) McDevitt, J. T.; Zhou, J.-P.; Jones, C. E.; Talvacchio, J. In *Proceedings of the 10th Aniversary HTS Workshop on Physics, Materials, and Applications*; Batlogg, B., Ed.; World Scientific: Houston, Texas, 1996, pp 177-178.

(13) Zhou, J.-P.; Lo, R.-K.; Savoy, S. M.; Arendt, M.; Armstrong, J.; Yang, D.-Y.; Talvacchio, J.; McDevitt, J. T. *Physica C* **1997**, *273*, 223-232.

(14) McDevitt, J. T.; Zhou, J.-P.; Zhao, J. In *PCT Int. Appl*; Board of Regents, The University of Texas System: USA, 1996.

(15) Zhou, J.-P.; Zhou, J.-S.; Goodenough, J. B.; McDevitt, J. T. *Journal of Superconductivity* **1995**, *8*, 651-652.

(16) Zhou, J.-P.; Savoy, S. M.; Lo, R.-K.; Zhao, J.; Arendt, M.; Zhu, Y. T.; Manthiram, A.; McDevitt, J. T. *Appl. Phys. Lett.* **1995**, *66*, 2900-2902.

(17) Zhou, J.-P.; Jones, C. E.; McDevitt, J. T.; Talvacchio, J.; Jia, Q. X. In *Advances in Superconductivity X: Procceding of the International Symposium on Superconductivity*; Osamura, K., Hirabayashi, I., Eds.; Springer: Gifu, Japan, 1997; Vol. 1, pp 289-292.

(18) Zhou, J.-P.; Lo, R.-K.; Savoy, S. M.; Arendt, M.; Armstrong, J.; Yang, D.-Y.; Talvacchio, J.; McDevitt, J. T. *Physica C* **1997**, *273*, 223-232.

(19) Zhou, J.-P.; Savoy, S. M.; Zhao, J.; Riley, D. R.; Zhu, Y. T.; Manthiram, A.; Lo, R.-K.; Borich, D.; McDevitt, J. T. *J. Am. Chem. Soc.* **1994**, *116*, 9389-9390.

(20) Zhou, J.-P.; Riley, D. R.; McDevitt, J. T. *Chem. Mat.* **1993**, *5*, 361-365.

(21) Zhou, J.-P.; McDevitt, J. T. *Chem. Mat.* **1992**, *4*, 953-959.

(22) McDevitt, J. T.; Mirkin, C. A.; Lo, R.-K.; Chen, K.; Zhou, J.-P.; Xu, F.; Haupt, S. G.; Zhao, J.; Jurbergs, D. *Chem. Mat.* **1996**, *8*, 811-813.

(23) Mirkin, C. A.; Xu, F.; Zhu, J. *Adv. Mat.* **1997**, *9*, 167-172.

(24) Ritchie, J. E. In *Department of Chemistry and Biochemistry*; University of Texas at Austin: Austin, Texas, 1998, p 166.

(25) Xu, F.; Zhu, J.; Mirkin, C. A. *Langmuir* **2000**, *16*, 2169-2176.

(26) Riley, D. R.; McDevitt, J. T. *Journal of Electroanalytical Chemistry and Interfacial Electrochemistry* **1990**, *295*, 373-384.

(27) Nicholson, R. S. *Analytical Chemistry* **1965**, *37*, 1351-1355.

(28) Riley, D. R. In *Department of Chemistry and Biochemistry*; University of Texas at Austin: Austin, Texas, 1993, p 199.

(29) Bard, A. J.; Faulkner, L. R. *Electrochemical methods: fundamentals and applications*; 2nd ed.; John Wiley & Sons, Inc.: New York, 2001.

(30) Schessler, H. M.; Karpovich, D. S.; Blanchard, G. J. *J. Am. Chem. Soc.* **1996**, *118*, 9645-9651.

(31) Bain, C. D.; Troughton, E. B.; Tao, Y.-T.; Evall, J.; Whitesides, G. M.; Nuzzo, R. G. *J. Am. Chem. Soc.* **1989**, *111*.

(32) Thomas, R. C.; Sun, L.; Crooks, R. M.; Ricco, A. J. *Langmuir* **1991**, *7*.

(33) Karpovich, D. S.; Blanchard, G. J. *Langmuir* **1994**, *10*, 3315-3322.

(34) Yitzchaik, S.; Marks, T. J. *Accounts of Chemical Research* **1996**, *29*, 197-202.

(35) Peterlinz, K. A.; Georgiadis, R. *Langmuir* **1996**, *12*, 4731-4740.

(36) Bansebaa, F.; Voicu, R.; Huron, L.; Ellis, T. H.; Kruus, E. *Langmuir* **1997**, *13*, 5335-5340.

(37) Eberhardt, A.; Fenter, P.; Eisenberger, P. *Surf. Sci.* **1998**, *397*, L285-L290.

(38) Xu, S.; Cruchon-Dupeyrat, S. J. N.; Garno, J. C.; Liu, G.-Y.; Jennings, G. K.; Yong, T.-H.; Laibinis, P. E. *J. Chem. Phys.* **1998**, *108*, 5002-5012.

(39) Wagnerud, P.; Jonsson, B. *Langmuir* **1994**, *10*, 3268-3278.

(40) Hatchett, D. W.; Uibel, R. H.; Stevenson, K. J.; Harris, J. M.; White, H. S. *J. Am. Chem. Soc.* **1998**, *120*, 1062-1069.

(41) Walczak, M. M.; Popenoe, D. D.; Deinhammer, R. S.; Lamp, B. D.; Chung, C.; Porter, M. D. *Langmuir* **1991**, *7*, 2687-2693.

(42) Schlenhoff, J. B.; Li, M.; Ly, H. *J. Am. Chem. Soc.* **1995**, *117*, 12528-12536.

(43) Hackett, D. W.; Uibel, R. H.; Stevenson, K. J.; Harris, J. M.; White, H. S. *Journal of the American Chemical Society* **1998**, *120*, 1062-1069.

(44) Chen, S. H.; Frank, C. W. *Langmuir* **1989**, *5*, 978-987.

(45) Popenoe, D. D.; Deinhammer, R. S.; Porter, M. D. *Langmuir* **1992**, *8*, 2521-2530.

(46) Lenhard, J. R.; Murray, R. W. *J. Am. Chem. Soc.* **1978**, *100*, 7870-7875.

Bibliography

Bard, A. J. and L. R. Faulkner (2001). Electrochemical methods: fundamentals and applications. New York, John Wiley & Sons, Inc.

Bourdillon, A. and N. X. T. Bourdillon (1994). High Temperature Superconductors: Processing and Science. New York, Academic Press, Inc.

Cyrot, M. and D. Pavuna (1992). Introduction to superconductivity and high-Tc materials. River Edge, NJ, World Scientific Publishing Co. Pte. Ltd.

Hazen, R. M. (1988). The Breakthrough: The Race for the Supercondcutor. New York, Summit Books.

Jenkins, R. and R. L. Snyder (1996). Introduction to x-ray powder diffractometry, Wiley - Interscience.

Kittle, C. (1976). An Introduction to Solid State Physics. New York, John Wiley & Sons, Inc.

Masel, R. I. (1996). Principles of adsorption and reaction on solid surfaces. New York, John Wiley & Sons, Inc.

Poole, C. P., H. A. Farach, et al. (1995). Superconductivity. New York, Academic Press.

Sands, D. E. (1975). Introduction to Crystallography. New York, Dover Publications Inc.

Simon, R. and A. Smith (1988). Superconductors: Conquering Technology's New Frontier. New York, Plenum Press.

Ulman, A. (1991). An introduction to ultrathin organic films: from Langmuir-Blodgett to self-assembly. San Diego, CA, Academic Press.

van der Put, P. J. (1998). The Inorganic Chemistry of Materials: How to Make Things Out of Elements. New York, Plenum Press.

Vita

William Reynolds Murray was born April 20, 1970 in Houston, Texas. He is the son of Richard and Rachel Murray. After graduating Magna Cum Laude from Washington an Lee University as an Honors Scholar with a B.S. in Chemistry in 1996, he enrolled at the University of Texas at Austin under the tutelage of Dr. John T. McDevitt.

Permanent address: 4243 Lakeshore Forest Dr. Missouri City, TX 77459

This dissertation was typed by the author.